Semitransparent Perovskite Solar Cells for Building Integration and Tandem Photovoltaics: Design Strategies and Challenges

Giuliana Giuliano, Aurelio Bonasera, Giuseppe Arrabito, and Bruno Pignataro*

Over the past decade, halide perovskite systems have captured widespread attention among researchers since their exceptional photovoltaic (PV) performance is disclosed. The unique combination of optoelectronic properties and solution processability shown by these materials has enabled perovskite solar cells (PSCs) to reach efficiencies higher than 25% at low fabrication costs. Moreover, PSCs display enormous potential for modern unconventional PV applications, since they can be made lightweight, semitransparent (ST), and/or flexible by means of appropriate design strategies. In particular, by enabling transparency and high efficiency simultaneously, ST-PSCs hold great promise for future versatile utilization in the context of building-integrated PVs (BIPVs) or as top cells to be coupled with conventional lower-bandgap bottom cells in tandem PV devices. The present review aims to provide a detailed overview of latest research about ST-PSCs for BIPVs and tandems, by critically reporting on the most updated and effective design strategies in view of these two possible future applications. The differences and similarities between the available approaches are punctually highlighted, emphasizing the importance of a rigorous application-orientated ST-PSC design. Finally, the main challenges and issues about device design, operation, and stability that need to be addressed before commercialization are thoroughly scanned.

1. Introduction

From a sustainable development perspective, transforming the global energy sector by switching from fossil fuels to renewable energy sources constitutes an absolute priority.[1–5] Solar

G. Giuliano, A. Bonasera, G. Arrabito, B. Pignataro
Department of Physics and Chemistry – Emilio Segrè
University of Palermo
Viale delle Scienze, bldg. 17, 90128 Palermo, Italy
E-mail: bruno.pignataro@unipa.it

A. Bonasera
INSTM – University of Palermo Research Unit
Viale delle Scienze, bldg. 17, 90128 Palermo, Italy

The ORCID identification number(s) for the author(s) of this article can be found under https://doi.org/10.1002/solr.202100702.

photovoltaics (PVs) offers one of the most effective strategy for producing clean and sustainable electric power by exploiting the unlimited, ubiquitous, and freely available energy of the sun.[6–9] However, the PV technology is still a minor player in the global power industry, providing less than 3% of the worldwide electricity demand.[10] This is mainly due to the higher production costs of today's applied wafer-based PV modules compared to other conventional carbon-based fuels. Moreover, their opaque/bulky nature hinders a more efficient PV integration into urban scenarios. These issues call for the development of novel, more adaptive, and cost-effective technologies to promote large-scale deployment of PVs.[11–13]

Nowadays, new-generation thin-film PV technologies are making inroads, including dye sensitized solar cells (DSSCs),[14,15] organic solar cells,[16–19] and perovskite solar cells (PSCs).[20–30] Among them, PSCs have recently gained much attention both from the academic and industrial communities, mainly because perovskite light harvesters have demonstrated extraordinarily high PCEs, with the current record certified efficiency being 25.5%.[29] In addition to the impressive PV performance, the possibility to make PSCs semitransparent (ST) has recently opened up new directions for sustainable energy development in the contexts of building-integrated photovoltaics (BIPVs), solar-powered automotive/portable electronics, and tandem solar cells (see **Figure 1**).[31–38] The state-of-the-art PSCs are nontransparent due to the use of opaque, highly reflective metal counter electrodes and the strong absorption of the perovskite film. Very recently, efficient ST-PSCs have been successfully demonstrated using suitable transparent electrodes, opportunely engineered perovskite layers, and advanced light manipulation strategies.[33] The integration of such devices into buildings and skyscrapers as power-generating solar windows, façades, skylights, or other aesthetic architectural elements is one of the most intriguing perspectives,[34,35] offering a sustainable solution to the tremendous and ever-increasing building energy consumption. For such BIPV purposes, specific transparency levels are typically required: For instance, an average visible transmittance (AVT) of at least 25% is taken as a benchmark for solar window applications.[39] In contrast, ST-PSCs with high transparency in the
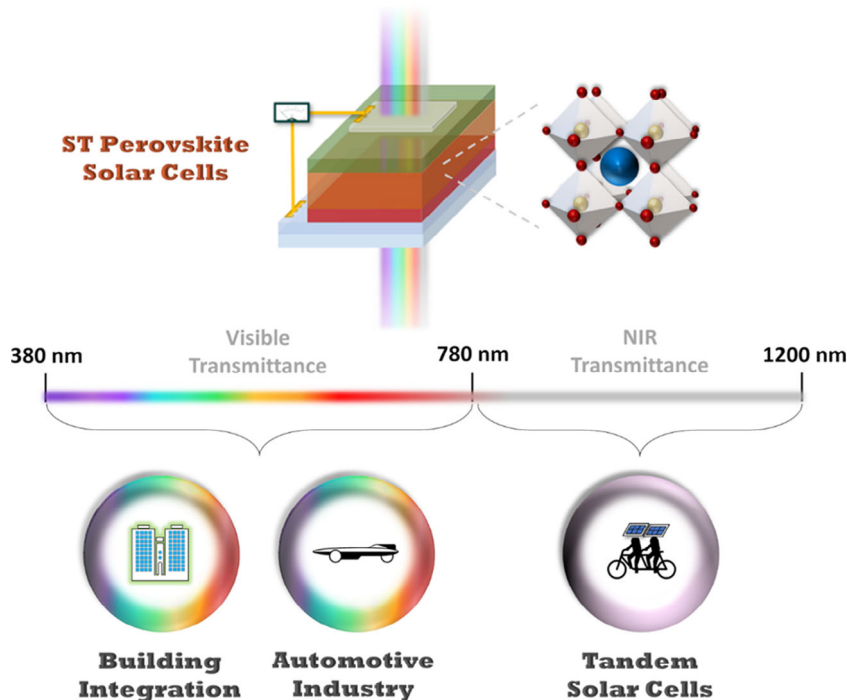
Figure 1. Potential application areas of semitransparent perovskite solar cells (ST-PSCs) based on the transparency wavelength range of interest, either the visible (380–780 nm) or the NIR (800–1200 nm) region of the solar spectrum. ST-PSCs with high visible transparency could find applications in BIPV systems or in the automotive industry (e.g., power-generating transparent car roofs), whereas NIR-transparent PSCs can be integrated as top cells in tandem PVs.

near-infrared region (NIR) of the solar spectrum (typically in the 800–1200 nm range) have recently demonstrated themselves as the ideal top cell candidates for integration into tandem PVs, coupled with lower-bandgap bottom cells, including crystalline silicon (c-Si) and copper indium gallium selenide (CIGS)-based cells.[36] Such multi-junction devices can offer promising new avenues for PV technology since they may boost the efficiency of already commercialized solar cells beyond their single-junction theoretical limit.

There are several recent reviews in the literature on the topic of ST-PSCs, mainly focusing on the optimization of each functional layer or on the manufacture of such devices from the perspective of one specific application.[32–38] Unlike those works, the present review aims to summarize the state-of-the-art progress in the fabrication of ST-PSCs, offering a critical vision and highlighting the key requirements that must be fulfilled depending on the possible future application, either in the context of BIPVs or tandem solar cells. Before presenting the most updated design strategies of ST-PSCs, the reader will be provided with the necessary background information about perovskites and PSCs in Section 2. Then, Section 3 is dedicated to describing the way in which ST-PSC architectures are derived from conventional opaque ones. In particular, the discussion will be divided into two main parts, the first dealing with the manufacture of ST-PSCs for BIPV systems, and the second concerning the design of ST-PSCs for different types of tandem cells; the differences and similarities between the two approaches will be highlighted, and the need for a more rational design of ST-PSCs based on "fitness-for-purpose" criteria will be emphasized. Finally, Section 4 provides some perspectives for the future development of ST-PSCs

by scanning the main challenges and issues about device design, operation, and stability that need to be addressed before any large-scale implementation. We hope that the guidelines reported later will help identify the most appropriate ST-PSC design and fabrication method in the prospect of BIPV or tandem applications.

2. Perovskite-Based PV Technology

2.1. Perovskite Materials

Generally speaking, the term "perovskite" is used to describe any material with the same crystal structure as calcium titanate ($CaTiO_3$) and general formula ABX_3, where X is an anion, and A and B are cations of different sizes. The chemical composition as well as the geometrical distortion from the ideal perovskite structure, which consists of a 3D cubic lattice as illustrated in **Figure 2**a, play a crucial role in tuning the physical properties such as the bandgap.[40–42] Historically, inorganic oxide-based perovskites ($CaTiO_3$, $BaTiO_3$, etc.) have been most actively studied for various applications due to their superior ferroelectric and superconducting properties; however, their wide bandgaps limit their use in solar applications. Instead, the perovskites of interest for photovoltaic purposes are halide-based perovskites (ABX_3, with $X = I^-$, Cl^-, Br^-), which are generally solution-processable semiconductors.[20,43] Typical inorganic A site cations that can form 3D halide perovskites include Li^+, Na^+, Rb^+, and Cs^+, while the B site can be occupied by any divalent metal cation, with the most relevant for optoelectronic purposes being Pb^{2+}, Sn^{2+}, and Ge^{2+}. The replacement of the inorganic A site
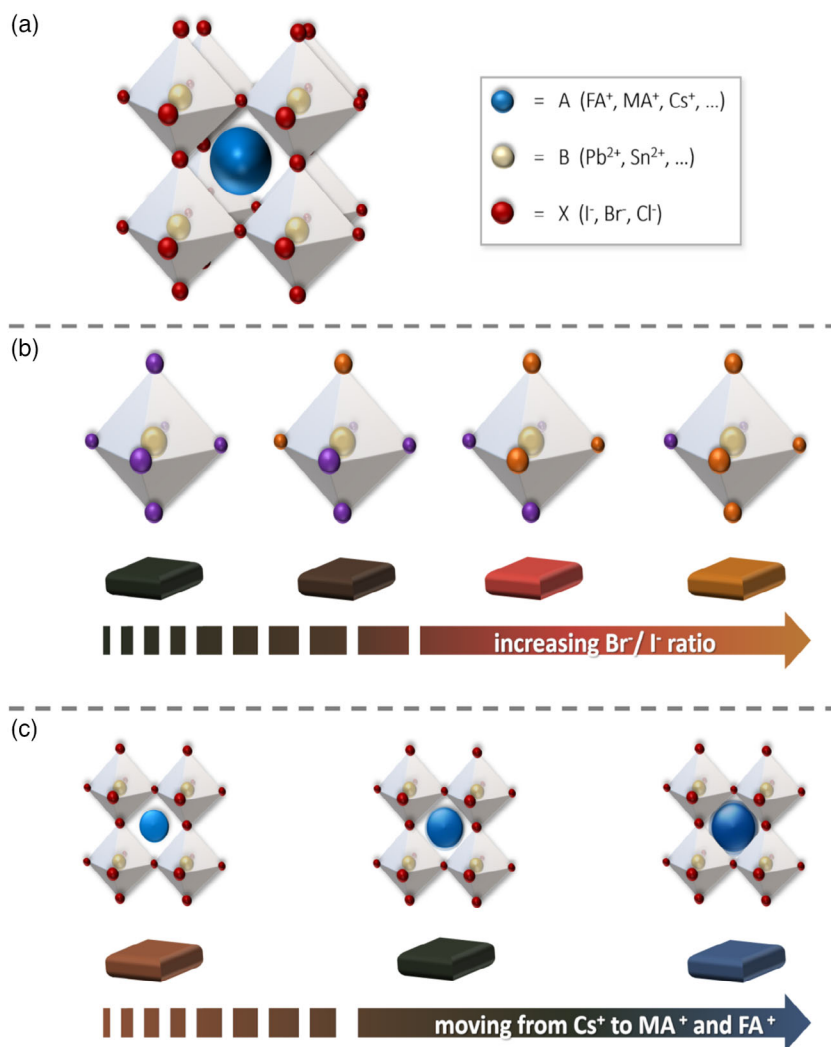
Figure 2. a) Ideal cubic structure of perovskite (ABX$_3$); simplified schematics showing the possible color tuning of hybrid halide perovskite films by b) increasing the Br$^-$/I$^-$ ratio or c) varying the nature of the A cation.

cation with an organic cation of properly small size leads to the formation of hybrid organic–inorganic halide perovskites, a class that has attracted huge attention since the 1970s due to their improved optical and electrical properties. The most commonly investigated hybrid halide perovskites to date have been based on methylammonium (CH$_3$NH$_3^+$, also referred to as MA$^+$) or formamidinium (NH$_2$CHNH$_2^+$, FA$^+$) as the organic cation.[20,42]

Since the first application of MAPbI$_3$ in solar PV devices in 2009,[44] several compositional modifications have been proposed, resulting in color variation and PCE modulation. Indeed, one of the key attributes of perovskite materials is that they possess excellent tunability of the bandgap, achievable through rational compositional engineering. This is a very attractive feature for solar cell applications, since it allows for devices with a specific color, or for ST solar cells with proper absorption characteristics that can be used as top cells in tandem PV devices, as will be discussed in Section 3.3. Bromide has been most effectively used to tune the bandgap of hybrid perovskites. Noh et al.[45] were first to investigate the effects of mixed

iodide-bromide MAPbI$_{3-x}$Br$_x$ compositions, realizing a tunable bandgap between 1.5 and 2.2 eV and a wide variety of film colors, as shown in Figure 2b. In 2014, Pellet et al.[46] demonstrated an improved PCE using mixed cation lead tri-iodide perovskites by gradually substituting MA with FA cations. The enhanced performance compared to pure MAPbI$_3$ was due to greater absorption in the red region of the spectrum (narrower bandgap), resulting in a higher photocurrent. Even though the nature of the organic cation does not directly affect the electronic band structure of perovskites, a variation of the bandgap can occur as a result of the change in crystal lattice geometry (see Figure 2c). Numerous other reports of (MA)$_x$(FA)$_{1-x}$PbI$_3$-based devices with respectful PCEs have been documented during the last years.[47–50] At present, there is an increasing interest in more complex, cesium-containing, triple-cation (Cs/MA/FA) perovskite compositions, which have recently shown impressive PCEs exceeding 20% and very stable performances against the long-term exposure to ambient atmosphere.[51–55] The incorporation of Cs apparently reduces the trap density and charge recombination rates in the

perovskite film, making it more thermally stable and less sensitive to processing conditions. Such robustness is important for providing PSCs with performance reproducibility and long-term lifespan in the prospect of a future commercialization. Furthermore, in the context of tandem PVs, triple-cation perovskites have demonstrated themselves as suitable tandem partners for silicon solar cells, exhibiting remarkable stability and proper absorption characteristics (see Section 3.3). As well as by varying the A and X site ions, another effective way to change the bandgap of perovskite is by replacing Pb^{2+} with alternative homovalent metal species (Sn^{2+}, Ge^{2+}) at the B site. A partial substitution of lead by tin was reported by Zuo et al.,[56] who demonstrated bandgap tuning through varying Pb:Sn ratios and PCEs higher than 10%. In general, tin-based perovskites show promising PV properties like narrower bandgap (1.2–1.4 eV) and higher carrier mobility, but they also suffer from rapid degradation due to the inherent instability of the Sn^{2+} oxidation state; this effect is even more prominent for the case of Ge^{2+}. Parallelly, the performances exhibited by fully lead-free perovskite-based devices are still very low,[57] and a complete replacement of toxic Pb^{2+} by more environmental-friendly metal cations without compromising on efficiency and stability remains an open challenge, as will be discussed in Section 4.1.

2.2. Device Architecture

After having recognized the relevance of halide perovskites as potentially high-efficiency PV materials, researchers focused their efforts on optimizing the PSC structure. PSCs were initially fabricated in the traditional DSSC architecture. In 2009, Kojima et al.[44] replaced the conventional dyes with $MAPbI_3$ and $MAPbBr_3$ perovskites, demonstrating PCEs of 3.8% and 3.1%, respectively. In 2012, the severe instability of such prototype PSCs was solved by replacing the liquid electrolyte with the solid 2, 2′, 7, 7′-tetrakis (N, N-p-dimethoxy-phenylamino)-9, 9′-spirobifluorene (spiro-OMeTAD) hole-transporting material (HTM).[58] Park and collaborators proposed a solid-state mesoscopic PSC architecture based on $MAPbI_3$ nanocrystals, spiro-OMeTAD, and 0.6 μm thick mesoporous TiO_2 film, achieving a maximum PCE of 9.7%. Since then, the further progress in the design of PSCs was propelled by the advances in film deposition techniques and the development of alternative device layouts.

Today, PSCs are most commonly designed as a solid-state n-i-p (or p-i-n) heterojunction architecture, either planar or mesoscopic, where the intrinsic (i-type) perovskite semiconductor serves as the light absorber for photogeneration of charge carriers, while n- and p-type materials are introduced in the device to provide the built-in potential and assist directional charge extraction (see **Figure 3**a, b). A typical PSC comprises a front transparent conducting electrode (TCE), which allows for the passage of light to the heart of the cell, a perovskite photoactive layer sandwiched between a hole-transporting layer (HTL) and an electron-transporting layer (ETL), and a metal reflective back contact. In the case of the n-i-p architecture (also called the "regular" architecture due to its popularity), the electron-transporting material (ETM) is deposited prior to the perovskite layer and is often made of TiO_2, an n-type material which forms a n-i

junction selective to the passage of electrons; the HTL is instead a p-type material located on top of perovskite, such as spiro-OMeTAD, poly(triaryl amine) (PTAA), or the inorganic copper thiocyanate (CuSCN), forming a i-p junction selective to the holes transport. In contrast, the p-i-n structure has an opposite sequence of HTM and ETM than the regular configuration, and it is often referred to as the "inverted" structure. Typically used charge-transport materials in planar p-i-n devices are poly(3,4-ethylenedioxythiophene) polystyrene sulfonate (PEDOT:PSS) or NiO_x as the HTM, and fullerene derivatives (e.g., phenyl-C_{61}/C_{71}-butyric acid methyl ester, $PC_{61}BM$/$PC_{71}BM$) as the ETM. Differently from planar devices, mesoscopic PSCs feature an additional mesoporous HTL or ETL, which can help facilitate the charge transfer at the interface with perovskite, giving rise to a significant improvement in PSC performance. The state-of-the-art PSCs with the record PCEs are predominantly fabricated in the regular mesoscopic configuration.[21–24] Although the traditional mesoscopic PSCs generally show higher PCEs compared with planar architectures, the latter typically offer low-temperature processing and reduced optical losses, which are great advantages for applications in the contexts of flexible and transparent PVs.

For all the aforementioned PSC structures, a proper energy level alignment is vital for obtaining a good PV performance. The photogenerated electron–hole pairs in the perovskite layer would experience charge separation at the interfaces between the perovskite and the ETL or HTL; therefore, suitable energy band offsets are to be provided at these junctions to enable efficient charge extraction and to minimize carrier recombination, ultimately resulting in an overall increase in the key cell parameters values (PCE; open-circuit voltage, V_{oc}; short-circuit current density, J_{sc}; fill factor, FF). This means that the HTL and the ETL should be selected with energy levels well matched to the perovskite material. Moreover, they should ensure efficient and selective charge transport by presenting high electron or hole mobility, as well as adequate bandgap to block the opposite charge carriers. The work functions (WFs) of the bottom and top electrodes should also match the energy levels of the charge-transport layers to facilitate charge collection. Figure 3c shows the band energy levels for the most commonly used materials and interfaces in PSCs.[59] Rational engineering of the PSC interfaces has recently become an important strategy for improving the charge extraction and reducing the gap between theoretical and practical PCEs.[60] A careful selection of materials and their interfaces is also critical for the performance of ST-PSC devices, as will be thoroughly discussed in Section 3.

2.3. Fabrication Techniques

As previously described, the PSC architectures incorporate different functional layers, including perovskite, charge-transport layers, interfacial buffer layers, and bottom and top electrodes. One of the key advantages of such PSC components over conventional inorganic PV materials is solution processability, which allows for the use of low-cost thin-film deposition techniques such as spin-coating, doctor blading, ink-jet printing, and spray-coating. Most of these technologies are compatible with roll-to-roll processing for industrial large-scale production.
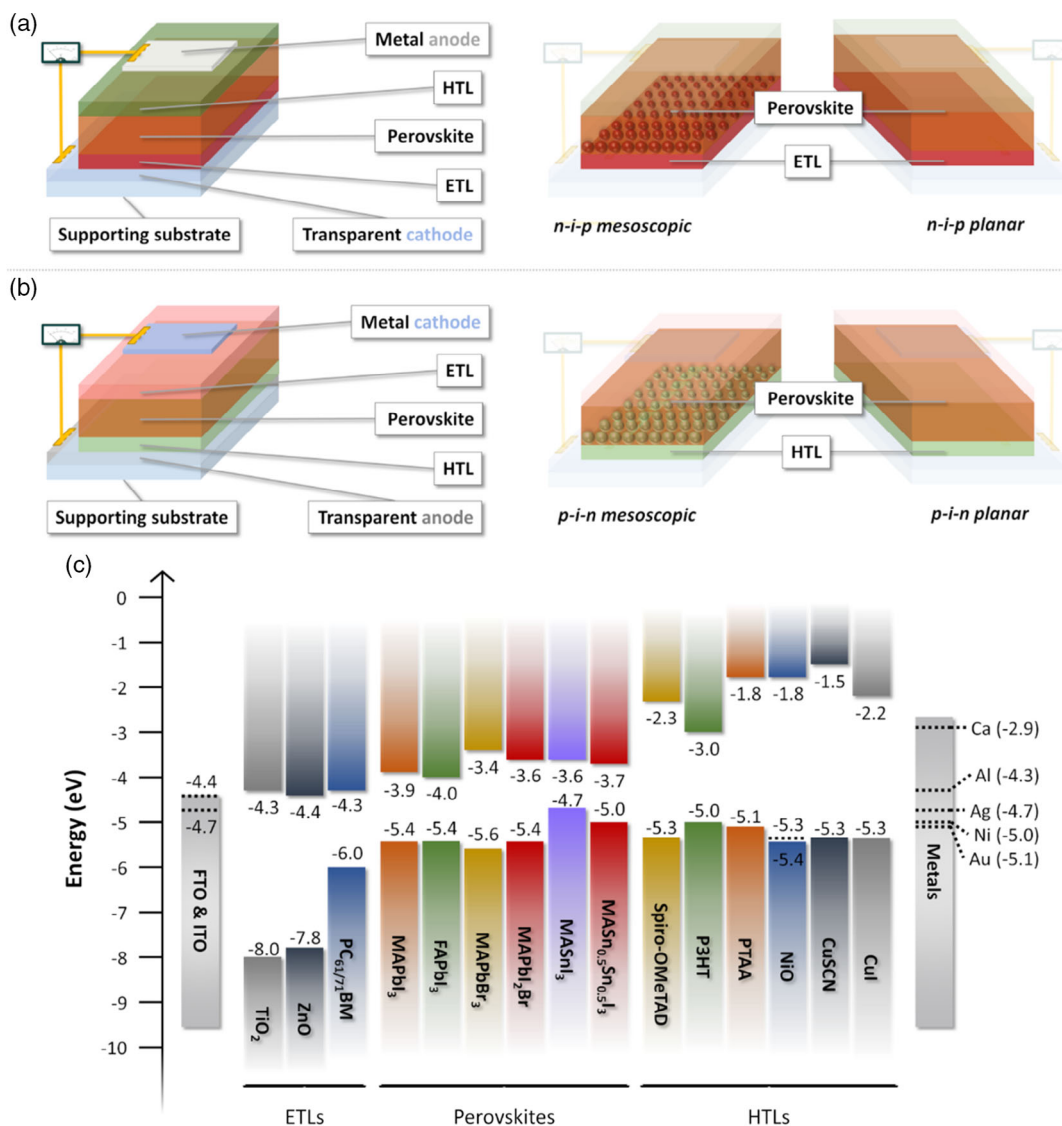
Figure 3. Schematic of the major PSC architectures: a) Regular n-i-p mesoscopic and planar; b) inverted p-i-n mesoscopic and planar. c) Schematic energy level diagram of the most commonly employed materials in PSC technology.[59]

Nevertheless, fabricating high-quality thin films from solution is not trivial, especially in the case of perovskite materials, and a careful control of each deposition step is necessary for obtaining high-performance PSC devices.

The fabrication of laboratory-scale PSCs typically starts from a glass (or plastic) substrate coated with a transparent conductive oxide (TCO) layer, such as indium tin oxide (ITO) or fluorine-doped tin oxide (FTO), which serves as the bottom electrode. TCO-coated substrates are generally prepared by magnetron sputtering and are commercially available. Nevertheless, some researchers have tried to deposit the bottom contact themselves by using alternative substrates/techniques or replacing the traditional TCO layer with other transparent conducting materials. As far as the substrate is concerned, glass has been a universal material of choice as transparent rigid support due to its low production cost, the consolidated fabrication strategies, and optical transparency. This makes the state-of the-art PSCs potentially compatible with all those urban and daily life scenarios that include sunlight-exposed glass surfaces. Nevertheless, PSCs could benefit of other materials which do not possess the high thermal conductivity and brittleness that glass shows. In this regard, it found quite a resonance in the scientific community the very fresh report by Li and co-workers,[61] who developed a new fabrication strategy based on the employ of transparent wood, demonstrating an encouraging PCE of 16.8%. The exceptional versatility of the PSC technology has also opened the possibility of constructing cells on top of various flexible substrates, including metal foils, ultrathin flexible glass, nanopaper, and plastic substrates, thus extending the possibility of practical integration. Many examples of flexible PSCs fabricated on polymer supports such as polyethylene terephthalate (PET),[62–64] polyethylene naphthalate (PEN),[65,66] and polyimide (PI)[67] are reported in the literature. However, still most PCE values of flexible cells lag behind those of their rigid counterparts, with the major issues

arising from the relatively low conductivity and poor mechanical properties of conventional TCO electrodes on flexible substrates. This is one of the reasons why TCO-free PSCs have recently become a popular research field, focusing on the development of alternative transparent electrodes, as will be discussed in Section 3.1.

Once the substrate and the bottom electrode have been selected/prepared, the subsequent steps of PSC fabrication involve the sequential deposition of the electron-transport, the perovskite, and the hole-transport layer. In particular, it is critically important to deposit a uniform, dense, highly crystalline, and pinhole-free perovskite film with high surface coverage and proper thickness to achieve high PCE and reproducibility.[68] Indeed, the presence of pinholes or other inhomogeneities in the perovskite layer will result in direct contact between the p- and n-type materials, leading to shunting paths and severe charge recombination. Various deposition approaches have been developed to build up high-quality perovskite films starting from the corresponding precursors (e.g., MAX and PbX_2 to form $MAPbX_3$), primarily: one- or two-step solution processing,[69,70] thermal vapor deposition,[71] and hybrid vapor-assisted solution process (see **Figure 4**).[72] The solution processing routes are the most attractive for the aforementioned reasons, but they often result in poorer film quality, especially when using the one-step method. To improve the performance of solution-processed perovskite films, several strategies have been proposed, including: 1) incorporation of more than one organic or inorganic precursors, 2) antisolvent dripping method, 3) use of binary solvent systems, 4) solvent annealing, and 5) use of additives.[68] The additive engineering strategy was recently exploited by our research group to boost the efficiency and stability of one-step solution-processed PSCs.[73] For a time, PSCs fabricated using the two-step solution process exhibited higher performances than those made using the one-step, but the situation drastically changed upon the introduction of the antisolvent dripping method. The latter is a modification of the one-step approach, consisting in the deposition of all perovskite precursors in a single step, during which a proper antisolvent is spin-coated to trigger the crystallization of the perovskite film; this solution-based technique is currently the most used and effective perovskite deposition approach, resulting in record high PCEs exceeding 24% (see Figure 4e).[22–25]

Concerning the charge-transport layers, several semiconductor materials have been successfully implemented as ETLs or HTLs in PSCs, including polymers, organic small molecules, and inorganic compounds, some of which have already been mentioned previously (see Figure 3e). These materials are typically processable from solution and therefore can be deposited by spin-coating or other simple solution-based techniques. As in the case of the perovskite film, several strategies have been proposed to enhance the film quality and performance, including doping strategies, nano-design, and additive engineering.[74] It is important to mention that conventional methods for fabrication of metal oxide mesoporous ETLs/HTLs (e.g., mp-TiO_2) typically involve the deposition of a metal alkoxide precursor solution (e.g., titanium (IV) isopropoxide) by spin-coating or spray-pyrolysis followed by a high-temperature (>400 °C) sintering step, which increases the costs and generally hampers the fabrication of flexible devices. Very recently, alternative low-temperature processing routes have been proposed, leading to encouraging PCEs higher than 20%.[65]

Finally, the last PSC fabrication step consists in the deposition of the metal counter electrode, which is typically carried out by thermal evaporation. Recently, alternative vacuum-free deposition methods have been developed, and fully solution-processed PSCs with printed back electrodes have been successfully fabricated, as reported in Figure 4f.[75] The possibility to separately fabricate the electrode by printing techniques, and then mechanically transfer it over the photoactive layer by lamination, is a remarkable advantage in terms of manufacturing costs and design flexibility, enabling the incorporation of printable conducting materials of various kinds and transparency levels as top contacts, as will be extensively discussed in the following section. The distinctive features of such devices, including low-cost processing, lightness, and compatibility with different substrates, further confirm the remarkable versatility and potential of this technology.

3. Semitransparent Design of PSCs

3.1. Strategic Tools and Requirements

Generally speaking, ST solar cells are a technology that combines the ability of light-to-electricity conversion with the benefits of light transparency in a specific wavelength range of the solar spectrum. The emerging interest devoted by the scientific community to ST-PSCs came up in a specific moment (2014) for a series of precise reasons. First, it was necessary for opaque PSCs to become an established technology, especially in terms of PCE values comparable with the more investigated and commercialized PVs. Second, that is a consequence of the previous issue, it is not worth investigating ST solar cells unless high efficiency is not achieved by opaque devices, considering that the inherent trade-off between absorbed light and transmitted light in ST devices typically results in lower PCEs compared to their opaque counterparts; this aspect makes the fabrication of high-efficiency ST-PSCs, in some respect, even more challenging. All those key issues were first and successfully faced in the milestone work by Eperon et al.,[76] whose results created excitement around perovskite-based ST devices, demonstrating performances competitive with other emerging classes of ST-PVs. Since then, different ST-PSC design strategies have been developed, targeting at the desired semitransparency while maintaining increased PCE values.[32–38]

The manufacture of a ST-PSC can be accomplished through different approaches depending on the target application, but there are some mainstream design keywords that remain constant. First, starting from a conventional opaque architecture, it is mandatory to replace the traditional, highly reflective metal top electrode with a proper transparent conductive alternative. In other words, both the front and back contact of a ST-PSC should be transparent to allow for the passage of a fraction of incident light through the entire device. This concept is schematized in **Figure 5**. Ideally, materials employed as transparent contacts should minimize absorption and reflection in the complete 350–1200 nm spectral range. However, the consequent lack of reflecting light from the top electrode into the perovskite film
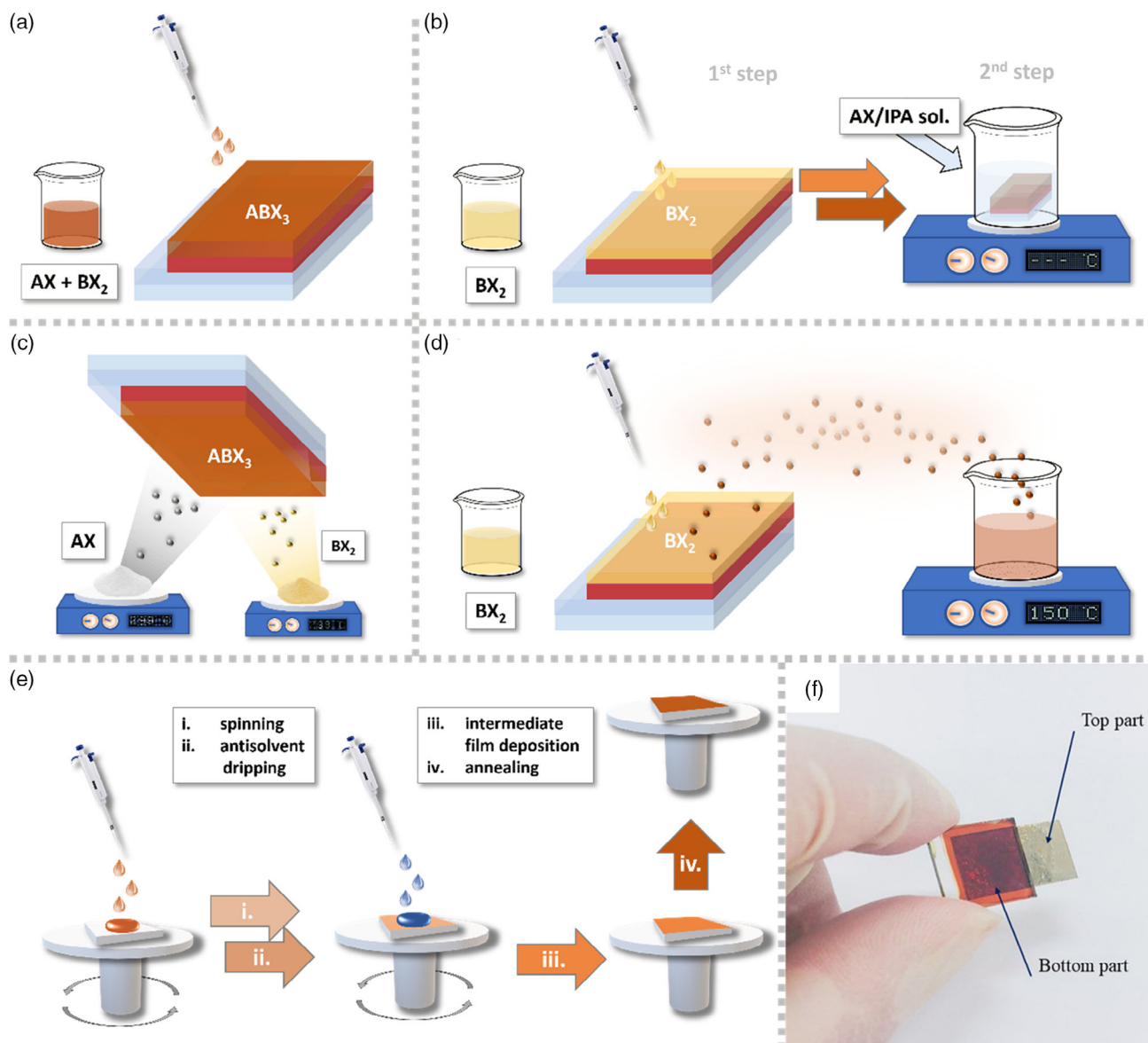
Figure 4. General deposition methods of perovskite film: a) One-step solution deposition; b) two-step solution deposition; c) vacuum deposition; d) vapor-assisted solution process (VASP); and e) antisolvent dripping method. f) Fully solution-processed PSCs with laminated nanoparticle silver inks electrodes. Reproduced with permission.[75] Copyright 2020, Elsevier.
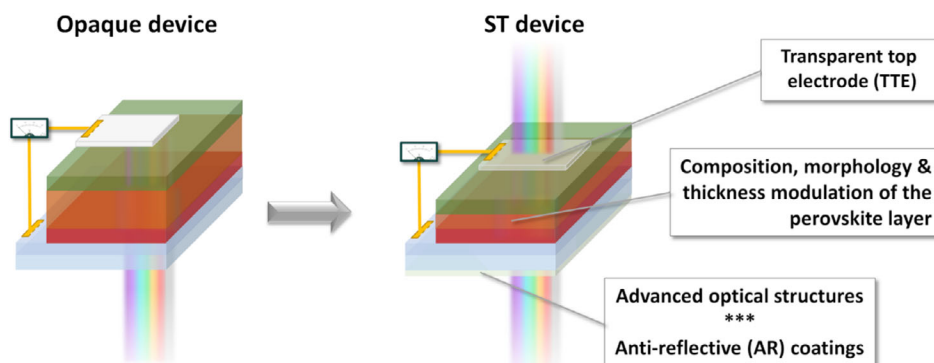

Figure 5. Schematic device design of a ST-PSC starting from a conventional opaque device.

will inevitably lead to an efficiency loss compared to the opaque device, in which, instead, the unabsorbed photons can alternatively be harvested by perovskite upon back reflection. Nevertheless, interestingly, it was shown that ST-PSCs may exhibit higher PCEs than conventional PSCs if implemented in a bifacial configuration, thanks to their intrinsic capability of receiving light from both the front and back side. Since bifacial PSCs will not be the main topic of the present review, we suggest to the readers that they consult the references to deepen their knowledge.[77,78]

Alongside transparent electrodes, the ST-PSC design typically involves the use of thinner or opportunely engineered perovskite films, so that they can only absorb a part of the incident photons. A careful optimization of the perovskite thickness, morphology, and composition is particularly important in the context of BIPVs, where a specific color or an appropriate visible transparency has to be provided, as will be detailed in Section 3.2. Last issue, the structure and composition of the charge-transport and interfacial layers, as well as the entire device structure, must be carefully selected to obtain the best trade-off between efficiency and transparency. To this end, additional antireflective (AR) coatings (e.g., LiF, MgF$_2$), optical outcoupling layers, or other advanced optical structures can also be inserted in the front and/or back side of the device to further enhance the transparency or the efficiency based on modern light manipulation strategies.[79,80] The performance of the final ST-PSC will be determined by the balance between PCE and optical properties such as AVT, average NIR transmittance, and color tinting/rendering metrics, and it should be optimized for the specific application, based on "fitness-for-purpose" criteria as highlighted in **Figure 6**. At the same time, chemical stability and simple/scalable processing of all the constituent materials and interfaces, along with high reproducibility and long-term durability of the device performance, should be guaranteed to enable the development of potentially marketable and reliable ST-PSCs.

It is intuitive to imagine that, before targeting at any specific feature, achieving electrodes transparency is the first and most relevant issue in ST-PSC design. The ideal transparent top electrode (TTE) should exhibit excellent electrical conductivity and maximized transparency simultaneously, along with low cost, robust chemical stability, and proper work function (WF) for efficient charge extraction.[81] Moreover, the TTE should be processable without damaging the underlying temperature- and solvent-sensitive layers in the device. Currently, transparent conductive oxides (TCOs) dominate the use of transparent electrodes in the optoelectronic industry, providing the best trade-off between conductivity and transparency. In the context of PSCs, FTO, and ITO have become a standard choice as bottom electrodes in ST-PSCs for most of the researchers, as already discussed in Section 2.3. However, whereas the bottom electrode has much less solvent/temperature restrictions, TCOs can hardly by employed as TTEs since they generally require high-energy deposition techniques (e.g., magnetron sputtering), which may damage the underlying perovskite and charge-transport layers from the high kinetic energy of the as-deposited particles. Recently, effective integration of various sputtered TCO-based TTEs, including ITO,[82–84] aluminum-doped zinc oxide (AZO),[85] indium-doped zinc oxide (IZO),[86] indium zinc tin oxide (IZTO),[87] zirconium-doped indium oxide (IZrO),[88] and multiple-element-doped tin oxide (MDO),[89] has been demonstrated by careful control of the sputtering parameters to minimize the damage or by incorporating suitable sputter buffer layers (e.g., ultrathin metal films or metal oxide nanoparticles) to protect the underlying materials. As an example, thermally evaporated molybdenum oxide (MoO$_x$) has been extensively adopted and used as anode buffer layer in n-i-p devices (deposited on top of the HTL prior to TCO sputtering), owing to its low processing temperature and desirable energy level alignment for hole extraction.[82] Despite these remarkable achievements, the increasing prices and very poor mechanical properties of TCOs remain undesirable for modern PV applications. For this reason, there has been a growing research interest in alternative materials to serve as transparent electrodes, such as ultrathin metal (UTM) films,[90–94] multilayered dielectric/metal/dielectric (DMD) structures,[95–100] metal nanowires,[101–103] conductive polymers,[104,105] graphene,[106–109] and carbon nanotubes (CNTs).[110,111] The pros and cons related to their use as TTEs compared to TCOs, as well as their performances in terms of
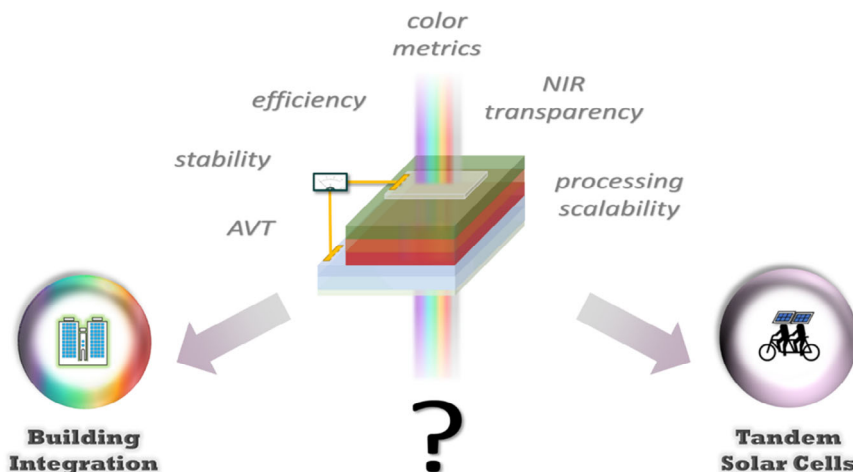

Figure 6. "Fitness-for-purpose" criteria for ST-PSC design: Efficiency, AVT, NIR transparency, color metrics, stability, and processing scalability should be precisely evaluated and carefully balanced to fit with the specific target application (BIPVs or tandem SCs).

sheet resistance (R_s) and average transmittance (T_{avg}) based on recent reports, are listed in **Table 1**.

By reducing the thickness down to tenths of nanometer or even below, metal top electrodes become sufficiently transparent to become suitable for ST applications.[90] Many examples of ultrathin Ag or Au films have been successfully implemented as TTEs in ST-PSCs, often by means of seed layer strategies helping in enhancing the wetting ability of the metal particles and obtaining a smooth, percolative metal layer with minimized thickness and acceptable transparency.[91–94] The optical transmittance of UTM film-based electrodes could be further enhanced without losing the electrical properties if the metal

(M) thin film is embedded between two dielectric (D) materials with high refractive indices to give multilayered DMD structures. Such composite electrodes generally exhibit ideal characteristics to serve as TTEs, such as: excellent electrical conductivity provided by the metal middle layer; improved overall transparency due to interference and antireflective effects occurring at the interfaces; low-temperature and solvent-free processability; and mechanical stability.[95] The multilayered architecture composed of MoO_x as the dielectric and Au or Ag as the metal is one of the most employed DMD electrode in regular ST-PSCs, showing performances competitive with those of conventional TCOs (see Table 1).[96–99] $SnO_x/Ag/SnO_x$ top electrodes have also been

Table 1. A comparison between different types of transparent conductive electrodes for use as TTEs in ST-PSCs. Typical ranges of sheet resistance (R_s) values and average transmittance (T_{avg}) values in the visible (380–780 nm) and NIR (800–1200 nm) spectral ranges are provided in square brackets for each type of TTE, together with the values corresponding to representative examples taken from the literature.

TTE composition	R_s [Ω sq^{-1}]	T_{avg} (vis.) [%]	T_{avg} (NIR) [%]	PROS	CONS
[ITO-based]	[10–100]	[80–90]	[>75]	Excellent trade-off between conductivity and transparency	High-energy sputtering; expensive; brittle; slightly yellow; unstable to acid
MoO_x/ITO[82]	40	>80	>80		
ITO[83]	9; 14; 27	–	76; 84; 81		
ITO/MgF_2[84]	44	≈83	–		
[Other TCOs]	[10–100]	[80–90]	[>80]	Low damage sputtering; improved mechanical properties; superior NIR transparency	Parasitic absorption and low carrier mobility; post-annealing treatments
AZO[85]	28.1	>85	>85		
IZO[86]	15.9	>80	81.96		
IZTO[87]	11.8; 17.3	81.3; 83.3	>85		
IZrO[88]	18	~85	>80		
MDO[89]	–	>80	81.6; 91.6		
[UTM films]	[1–50]	[50–70]	[50–70]	Low-temperature solvent-free deposition; high conductivity, flexibility	Often based on precious metals (Ag, Au); parasitic absorptions; corrosion/ diffusion issues
Au/LiF[91]	–	56	–		
Cu-seeded Ag[92]	23	≈70	58.6		
Cu-seeded Au[93]	23	–	≈60		
Cr-seeded Au[94]	16.3	≈70	66.6		
[DMD structures]	[1–50]	[70–85]	[>70]	Tunable opto-electrical properties; high transparency; flexibility	Often based on precious metals (Ag, Au); parasitic absorptions; corrosion/ diffusion issues
$MoO_x/Au/MoO_x$[96]	13	≈80	–		
$MoO_x/Au/MoO_x$[97]	15	–	73		
$MoO_x/Au/MoO_x$[98]	19.6	–	74		
$MoO_x/Au/Ag/MoO_x$[99]	≈16	>70	–		
$SnO_x/Ag/SnO_x$[100]	10	81	–		
[Metal NWs]	[1–200]	[70–95]	[>80]	Easy solution processing; flexibility; transparency; colorless	Challenging fabrication; high roughness; poor adhesion; haze; corrosion/ diffusion issues
AgNWs[101]	12.4	≈90	>85		
AgNWs[102]	18; 78	85.4; 93.4	~80; ~90		
AgNWs[103]	16; 120	≈80, >90	≈80, >90		
[Conductive polymers]	[15–1000]	[75–90]	[>70]	Low cost; solution processing; flexibility	Degradation under humidity, high T and UV; color tinge
PEDOT:PSS[104]	77; 15	78; 76	–		
PEDOT:PSS[105]	≈121	≈90	–		
[Carbon-based mater.]	[50–2000]	[50–97]	[60–90]	Low cost; flexibility; environmental stability; colorless	High resistance; high roughness (CNTs); sensitive to defects and impurities (graphene)
Graphene[106]	140	≈90	–		
Graphene[107]	552	97	–		
Graphene[108]	96	90	–		
CNTs[110]	≈2000	≈60	–		
CNTs[111]	–	50–85	60–90		

incorporated in inverted ST-PSCs, demonstrating additional self-encapsulation abilities.[100] Another remarkable advantage of such DMD structures consists in the possibility of tuning their transmittance/reflectance properties by simply varying the thickness of the constituent layers. In particular, several recent studies have reported on the optimization of the bottom and top D layers thicknesses toward the best transparency in the wavelength range of interest. The fact that one specific thickness value may correspond to the highest AVT suitable for BIPV purposes, while another value may lead to the maximum transparency in the NIR region in view of tandem integration, further confirms the importance of a rigorous application-oriented ST-PSC design.

Solution-processed metal nanowires or meshes are also promising alternatives to the commonly incorporated sputtered TCO electrodes. Among several materials, silver nanowires (AgNWs) have the potential to be among the best choice for researchers due to the elevate transmittance ($\approx$90% at 550 nm) and resistance value (10–20 Ω sq^{-1}), which make them comparable with commercial ITO electrodes.[101] The biggest limitation is the high reactivity of Ag with halogens, whose combination causes disruption of the optimal perovskite crystal structure. The pivotal work by Guo and co-workers circumvented this issue by simply introducing a thin layer of zinc oxide nanoparticles beneath the top AgNW electrodes.[112] On the one hand, the metal oxide layer provided a physical barrier to Ag diffusion to the perovskite layer; on the other hand, it guaranteed excellent ohmic contact between the AgNWs electrode and the underneath layers. According to the high costs and instability issues of precious metals as TTEs, one of the very first examples of indium-, gold-, and silver-free transparent electrode was proposed by Bryant and co-workers, who obtained encouraging results combining a corrosion proof Ni mesh grid (embedded in a PET film) with a transparent conductive adhesive; this cheap strategy offers the possibility to separately fabricate the electrode, and then deposit it over the photoactive layer by lamination.[113] A more recent example of mechanically transferable TTE for ST-PSCs was reported by Lee et al., who demonstrated high-performance flexible devices (PCE > 13% at 1 cm^2 active area) by reproducible dry stamping transfer of a polymeric PEDOT:PSS (PH1000)-based flexible TTE.[105]

In addition to TCO- and metal-based TTEs, carbon nanomaterials such as CNTs and graphene have also been deeply studied and tested in ST-PSCs as grounding materials for transparent conductive electrodes.[114–116] They possess appealing features such as electrical conductivity, hydrophobicity, both of them contributing to the stability and the performance of the final devices, and a relatively low production cost, which is a further plus looking at the final price of the PVs on the market; furthermore, chemical and mechanical robustness are appealing extra features. One of the very first attempts to produce carbon-based electrodes was reported in 2014 by Li et al., who investigated the fabrication of a hole collector by laminating films of CNTs onto the perovskite layer.[110] The study demonstrated the achievement of efficient electrodes bypassing expensive metal deposition by vacuum techniques. Very recently, a CNT electrode was implemented for the first time to 4-terminal perovskite/silicon tandem cells, proving to be an ideal candidate as TTE for tandem purposes due to its higher transmittance than the

ITO electrodes in the infrared region.[111] Taking advantage of its atomic-scale flatness, You and others reported the employ of graphene as TTE; the stacked multilayered graphene was prepared by chemical vapor deposition (CVD) followed by a lamination procedure[106]; a thin layer of PEDOT:PSS was coated onto the electrode both to improve the electrical conductivity and contribute to the formation of an efficient interface with the perovskite film. More specific examples of application of different transparent electrodes as TTEs in ST-PSCs will be provided in the next two sections, where a clear boundary between BIPV and tandem applications will be drawn.

3.2. ST-PSCs for Building-Integrated PVs

Nowadays, the electricity consumption of buildings is tremendous, accounting for nearly one third of the total global energy demand.[10] A low-cost and sustainable solution to this issue is to implement BIPV systems on the building themselves, with the ultimate goal of turning any urban infrastructure into a green and self-powered asset. In the early days, it was necessarily silicon solar cell technology to dominate the field, since it was the sole PV technology to guarantee reliability, stability, and performance. The possibility to introduce modern aesthetic criteria for building design quickly began to attract architects, investors, and public institutions, aiming at boosting the energy transition and shaping the landscapes of the near-future urban projects.[117] Currently, the BIPV market is very florid and dynamic; considering the recent trends in Europe, data evidence the consistent growth of solar power installed into buildings within the last 6 years, with an increase of one order of magnitude up to 5 GW,[118] providing a breeding ground for innovation and new technologies. In this context, modern architectures are often producing buildings and skyscrapers based on a harmonic combination of steel and glass, where wide portions of the façades result in immense windows, providing elevate brightness in the inner space and limiting electricity consumption for indoor lighting; however, buildings with elements such as windows and transparent walls/rooftops are generally excluded from this advantageous PV integration to comply with the intrinsic opacity and rigidity of silicon-based devices.[119,120] In fact, due the lack of transparency and design flexibility, silicon solar panels are typically mounted at the limited rooftop of the building in the form of building-added/applied PV (BAPV) systems, which are added on rather than integrated in the building envelope, thus requiring extra space and relatively high additional costs for implementation. For a more sustainable and effective PV integration into buildings, alternative PV technologies are needed that can be architecturally integrated into all the available surfaces of the building structure, including rooftops, windows, façades, balconies, shading systems, parapets, and skylights, thus serving as a functional covering material in addition to producing sustainable electric power. Indeed, the key concept behind the definition of BIPV is that PV modules can also offer more architectural functions and aesthetic possibilities rather than only energy production. To this end, appropriate transparency in the visible spectral range, along with the possibility of color tunability and the simplicity/scalability of the fabrication processes, are highly desirable features in an alternative PV technology candidate. In

particular, transparency has become a crucial issue to encourage further investment in PVs, and third-generation solar cells (including PSCs) are currently under the lens as a possible game changer. By enabling superior performances and transparency simultaneously, and eventually tunable color, ST-PSCs represent the most promising technology among emerging PVs in view of this application. In support of this, it is worth mentioning the recent work of Cannavale and co-workers,[121] who evaluated the benefits related to the installation of perovskite-based ST-BIPVs in an office building, considering different climate conditions and photovoltaic surface areas; the analysis concluded that, with the available technology in 2016, the amount of produced electricity could overcome the artificial lightning expenses in most cases, providing stronger support to proceed with this revolution of the electrical power market and politics.

On a technical level, the main challenge in PSC design for BIPVs consists in the manufacture of solar panels that must respond to specific aesthetic requirements in terms of size, shape, texture, transparency, and color, while at the same time maintaining competitive PCEs. Explicit criteria for ST-PSC design and performance assessment are presently quite unclear, making it challenging to directly compare the countless ST-PSC devices proposed in the literature. Similar to opaque devices, PCE is a fundamental factor denoting the performance of ST-PSCs; a PCE of 5–10% is generally required as an entry application threshold for façade-integrated PVs and tinted architectural PV glass, whereas 2–5% PCE would be sufficient to self-power smart window technologies (see Section 3.2.3).[31] Since the PCE varies with the transmittance, another important parameter that must be considered when comparing the PCEs of ST-PSCs is the AVT, which is generally defined as the average value of the transmittance in the wavelength range of 380–780 nm visible to the human eye. Because the efficiency and transparency of ST solar cells typically compromise each other, there is plenty of literature reports providing a wide array of AVT-PCE values, as shown in **Figure 7**a. Recent advances exhibit PCEs beyond 10% under 1 sun illumination at over 25% AVT, which is considered as a benchmark for practical solar window applications.[39] In contrast, ST-PSC devices with similar PCEs but lower AVT values are equally attractive for application in different BIPV systems with less stringent transparency requirements (e.g., façade-integrated PVs, decorative construction exteriors). It should be noted that many articles report AVT by measuring the relative transmission spectra with unnecessary reference samples and simply averaging it over an arbitrary wavelength range. However, as well explained by Yang and co-workers,[122] it should be instead indicated as the integration of the absolute transmission spectrum of the entire device, weighted against the photopic response of the human eye as requested by the window industry. The fact that the AVT has no specific evaluation standard further complicates a clear comparative analysis between different developed ST-PSCs. Moreover, as the required transmittance varies across the different application fields, researchers generally propose various approaches to obtain different pairs of AVT-PCE values by using the same device architecture, thus providing various solutions according to need (see Figure 7a). Even though this certainly corresponds to an enrichment in terms of scientific data and possibilities, it is also a sign of inefficient methodology in terms of application-orientated design, dictated by the lack of clear assessment criteria, causing an inevitable dispersion of knowledge.

The aforementioned issues invoke the development of more application-specific figures of merit and a precise definition of key individual thresholds for all the performance/aesthetic metrics according to the purpose. In this direction, Traverse et al. have recently introduced the concept of light utilization efficiency (LUE), corresponding to the product of PCE and AVT values, as a convenient figure of merit for assessing and comparing the performance of ST-PSCs relating to the AVT.[31] However, acceptance in the building industry requires more aesthetic requirements than the simple AVT that should also be considered. Other figures of merit for the accurate evaluation of the aesthetic factors include the transmission haze ratio (H), the color rendering index (CRI), and the CIELAB color
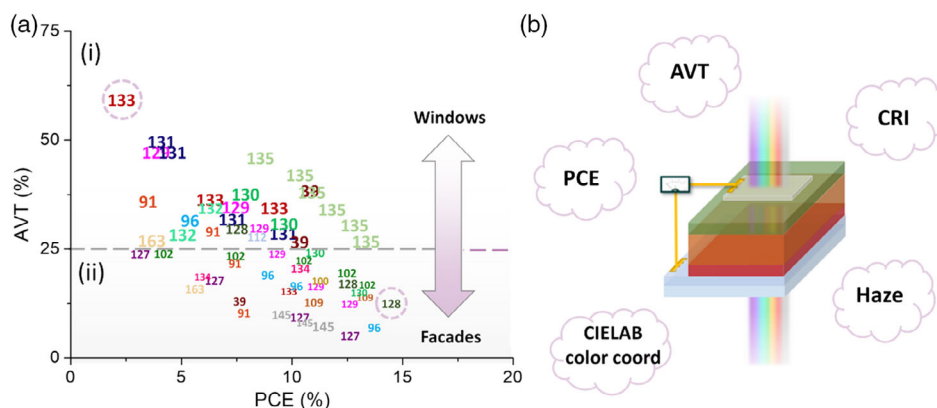

Figure 7. a) PCE-AVT diagram reviewing the most recent literature reports in the field of ST-PSCs for BIPVs. In the panel, data points are labelled with the number corresponding to the reference paper reported in the bibliography list. Note that the 25% AVT threshold is reported, to opportunely reveal the existence of: Zone (i) devices with >25% AVT, possessing minimum acceptable transparency for solar window applications; Zone (ii) ST-PSC devices, whose lower AVT can rather suggest application in different BIPV systems with less stringent transparency requirements, such as façade-integrated PVs. Devices described in refs. 128 and 133 are localized at the opposite edge of a diagonal area collecting most data points, driving the reader's eye to visualize how AVT and PCE move ST-PSCs in opposite directions, with high transparency penalizing photovoltaic performance, and vice versa. b) Key performance/aesthetic metrics of ST-PSCs for BIPV applications (PCE, AVT, CRI, haze, CIELAB color coordinates).

coordinates.[122,123] The H metric is a measure of the degree to which light passing through the ST solar cell is scattered or reflected, causing objects seen through the device to be blurred; it can be estimated as the ratio of the diffuse transmittance (T_d) to the total transmittance (T_t). The other two figures of merit are color standards that indicate the color rendering and the absence or presence of color, respectively; both should be measured under the same standard illumination (AM1.5G) as that used for PV performance assessment. More specifically, the CRI is a quantitative measure of the color rendering capacity calculated by comparing the color of an object located on the back of the device with the original color under reference illumination source; a CRI close to 100 indicates that the color is almost identical to the original one. In contrast, the CIELAB color coordinates consists in three coordinates (L*, a*, b*) that can describe the color sensations registered in the human eye by displaying both chromaticity and brightness values: The L* value indicates lightness from black (0) to white (100), whereas the a* coordinate represents green to red and the b* coordinate shows the blue-yellow opponent colors; when a* and b* are closer to 0, the color is more neutral (see Section 3.2.1). The CIELAB (or CIE 1976) color space was created by the International Commission on Illumination (CIE) in 1976 with the intention of providing a more perceptually uniform color system compared to the other traditional CIE 1931 color spaces, which are still widely used. As highlighted in Figure 7b, all the above figures of metric are equally important in demonstrating the feasibility of the developed ST-PSCs to specific BIPV applications.

Based on these premises, the following lines will be focused on the presentation of various examples taken from the most recent reports in the literature, in the purpose of presenting the actual trends in ST-PSC technology evolution for BIPVs and underlining the necessity to develop certain approaches, and the reason why some other are not anymore further investigated. To rationalize the number of examples, the first two subsections will be dedicated to describing the available strategies for obtaining ST solar cells with specific aesthetic features, namely *neutral-colored ST-PSCs* and *colorful ST-PSCs*. The target applications and go-no-go criteria for practical BIPV integration of such devices will be opportunely discussed. The third subsection will be dealing with ST-PSC design for smart photochromic windows, in which light transmission, haze, and color can be controlled in a "smart" and "active" way.

3.2.1. Strategies for Neutral-Colored ST-PSCs

ST-PSCs are destined to be more and more integrated into buildings, creating a delocalized power-generating network. But, aiming at the best functional and visual integration, ST-PSCs are evolving into specialized devices. Looking at modern buildings, they usually present façades with wider external openings and glazing systems—including fixed or operable windows, skylights, jalousie windows, French doors, roof lanterns, etc.—to provide optimum daylighting to the inner volumes and ensure energy savings by reducing the need of artificial lighting; as a direct consequence, solar PV windows are becoming one of the most targeted applications in the scientific and industrial

research. Generally speaking, a careful design of building openings and glazing is essential to achieve a pleasant, energy efficient, and well-illuminated indoor environment. The implementation of power-generating windows in place of traditional ones must guarantee the same conditions in terms of visible light transmittance and visual comfort: If this assumption is disregarded, the principal function is lost and the device not worth being installed. Of course, transparency is a pivotal feature: A specific survey by Boyce et al. determined that minimum acceptable glazing transmittance for office buildings should fall within the range between 25% and 38%.[124] It follows that an AVT higher than 25% is generally considered to be acceptable for solar window applications, but the necessity for transparent composing layers inevitably compromises the efficiency. Moreover, in a real environment where the position of the sun varies continuously, proper strategies to minimize PCE degradation due to the change in the angle of the incident light should be developed before any commercialization. Coloring is another important aspect that was barely mentioned before. As a PV window should resemble in its primary function a traditional colorless glassy panel, stringent aesthetic requirements in terms of color coordinates and CRI values must be fulfilled to enable practical window deployment. Considering that a* and b* color coordinates at the origin (0,0) correspond to the absence of color (neutral color), the region of visually acceptable tinting in the window field is $-5 < a* < 1$ and $-5 < b* < 5$, while CRI values higher than 90 are typically needed to ensure acceptable color reproduction.[122,125] In addition, it is also necessary to develop a ST-PSC with a low haze ratio to ensure a high degree of clearly visible transmitted light; the H value should be opportunely compared with those of architectural glass products ($\approx$1%) currently employed in the window/glazing industry. Since the photoactive layer in ST-PSCs is necessarily colored as it is interacting with photons in the visible range to produce a photocurrent, many ST-PSC structures proposed in the literature maintain the typical brownish color provided by the perovskite film, resulting to be not neutral-colored, so far. Thus, specific approaches were developed in the last years to make the devices meeting those expectations, including rational modulation of the perovskite thickness, morphology, and composition.

Modulation of Perovskite Layer Thickness: One well-established approach to fabricate neutral-colored ST-PSCs consists in controlling the photoactive layer thickness. The logic behind this choice comes from the simple assumption that, if the photoactive layer is the one deputed to collect photons of light to be used to generate charge carriers, a minor quantity of light absorbing centers will guarantee higher transparency. This strategy comes to provide devices with relatively high values of AVT, but obliges to face power efficiency issues due to the now-inferior density of photoactive material. In this scenario, optical properties and PV performances are at the edges of the playboard, and limited achievements are targetable. To this regard, one of the very first dedicated investigation was reported by Ono and colleagues,[126] who described in 2014 an alternative hybrid evaporation technique for attaining large-area $MAPbI_{3-x}Cl_x$ perovskite films as thin as 135 nm with centimeter-scale uniform semitransparent color. The proposed fabrication method returned solar cells with 9.9% PCE and a high V_{oc} value of 1.09 V, and it was also tested to be of general use for other combinations of MA halides and Pb

halides, providing flexibility on perovskite film color choices. However, it is worth considering that the final electrical/optical properties of ST-PSC devices are ruled not only by the perovskite layer thickness, but also by the transparent top electrode incorporated in the final design. In 2014, Roldán-Carmona et al. reported a detailed investigation on the optimization of neutral-colored ST-PSCs through both rational design of the perovskite film and judicious selection of the top electrode.[91] In their report, an Au film with thickness as low as 6 nm was deposited to act as the TTE. The authors' efforts to avoid surface diffusion and aggregation of the Au atoms, ultimately causing the formation of a rough interface at the top of the metal layer (resulting in poor electrical performances)[90]; a second and not-trivial issue concerns the optical properties, and in detail the appearing of greenish and bluish shades, arising from the presence of localized surface plasmon resonance phenomena, plus scattering losses, which definitely affect the overall transparency of the device. To circumvent those issues, the use of LiF as capping layer provided stability to the metal layer; moreover, it usefully reduced the energy lost by the light specular reflection of the device, acting as an effective AR coating while enabling higher transparency and keeping an elevate J_{sc} value. Once the top electrode was optimized and stabilized, the thickness of continuous perovskite films was precisely controlled by thermal evaporation, and PCEs as high as 6.4% with AVT close to 29% were successfully achieved. However, typical samples looked yellowish/light brown depending on the perovskite thickness, suggesting that they would need more fine-tuning of the perovskite structure and composition to meet the requisites for solar window deployment.

In 2015, Guo et al. proposed an alternative layout incorporating a one-step solution-processed MAPbI$_{3-x}$Cl$_x$ perovskite film as the photoactive layer and AgNWs as the TTE. The electrode was deposited by spray-coating on top of the PC$_{60}$BM ETL with an underlying ZnO NP-based protecting layer to prevent any solvent damage or chemical reaction between Ag and halogens from perovskite. By integrating this transparent electrode and applying AR LiF coatings on both the top and bottom sides of the device, they managed to obtain PCEs as high as 8.5% at an AVT of 28.4%. In the same year, Della Gaspera et al.[96] documented the design of an alternative DMD-structured TTE with an optimized MoO$_x$ (5 nm)/Au (10 nm)/MoO$_x$ (35 nm) multilayered composition. In their work, MAPbI$_3$ perovskite films in a range of thickness values between ≈50 and 300 nm were successfully fabricated via a gas-assisted solution method; as it can be expected, thick-layered devices achieved higher PCE values (up to 13.66%), but an AVT (calculated between 370 and 740 nm) as low as 7% was obtained in turn, while 50 nm thick photoactive layers provided devices with inferior PCE (5%), a more acceptable 31% AVT, and a color hue closer to neutrality. A different investigation came later from our research group, reporting on the development of a nonprecious copper-based DMD transparent electrode to be used as an alternative, cost-effective top anode in regular planar ST-PSCs.[127] The electrode design goes around the choice of MoO$_x$ as the dielectric, being proven effective as anode buffer layer, and the deposition of a compact Cu film as thin as 9.5 nm as the metal middle layer, whose quality was improved by incorporating an ultrathin Au seed layer, also acting as an effective Cu diffusion barrier. Benefitting from further optimization of the perovskite layer thickness and

transparency, the final devices achieved PCEs of 12.5%, 10.2%, 6.4%, and 3.1% with corresponding AVT values of 5%, 9%, 18%, and 24%, and increasing color neutrality.

Researchers continued with pursed further developments in this direction, as Yu and others kept on preparing perovskite layers using precursors solutions with different concentrations, to obtain ST devices with higher AVTs and getting as close as possible to the neutral color. The most transparent ST-PSC, incorporating a 120 nm thick, triple-cation (Cs/MA/FA) mixed-halide perovskite film and a MoO$_x$/Au/MoO$_x$ DMD TTE, exhibited a PCE of 7.4% with an AVT of 29.5%, whereas the thickest device with 500 nm thick photoactive layer showed a PCE as high as 16.1% with an AVT of 10.1%.[128] These results are remarkable when you consider that an alternative solution-processed cross-linked HTL was used in place of the traditional spiro-OMeTAD, with significant improvements in long-term device stability. Another interesting work highlighting the importance of selecting an appropriate HTM in ST-PSCs had already been reported a few years earlier by Jung et al.,[39] who fabricated their devices using a highly transparent CuSCN-coated ITO/glass substrate, taking advantage of the exceptional optical transparency in the visible range (see **Figure 8**c). In their study, a planar inverted PSC configuration was selected, possessing appealing advantages over mesoscopic structures owing to its simple layered configuration allowing high transmittance and low scattering/haze. Also, a range of different CuSCN HTL thicknesses was explored, with the best electrical performance obtained with the thinnest layer (40 nm). Anyway, the overall transparency and color neutrality mainly resulted from the optimization of the perovskite layer thickness, with the AVT optimum reached for a 60 nm thick perovskite film; the best compromise between electrical and optical features was reached for a ST-PSC using a 180 nm thick perovskite layer (PCE = 10.3%, AVT = 25.1%).

When researchers have to reduce the thickness of the photoactive layer down to tenths of nanometers, it is important to have strict control of the preparation conditions, to obtain high quality films with minimized surface defects and pinholes; this issue is particularly critical for solution-based procedures, where temperature could have dramatic influence over the perovskite crystallization dynamics. One simple procedure has been reported by Bag and Durstock,[129] who documented the employ of a thiourea vapors treatment to produce stable 100 nm thick films; the thiourea is believed to act as "molecular glue," favorably engineering the perovskite interface with the underlying PEDOT:PSS and minimizing pinholes generation over the perovskite film (see Figure 8d). The final devices were obtained by evaporating an ultrathin (10 nm) Ag film as the TTE. This approach returned ST-PSCs with 8.2% PCE and 34% AVT and can be easily implemented into other protocols; a PCE higher than 10% at an AVT of 24% was also demonstrated when the active layer reached about 180 nm of thickness. If these results were achieved by proofing the positive effect of an additive introduction, Quiroz et al. developed a solvent-solvent extraction protocol, managing to obtain active layer films as thin as 40 nm following a room-temperature crystallization in few second time span and avoiding the employ of any inert atmosphere.[130] By combining this strategy with a performing spray-coated AgNW semitransparent counter electrode (R_s = 10–20 Ω sq^{-1}; $T \approx$ 85% at 550 nm), they demonstrated a striking AVT of 46% with an efficiency of 3.6%.
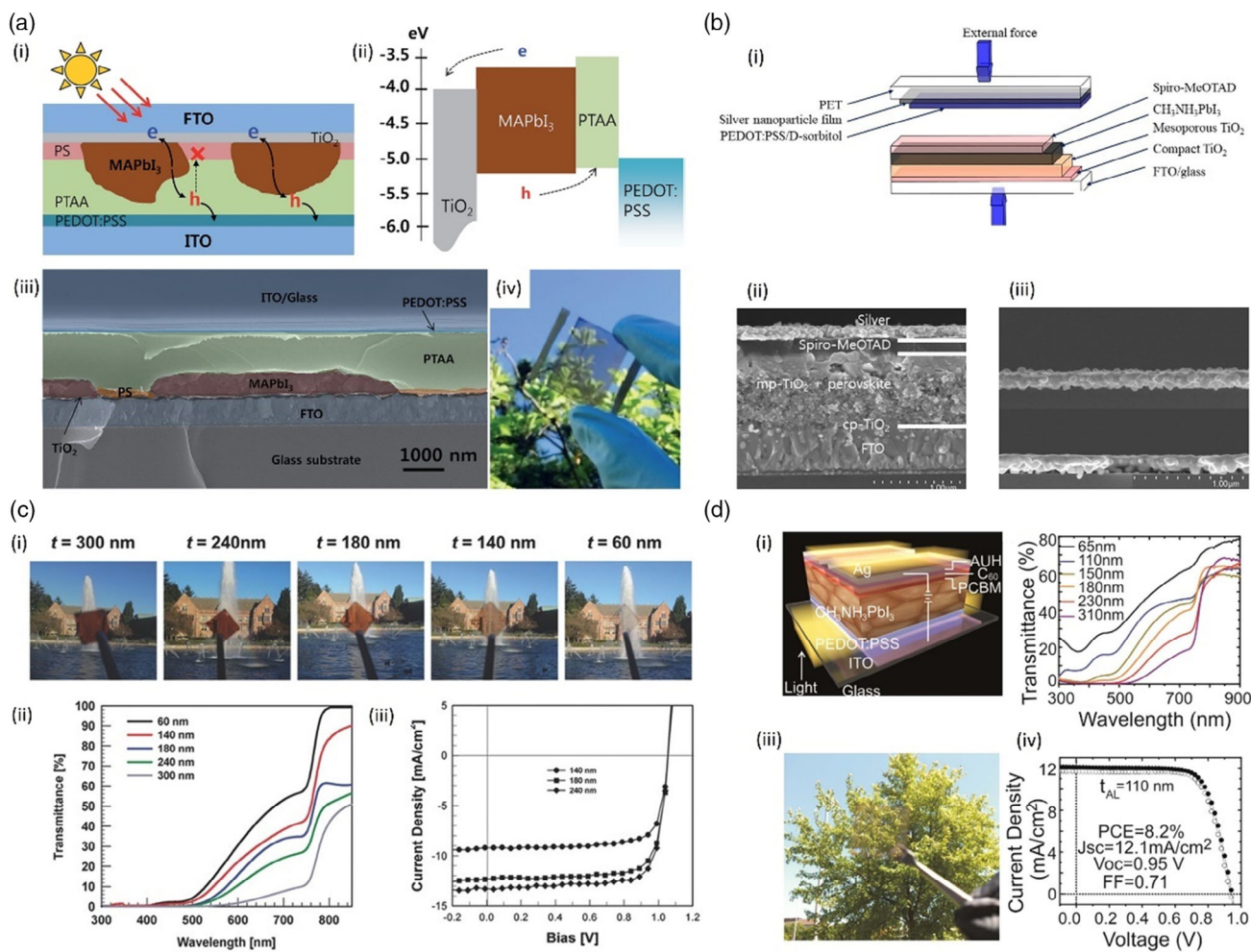
Figure 8. A collection of neutral-colored ST-PSC fabrication examples. a) Morphology control over perovskite active layer: (i) Schematic device architecture; (ii) ST-PSC energy band diagram, (iii) SEM cross-sectional image of a representative device; (iv) a photograph of the as-fabricated ST-PSC showing its high transparency and neutral color. Reproduced with permission.[134] Copyright 2016, RSC Publishing. b) Transparent electrodes integration: (i) schematic illustration of lamination process for ST-PSC fabrication; (ii) cross-section image of the fabricated device; (iii) the microstructure of silver nanoparticle film annealed at 150 °C (top) and 180 °C (bottom) for 5 min. Reproduced with permission.[75] Copyright 2020, Elsevier. c) Investigation of new HTL materials: i) Photographs of MAPbI$_3$ films (with different thickness) on CuSCN/ITO-coated glass; ii) UV–visible transmittance of the corresponding films; iii) J–V curves of the ST-PSCs. Reproduced with permission.[39] Copyright 2015, John Wiley & Sons, Inc. d) Application of additives to obtain low thickness, defect-free perovskite active phases: i) ST-PSC device structure; ii) UV–visible transmittance spectra through the complete ST device for different perovskite layer thicknesses; iii) photograph of the ST-PSCs with an AVT of ≈34% and an ≈110 nm thin MAPbI$_3$ active layer; iv) J–V characteristics of the 8.2% ST solar cell having similar AVT (open circles: forward scan, closed circles: reverse scan). Reproduced with permission.[129] Copyright 2016, Elsevier.

Modulation of Perovskite Morphology: Another investigated aspect concerns the control over the perovskite layer coverage, targeting at higher AVTs and a more visually acceptable tinting as requested by the window industry. Following this approach, the research equip lead by Snaith proposed a successful protocol consisting in the preparation of an island-structured layer of perovskite with incomplete coverage, resulting in a substantial attenuation of the typically brownish color associated to perovskite films.[131] The investigation focused on planar heterojunction PV devices; as reported by them, a precise control over the dewetting process conditions (temperature, film thickness, etc.) guides the polycrystalline photoactive film to have access to

micro-structured arrays of perovskite "islands" which possess, according to the SEM images, an average width of 5 and 1 μm thickness.[132] Such morphology guarantees elevate AVT values, color neutrality, and optimal PV efficiency. This group kept on the investigation moving in different directions, and one year later, they reported the employ of a templating highly ordered metal oxide honeycomb structure, resulting in a precise control over crystal growth, and finally over domain size and the overall morphology of the film.[133] A monolayer of poly(styrene) microspheres was employed as sacrificial agent to prepare the metal oxide honeycomb microfilms, which is deputed to drive perovskite crystallization in these confined areas. After comparing

the results obtained using TiO_2 and SiO_2 templating scaffolds, the latter resulted in a more contiguous microstructure, providing the final device with sufficient AVT (37%) and PCE (not far from 10%). Similarly, a passivation poly(styrene) interlayer was introduced by Heo and co-workers to prevent direct contact between HTL and ETL,[134] obtaining devices with improved performances due to the suppression of charge carrier losses (see Figure 8a). Kwon et al. considered to go deeper in the attention to the morphology control and decided to develop nanostructured perovskite layers based on the use of anodized aluminum oxide (AAO) nanopillars as templating network, achieving a satisfying 9.6% PCE at 33.4% AVT value.[135] These parallel nanopillars allowed a precise control over the pores size within the AAO volume, thus controlling the dimension of the vertically aligned perovskite pillars. Such approach provided cells with negligible hysteresis, and a remarkable improvement in long-term stability under continuous illumination, as well as suppression of internal ion diffusion; high transparency was achieved by a combination of the so-nanostructured photovoltaic layer and the employ of a transparent cathode (made of ITO) and an accompanying buffer layer (MoO_x).

Other Approaches: A completely different strategy to produce highly transparent PVs for solar window purposes consists in creating ultraviolet (UV)-harvesting ST devices based on halide perovskite semiconductors where the bandgap is sensitively tuned with a range of compositions to selectively harvest only UV photons from solar radiation. In a recent work by Liu and co-workers,[136] UV-selective ST-PSCs based on doped compositions of $MAPbCl_{3-x}Br_x$ with ideal bandgaps and visible absorption cut-offs (at around 435–440 nm) were successfully demonstrated, enabling exceptionally high AVT (73%) and CRI (over 93) values at 0.52% PCE. This approach offers theoretical efficiencies up to 7% with >99% AVT, providing an effective route to potentially surpass state-of-the-art NIR-harvesting ST-PVs.

So far, research and development of ST-PSCs for solar window purposes was mainly focused on the optimization of visible light transmittance and aesthetic appeal in view of a possible future building integration. Less attention has been paid to another important aspect concerning the solar heat transmittance of the devices. Considering the enormous amount of energy spent on indoor air-conditioning worldwide, high-performance PV glazing systems are needed that not only generate electrical energy but also allow smart management of photons in the NIR part of solar radiation to reduce indoor overheating and maximize energy savings. In this direction, Kim et al. developed ST-PSCs that not only exhibit high values of PCE (13.3%), but also show remarkable heat rejection capability, reflecting 85.5% of incoming infrared light.[137] To realize thermal-mirror functionality, they employed a sophisticated dielectric-capped metal-based TTE incorporating a thick Ag layer in conjunction with ZnS as a high-index capping layer, thus selectively maximizing transmission at visible and reflectance at NIR region. Despite the quite low AVT value (7.43%) and brownish appearance of the final devices, this study constitutes a step forward toward the development of "electricity-generating and heat-rejecting" solar windows with ideal energy management capability.

3.2.2. Colorful ST-PSCs

Neutral-colored photovoltaics are the mandatory choice when the final user considers clear visibility as an essential requisite the solar window must possess. However, in a different scenario, for design/aesthetic purposes (e.g., façade-integrated PVs, decorative exteriors), light filtering could be a desired feature, and colorful PSCs meet these expectations. In this review, the attention is focused on ST-PSC devices, thus the transparency requirement remains pivotal, as well as the necessity to target simple, scalable fabrication protocols, but the color-neutrality is abandoned in favor of different and more evident optical properties. Importantly, colorful ST-PSCs should not be envisaged as a device whose appearance is characterized by a darkening of the canonic coloration of the perovskite, but it is rather the result of a precise strategy aiming at fabricating cells with a precise color hue in the visible range.

Several components can be evaluated in a ST-PSC to make it colorful. In a simple vision, the most effective way can be envisaged in the photoactive layer engineering. but the manipulation of the charge transport layers (both HTL and ETL) or the electrodes can be taken in account as well. Such approaches can be based on chemical modification (e.g., varying the composition of the perovskite by adding dopants) or morphological modification (the introduction of photonic nanostructures, optical cavities, grating patterns, etc.), and usually oblige to develop a specific fabrication procedure. In a recent perspective paper,[138] these approaches have been labeled as "internal modifications," as they focus on the main constituents of the solar cell; in opposition, "external modifications" concern the deposition of an external coating made of dyes/pigments, or a new layer made of dielectric mirrors. The addition of those new layers does not interfere or modify the stability of the solar cell, neither has it a negligible impact over the device's properties; however, the final effect is the introduction of a light filter, and it could eventually penalize the overall performance.

Tuning the Perovskite Composition: 2013 is the year of the report by Noh and coworkers,[45] a cornerstone article demonstrating how perovskite optical features can be thoughtfully shifted to the orange-red range by simply substituting part of the iodide anions with bromides and exploring different Br^-/I^- ratios. The investigation over the photoactive layer composition returned a PCE of 12.3% in a time when the efficiency was compatible with the best PSCs based on opaque back electrode, destined to non-ST applications. The year after, Eperon et al. moved their attention over the organic cation of the perovskite structure, and they managed to tune the bandgap by replacing methylammonium with formamidinium cation, modulating the bandgap between 1.48 and 2.23 eV and achieving up to 14.2% PCE values (see **Figure 9**a).[139] Considering that these pioneering works achieved successful results in terms of optical tunability and device performance, most subsequent studies on colorful ST-PSCs focused on the perovskite layer and at tuning its properties; most research reports are experimental studies, nevertheless some theoretical works started to appear,[140] trying to identify the key parameters and mechanisms ruling the final perovskite optical properties. Other research teams went on investigating new procedures and optimizing protocols to achieve fine control
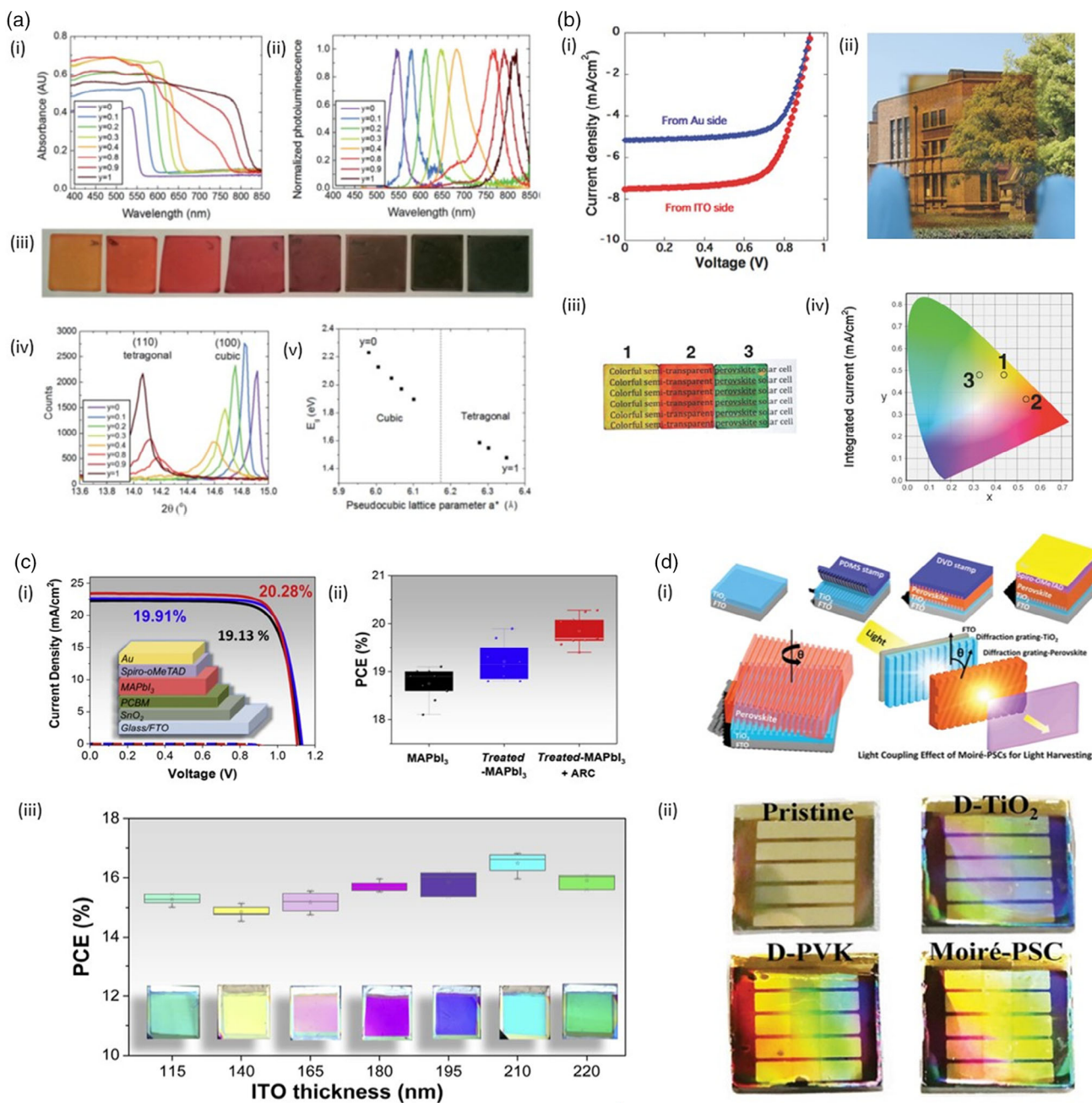
Figure 9. Compared examples aiming at colorful ST-PSC fabrication, following different approaches. a) Tuning the perovskite composition: i) UV-visible absorption spectra of the FAPbI$_x$Br$_{3-x}$ perovskites; ii) steady-state photoluminescence spectra for the same films; iii) photographs of the FAPbI$_x$Br$_{3-x}$ perovskite films with increasing bromine content (from right to left); iv) XRD spectra of FAPbI$_x$Br$_{3-x}$; v) bandgap modulation with pseudocubic lattice parameter as determined from XRD spectra. Reproduced with permission.[139] Copyright 2014, RSC Publishing. b) Depositing a dye/pigment over a neutral-colored ST-PSC: (i) J–V curves of the ST solar cell with light from ITO side (red) and Au side (blue); ii) picture of the reference ST device; iii) resulting colored ST-PSCs after spin-coating deposition of different pigment materials on Au surface; iv) color coordinates of the colored cells shown at panel (iii). Reproduced with permission.[155] Copyright 2015, John Wiley & Sons, Inc. c) Modulating the electrode thickness: i) Schematic representation of the fabrication design and J–V curves under reverse scan; ii) PCE statistical distributions; iii) PCE as a function of the ITO electrode thickness. Reproduced with permission.[147] Copyright 2020, Elsevier. d) Playing with light interference phenomena: i) Schematic description of the PSCs with dual diffraction gratings imprinted by a PDMS stamp and a commercial DVD disc; ii) comparison of the visual effect offered by devices incorporating different light-trapping materials, and the pristine sample with standard architecture. Reproduced with permission.[149] Copyright 2020, John Wiley & Sons, Inc.

over perovskite composition,[141] bandgap tuning,[142] and increased film quality in terms of homogeneous morphology.[143] Some original strategy has been recently reported by Xiong and colleagues.[144] In their work, 5-chloroisatin, a yellow orange organic dye, was incorporated as additive in the perovskite precursor solution, to stabilize the formation of crystalline microphases by means of hydrogen bonds directed to the MA organic cation. Such strategy enhanced the stability of the photoactive layer, but tuned as well the optical properties. Although the authors did not focus over semitransparent designs, the strategy can be easily implemented into ST devices.

Engineering the Electrodes and Charge-Transport Layers: Playing with the photoactive layer composition is not the sole strategy to make PSCs colorful; interesting results are targetable playing with the morphological profile of different constituting layers. For example, Jiang and others proposed a method to engineer the top electrode to obtain vividly colored ST-PSCs taking advantage of light interference phenomena.[145] In their study, PEDOT: PSS polymer electrode thickness was precisely governed by controlling spin-coating conditions or by depositing different number of layers of PEDOT:PSS with a given thickness via transfer-printing technique resulting in the fabrication of efficient devices, characterized by PCE values from 12.8% to 15.1% (from red to blue cells) when illuminated from the bottom electrode (FTO/glass) side and from 11.6% to 13.8% (from red to blue) when illuminated from the PEDOT:PSS side. The reflection peak of the ST-PSCs is modulated in its position by Wang et al.,[146] who obtained a library of colored cells by modulation of both the bottom electrode (ITO/glass) and HTL (CuSCN), obtaining devices with PCE values >10% in all the cases. Similarly, Li and colleagues by simply tuning the thickness of the ITO electrode,[147] resulting in a wide range of available colored cell (see Figure 9c), and superior performances compared to the previous example (>15% in all the cases, but resulting also of further optimization in the photoactive layer preparation procedure that is not solution-processing but more expensive thermal evaporation approach).

The engineering of the ETL morphology can bring color to the ST-PSCs. Deng and co-workers introduced diffraction grating pattern into the TiO$_2$ layer, inducing a modulation of the optical profile by light trapping phenomena.[148] Similarly, Wang et al. prepared PSCs based on diffraction grating layers[149]; also in this case, the range of obtained colors is more limited, or better saying that a specific color cannot be targeted, but a wide range of hue will be visible as function of the relative angulation between PSC and observer (see Figure 9d). Looking at strategies to obtain a more strictly defined coloration of the device, the preparation of TiO$_2$-nanobowl arrays as a structured electron transport layer returned better results.[150]

In a different approach, similarly to the DMD electrodes, some researchers report MDM electrodes; such attempt to face the problem should not be surprising, since it has already been successfully tested in amorphous silicon (a-Si) solar cells,[151] which are definitely a more mature technology and praised by global market. Here, a dielectric is sandwiched in between two thin metallic layers, and playing with the thickness of the central layer modulates the resonance transmission of a specific wavelength. In principle, the advantage lies in the employ of standard materials and procedures, with specific control over a single step.

One of the first reports by Lee and co-workers employing a combination of Ag and WO$_3$ didn't return elevate efficiency of the final devices (3.86% for the best example),[152] but soon the work by Lu and colleagues,[153] which documented the employ of ITO as dielectric and Ag as metallic counterpart, gave access to devices with more encouraging values (7.4%). Recently, this approach was further investigated by Lee et al.,[154] with a more complex electrode constituted by sequential layers of silver and zinc sulfide, producing "red," "green," and "blue" prototype cells with PCE values high as 10.47%, 10.66%, and 11.18%, respectively.

External Modifications: Among the strategies implemented to introduce an external, filtering layer made of chromophores, the early report by Guo and co-workers is an example of how simple and successful this approach results to be (see Figure 9b).[155] Along with their investigation of a new fabrication method, where poly(vinylpyrrolidone) (PVP) acts as additive able of strict control over perovskite crystal sizes (thus, contributing to the modulation of the bandgap, improving its processability at low temperature, and enhancing the transparency of the final device), they describe a simple method to "color" ST-PSCs by spin-coating solutions of different commercial pigments in propylene glycol monomethyl ether acetate; "red," "yellow," and "green" solar cells are presented, opening the way to the realization of devices characterized by infinite possibilities of color hue. Instead of color filtering, another approach investigated by Schlisske et al. moves to the introduction of luminescent species.[156] In their vision, high energy photons in the ultraviolet/blue region in the spectrum are absorbed by the luminophore, being emitted at longer wavelength; in this way, photons whose absorption has little contribution in the ST-PSC can now be usefully employed for photocurrent generation, thus enhancing the overall efficiency of the device, and modulating the color perception of the PSCs, keeping elevate (≈17%) the power conversion efficiency. "Red," "green," and "blue" prototypes, a sort "power generating pixel" for graphic and design applications, they are fabricated accordingly to a totally solution-processed approach (devices' layers are produced by sequential inkjet printing), providing an appealing example of a protocol which can be easily transferred on industrial scale. Other approaches privileged investigations focusing on light-matter interaction phenomena (reflection, diffraction, etc.) to achieve color modulation avoiding the introduction of any pigment, as previously seen for some examples related to charge transport layers. Among the most representative works, the report by Quiroz and co-workers succeeded in tailoring the color hue of ST-PCSs after introducing dielectric mirrors (or Bragg reflectors).[157] These are a sequence of layers characterized by high and low refractive index materials; depending on the number of layers color profile can be tailored, as well as the final AVT and PCE values. The best scenario with 31% AVT provided only a 4.2% PCE; however, the full printability of the device remains an attractive feature. This approach has been more recently exploited by Lee et al. preparing a sequence of SnO$_2$ and SiO$_2$, achieving a more encouraging 9.52% PCE.[158] Finally, the fabrication of ultrathin metal nanostrips has been explored by Lee and coworkers to introduce localized surface plasmon nanoresonators.[159] Highly efficient and colored ST-PSCs were prepared using nanoimprint lithography of AgNWs, producing sharp reflection features and

angle-insensitive color profiles, keeping elevate AVT values and PCE as high as 10.12%, 8.17%, and 7.72% for the red, green, and blue devices.

3.2.3. Perovskite-Based Smart Windows

In the previous sections, starting from ST designs targeting at color neutrality, we moved to colorful ST-PSCs; as underlined, the absence of any color tone or the opposite situation are not a mere aesthetic requirement but the technological answer to specific requirements the PV panel has to meet, depending on its function as part of the building envelope. However, a further evolution step of ST-PSCs is investigated by the scientific community and consists in the combination of both the two functionalities in a sole, remotely controlled technological device. This strategy would offer higher filtering features when the incident radiation is more intense (under the daylight or in the hot seasons), and returning color-neutral in case of negligible light irradiation (night time or fall/winter). Such systems are generally referred to as "smart window" or "switchable windows," namely devices whose light transmission and color properties can be favorably altered by an external stimulus and, most importantly, in a reversible fashion.

Generally speaking, the trigger event for spectral modulation in smart windows can be an optical, thermal, or electrical one; in the latter case, we talk about electrically activated switchable smart windows, whose operating principles and different architectures have been thoughtfully reviewed in a recent work by Nundy et al.[160] This class of devices includes the so-called electrochromic (EC) systems, which require an external direct-current supply to change their state from bleached to colored. A technological evolution of such devices consists in the combination of PV and EC behaviors in photovoltachromic (PVC) windows, in which the photogenerated current from the PV system is used as a source for EC switching, but it enables the generation of surplus energy as well, for additional building uses. Such stand-alone, self-powered PVC systems are the most intensively investigated architectures.[160] Importantly, they allow for an "active" control over the windows properties, which is a major distinction from other smart devices such as thermochromic (TC) windows, where the switching among color-neutral and colored state cannot be ruled by the user, whose lack of control makes him/her a "passive" user. Looking at the global PV market, smart window technologies are gradually attracting more interest for their energy-saving properties,[161] although an intrinsic higher degree of complexity in terms of fabrication approach (and final cost) of the device must be accounted. Moreover, as in the case of solar windows, specific requisites must be fulfilled before practical building integration. According to a specific survey, effective smart glazing should be capable to switch their AVT from 50% to 70% at the bleached state to 10–20% at the colored state, with recommended contrast ratio (the ratio between the transmission of bleached and colored states) values between 5:1 and 10:1.[162] For what concerns the optical modulation kinetics, the response time (which is the time needed to activate the transition between the two states) of the device can range between 10 s and 5 min for architectural applications.

Perovskite Photovoltachromic Windows: As revealed in the previous sections, the group lead by Prof. Snaith has been very active in the early days of PSC technology, and again the first report on a perovskite photovoltachromic device (PVCD) comes from his laboratory in 2015, reporting the fabrication of a self-adaptive device, capable to move from a transparent, color-neutral state (26% AVT and 3.7% PCE) to a blue-tinted device with 8.4% AVT upon self-activated switching under illumination.[163] The PVCC architecture implies the combination of a standard ST-PSC as described in an earlier paper,[76] with the integration of a solid polymer electrolyte prepared using a mixture of polyethylene oxide (PEO), lithium iodide (LiI), and polyethylene glycol (PEG), which is deposited over an EC WO_3 film serving as ETL. The mechanism concerning WO_3 electrochromism relies on the insertion of protons and charge-compensating electrons to fill into its conduction band, with consequent variation of its electrical resistivity and optical transmittance.[164] Most of the research on perovskite-based PVCDs focused on the integration of WO_3-based EC films and capacitor components (see **Figure 10**a),[165,166] with the highest goal reached by Pugliese et al.,[167] who reported the fabrication of an all-solid-state PVCD in which a monolithic WO_3-based EC unit was combined with high-performance ST perovskite cells (see Figure 10b). In their work, the optimized ST-PSC device showed an AVT of 27%, a high PCE of 14.2%, and a V_{oc} of 1.06 V; three ST perovskite cells were connected in series to reach an adequate voltage to supply power to the EC module, and then the PV ad EC components were assembled on a single-glass substrate, resulting in a monolithic self-powered device. Such simplified architecture avoided previous complication due to the necessity of a complex sealing procedure for the liquid or gel electrolyte and of an additional lamination step of the two glass electrodes. Their best PVCC device exhibited an AVT of 23% in the clear state, then switching to an intense coloration when powered by the three series-connected perovskite cells (4.4% AVT), with very fast bleaching/coloring dynamics (≈15 s). Beside this relevant progression, the limitation of WO_3 films lies on the availability of a restricted gamut of coloration, limited to blue hues. Some last-minute research works moved away from inorganic materials and started to use alkyl viologen derivatives (see Figure 10c,d).[168,169] The strategy aims at finding new candidate molecules (with varied optical properties) and relies on organic chemistry synthetic protocols, to produce from a simple common scaffold a library of compounds with modulated colors. Moreover, organic compounds guarantee solution processability and more eco-friendly fabrication procedure. As an example, Liu et al. managed to fabricate high-performance PVCDs based on halide-exchanged perovskites and viologen derivative gel films,[75] exhibiting full-frame size (100% active area), excellent CRI (96), a wide contrast ratio (>30%), a coloring period of ≈200 s, and a self-bleaching time by disconnection of ≈300 s (see Figure 10c).

Thermochromic Perovskites: Perovskite thermochromic solar panels (PTC-PVs) are another approach to the problem, based on a specific perovskites' physical parameter, the crystallization temperature. It is reported that perovskites solubility is a function of the solvent, generally decreased when temperature raises up, and it is function of its halogen anions composition.[170] Based on this consideration, it was envisaged the possibility of fabricating device where the energy received by incident light
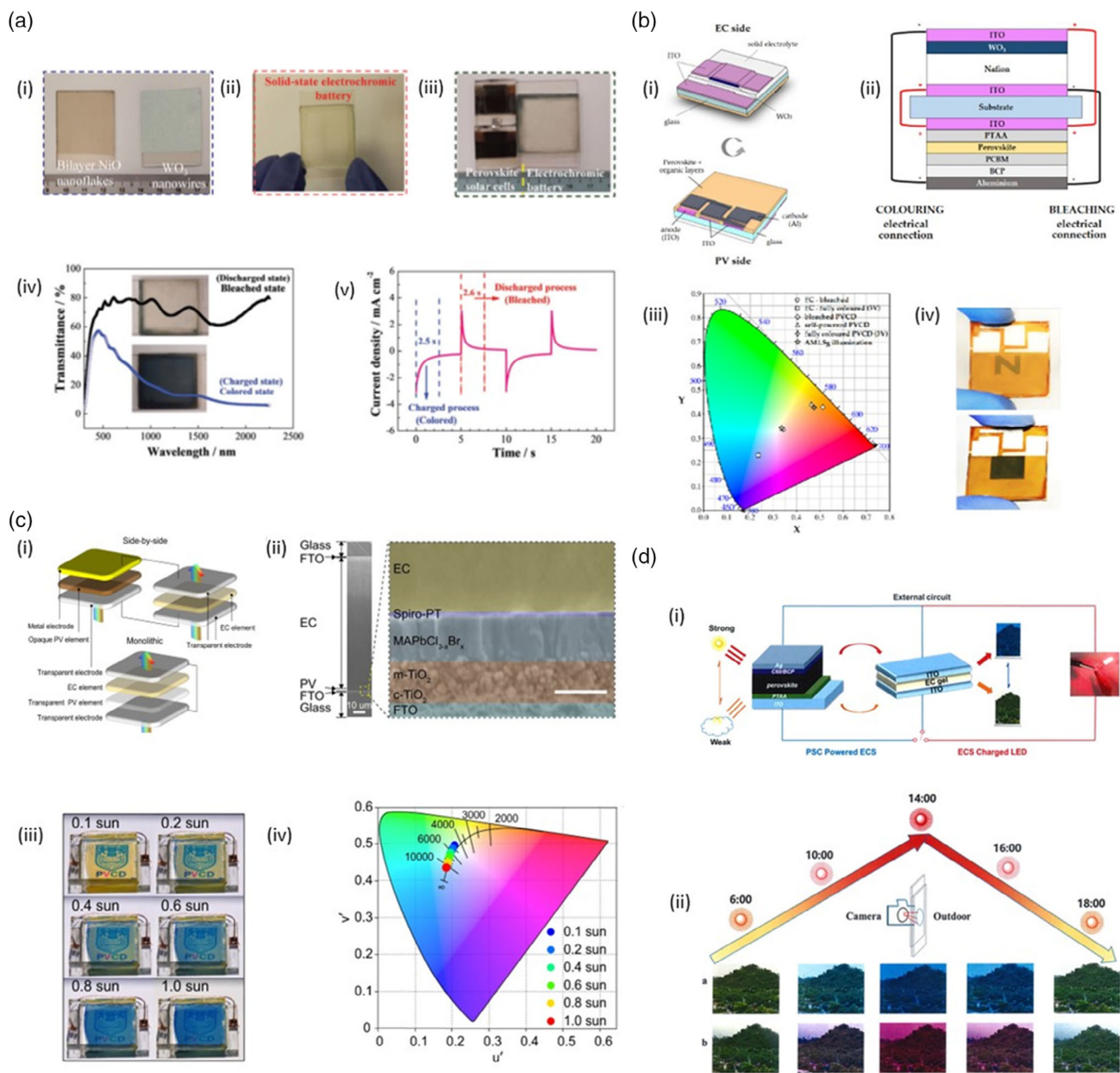
Figure 10. Pictorial résumé comprising the most notable examples of perovskite-based smart devices. a) Photos of different samples of: i) WO$_3$ nanowire arrays and rGO-connected bilayer NiO nanoflake arrays; ii) solid-state electrochromic (EC) battery based on (i); iii) a PSC and solid-state EC battery; iv) transmittance spectra of the solid-state EC battery in the visible and near-IR region at bleached and colored states (v) voltage–time responses of the solid-state EC battery during the charged (colored) and discharged (bleached) processes. Reproduced with permission.[165] Copyright 2016, RSC Publishing. b) Photovoltachromic device: i) fabrication scheme provided for the EC and PV sides; ii) device structure with electrical connection between the EC and PV device for coloring and bleaching phases; iii) color coordinates of the device with transmittance spectra under AM1.5 illumination, plotted on the CIE XY 1931 chromaticity diagram; iv) pictures of the photovoltachromic device in bleached and colored states. Reproduced with permission.[167] Copyright 2020, American Chemical Society. c) Four-terminal side-by-side PV-EC device: i) schematic representation of the investigated architecture; ii) cross-section SEM images of a monolithic PVCD as glass/FTO/PV/EC/FTO/glass device structure, with the detailed architecture of PV semi-module as c-TiO$_2$/m-TiO$_2$/MAPbBr$_x$Cl$_{3-x}$/Spiro-PT; iii) photographs of PVCD at different sunlight intensities; (iv) color coordinates of the devices reported at panel (iii), plotted on the CIE 1976 (u′,v′) chromaticity diagram. Reproduced with permission.[169] Copyright 2021, Nature Publishing Group. d) PSC-powered EC device: i) pictorial representation of the device' architecture; ii) digital images of outdoor sceneries viewed through PSC-powered ECDs by blocking device on the lens of the camera at different times (a: DPV; b: MPV). Reproduced with permission.[168] Copyright 2021, Nature Publishing Group.

is partially dispersed as thermal energy and, as the light intensity increases, the perovskite crystalline, photoactive phase appears, thus powering the photovoltaic panel and acting as light filtering. De Bastiani and co-workers were the first to document in a preliminary study the possibility to modulate this temperature-sensitive crystallization process of Br-doped perovskites to prepare inks characterized by reversible chromatic variation ranging from yellow to black as the temperature increases from 25 to 120 °C, aiming at the fabrication of PTC-PVs.[171] Shortly later, it came out a brilliant example reported by Lin et al.,[172] who fabricated performing PTC-PV devices utilizing thermally driven, moisture-mediated structural phase transitions of inorganic cesium-based mixed iodide/bromide perovskite. The solar panels were able to switch from a transparent, non-perovskite, noncolored state (AVT = 81.7%) with low power output to a deeply colored perovskite phase (AVT = 35.4%) with high power output. Moving away from this pioneering work, research is still in progress, however some trends can be revealed. On the one hand, researchers are actively working on the optimization of the perovskite phase composition and fabrication protocol conditions,[173] until passing in the very last reports to lead-free organic hybrid perovskites, aiming at more environmentally friendly formulations.[174] On the other hand, stepping into cesium-free organic hybrid perovskites allowed a finer tuning of the phase transition temperature,[174–176] as lower values would better fit with the commercial application, with the last reports fixing the benchmark at 60 °C.[176]

This parade of examples clearly demonstrates how ST-PSCs can be a primary player in the evolution of environmental and energy politics. In a short span of time, the technological progression returned not only more efficient and robust devices, but also compatibility with the urban setting; new applications and possibilities to solve the high energy consumption in buildings were granted by meeting specific semitransparency and aesthetic requirements, thus supporting a relevant position in the future energy market. The last part of this section evidenced an even newer generation of smart ST-PSCs, whose sophistication and final cost are definitely counterbalanced by a valuable adaptability to the light exposure condition, thus offering a new paradigm for the future products in the field of BIPVs.

3.3. ST-PSCs for Tandem PVs

To enable the expansion of solar PVs on a terawatt scale, the levelized cost of electricity (LCOE) of a PV system needs to be reduced. The most viable pathway for reducing the LCOE is by increasing the PCE of industrial PV modules, as this would correspond to a smaller area of solar panel required at constant electric power installed, and hence to a lower balance-of-system cost. The efficiencies of well-established PV technologies such as c-Si, CIGS, and gallium arsenide (GaAs) solar cells, have consistently progressed during the last decades, up to the current record certified research-cell PCEs of 26.7%, 23.4%, and 29.1%, respectively.[29] However, it was rigorously demonstrated that the PCE of solar cells is limited by the fundamental Shockley–Queisser (S–Q) theoretical limit of 33.7%, which is specifically valid for a single-junction PV cell possessing a bandgap (E_g) of 1.34 eV under standard illumination conditions

(AM 1.5G solar spectrum, unconcentrated).[177] For the case of silicon, which possesses a less favorable and indirect bandgap of about 1.1 eV, the theoretical upper limit results in a maximum PCE of about 29%. According to the S–Q limit model, the photons having less energy than the bandgap cannot be absorbed, and those possessing higher energy are wasted as heat due to a process known as thermalization.[178] Such nonabsorption and thermalization losses inevitably restrict the spectral utilization, and ultimately, the performance of commercially available single-junction solar cells, leaving limited room for further improvement in their PCE. The current research on tandem PVs aims to overcome such S–Q limit by an engineered configuration which stacks together different sub-cells (possessing different bandgaps), each of them able to absorb a different portion of the solar spectrum. More specifically, a wide-bandgap top cell can be stacked onto bottom cells having lower bandgap values. In a standard double-junction (2-J) configuration, the highest energy photons are captured by the material with the largest bandgap in the top cell, whereas the lower energy photons are allowed to pass through the top cell and reach the smaller bandgap semiconductor bottom cell, where they can be absorbed and converted, thus enabling a more efficient use of solar energy with overall reduced thermalization losses. In principle, by taking the number of stacking monochromatic sub-cells to an infinite number, it is possible to obtain a maximum efficiency of 68.7% at normal sunlight, or 86.8% using highly concentrated sunlight.[179] These numbers are very intriguing in theory but constitute an arduous target in real world devices. The present technology based on multi-junction (M-J) solar cells with inorganic III–IV semiconducting materials offers impressive performances, reaching PCE values as high as 39.2% by a six-junction inverted structure under 1 sun illumination.[180] However, the high costs involved, along with complicated fabrication procedures and poor scalability of the devices, limit the practical deployment of such M-J systems to space applications. For this reason, researchers have leveraged perovskite-based materials to ideally meet the needs of suitable bandgap tunability, along with exceptional opto-electronic properties and low-cost/versatile processability by solution dispensing approaches, that make them suitable for large-scale device fabrication. The current research focuses on perovskite-based 2-J tandem architectures, which show the best trade-off between efficiency gain and cost-effectiveness compared to other multi-junction solar cells.

The integration of perovskite into a 2-J tandem solar cell (TSC) can be obtained for instance by using the MAPbI$_3$ system (1.55–1.60 eV) or other higher-bandgap perovskites as the photoactive material for the top cell; conversely, the bottom cell can be obtained by integrating low-bandgap inorganic materials such as c-Si (about 1.1 eV) or CIGS (1.0–1.1 eV), or also opportunely engineered Sn-based perovskites showing a narrower bandgap down to 1.2–1.4 eV. To get high-efficiency perovskite-based TSCs, a careful design/selection of both the top and bottom cell is needed. As a primary purpose, the perovskite top cell should be able to convert UV/visible light as efficiently as possible, and, at the same time, it should be highly transparent to those lower-energy photons in the NIR spectral range that will be absorbed by the bottom cell. In this context as well (as for BIPVs), we can talk about "semitransparent design" of the

perovskite top cell, but, in the present case, the optical transmittance of the ST-PSC should be maximized in a different spectral range (typically 800–1200 nm), as dictated by the bandgap of the bottom cell. Any further requirement in terms of AVT, color, and aesthetics (typical of BIPVs) falls apart, at least at this stage of development, shifting the focus toward alternative device layouts and light management strategies aimed to achieve the best trade-off between efficiency and NIR transparency. To this end, perovskite materials with suitable bandgaps, as well as transparent electrodes with maximized NIR transmittance, should be developed and selected. Moreover, all the ST-PSC components should be processable by cost-effective fabrication methods compatible with the specific tandem configuration; challenges like up-scaling and long-term stability should also be considered and opportunely tackled before practical integration. Parallelly, the bottom cell should be optimized in terms of ideally matched bandgap, PV performance, costs, and compatibility with the subsequent processing steps. This is especially the case for emerging solar cells like low-bandgap PSCs, which needs to be improved with regard to the operation, composition, and stability of the devices for practical use as bottom cells.

After optimizing the design of the ST perovskite top cell and selecting the best-suited bottom cell, both with well-matched bandgaps and decent PCEs, the two sub-cells are ready to combine in a 2-J tandem device. Most recent studies have focused on two different tandem configurations, namely monolithically integrated two-terminal (2T) and mechanically

integrated four-terminal (4T) configuration. **Figure 11**a illustrates a typical 2T tandem architecture, in which the top cell is processed directly onto the bottom cell, with the two sub-cells being electrically connected in series via a recombination contact, also called interconnecting layer (ICL). According to Kirchhoff's law, the total voltage of such 2T devices corresponds to the sum of the sub-cell voltages, whereas the overall tandem current is dictated by the limiting sub-cell producing the least current. In contrast, in a 4T TSC, the top and bottom cells are stacked only mechanically on top of one another and have individual electrical contacts, without the need of any recombination layer (see Figure 11a); the overall PCE of the device is the sum of the PCEs of the two electrically independent cells, which are allowed to work separately at their own maximum power output. In general, 2T tandem devices are more attractive with respect to practical PV installation owing to their overall simpler architecture presenting fewer power electronic circuits, lower manufacturing costs, and potentially lighter weight. As they are monolithically integrated, 2T TSCs require only one TCE in their structure to serve as the front contact, with consequent reduction of associated costs and parasitic optical losses. Despite these advantages, obtaining high-performance 2T TSCs remains a great challenge mainly due to the requirement of current-matching and processing compatibility between the two sub-cells. Indeed, to obtain the maximum power output, the top and bottom cells should work near current-matching conditions, which means that they should generate the same photocurrent;
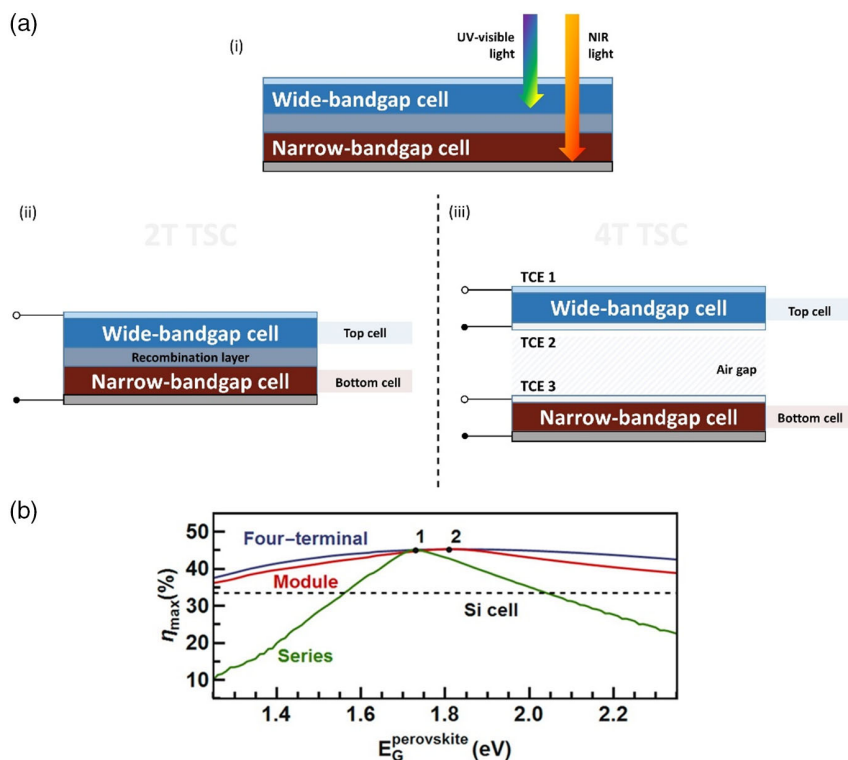

Figure 11. a) Structural features and main properties of tandem 2-J PVs: i) NIR transparency of the bottom cell; structural schemes for ii) 2-terminal (2T) and iii) 4-terminal (4T) tandem cells. b) Theoretical efficiency limit for three perovskite/Si TSC configurations (series, module, 4T) through detailed-balance simulations under standard test conditions (AM 1.5G). The dashed line corresponds to the SQ limit of Si. Reproduced with permission.[185] Copyright 2016, American Chemical Society.

this can only be achieved by sophisticated engineering of the bandgap and thickness of the photoactive layer of each sub-cell, as well as by implementation of advanced light trapping strategies (e.g., textured surfaces). At the same time, a careful optimization of the processing parameters (temperature, utilized solvents, etc.) of the top cell is needed, but the inherent properties of the bottom cell inevitably complicate tandem integration. Temperatures higher than 200 °C may cause degradation of the bottom cell, forcing researchers to adopt alternative PSC fabrication protocols (without sintering of metal oxides) or device layouts (less-performing p-i-n structures instead of conventional n-i-p PSCs); moreover, the surface topology of the bottom cell (e.g., textured Si or CIGS) may strongly differ from that of the glass substrates typically used in PSC fabrication due to their much higher roughness, which requires the adoption of conformal deposition methods (e.g., thermal evaporation or hybrid processes), or other strategies resulting in sufficiently thick perovskite films. These hurdles are solved in the 4T configuration, which enables each sub-cell to be fabricated and optimized independently with fewer restrictions imposed by the other sub-cell with regard to texture, processing method, and device layout. In 4 T tandem devices, n-i-p ST-PSCs showing the highest PCEs can be easily used as top cells, even when processed at high temperatures, and coupled with Si bottom cells with different structures (including double-side textured Si cells). This results in a relatively easier tandem integration and a more feasible way to obtain higher PCEs with respect to 2T tandem cells.[181] As a drawback, the 4T configuration is based on a more complex assembly, involving the use of multiple substrates and the fabrication of four different electrodes, with three out of the four which have to be transparent (see Figure 11a), resulting in relatively high manufacturing costs. Consequently, albeit the high potential of 4T TSCs, their implementation into large-scale devices at low cost is still a challenge. In particular, the selection of suitable TCEs with high conductivity and maximized transparency is crucial: Absorption and reflection losses should be minimized in the whole 300–1200 nm spectral range for the front contact of the perovskite top cell (TCE 1) to let UV/visible light reach the perovskite layer and NIR photons overpass the top cell, whereas both the back contact (TCE 2) of the top cell and the front contact (TCE 3) of the bottom cell should be highly transparent to the incoming NIR photons to let them pass and reach the smaller-bandgap photoactive material. The implementation of computational modeling is a powerful tool to rapidly optimize cell design and reduce electrical/optical losses. Several analyses on 2-J TSCs have been performed using detailed-balance calculations, shedding light on the maximum efficiencies attainable using 2T or 4T tandem configurations depending on the bandgap values of the top and bottom cells.[182] While the 2T structure imposes a stringent restriction on the optimal bandgap values due to the current-matching requirement, the choice of the bandgap is much more released in the 4T configuration, allowing for a wider selection range. The suitable bandgap tunability of the perovskite absorber, along with its high defect tolerance and compatibility with solution and vacuum fabrication methods, make PSCs an ideal choice as top cells to be combined with nearly any types of bottom cells in TSCs with both 2T and 4T architectures.

To date, high-performance perovskite-based 2-J TSCs have been mainly demonstrated by combining established PV devices (e.g., c-Si or CIGS) with ST perovskite top cells of different bandgaps into 2T and 4T configurations. Efficiency-wise, the most relevant researches during the last 5 years have focused on the development of perovskite/Si TSCs, whereas perovskite/CIGS cells have had a limited interest, being more than 400 and only about 40 the research articles dealing with the two technologies, as retrieved from the Scopus database. An outstanding record PCE of 29.5% for monolithic perovskite/Si TSCs was established by Oxford PV and certified by the National Renewable Energy Agency (NREL),[29] significantly exceeding the PCE of both Si- and perovskite-based single-junction solar cells. Although perovskite/Si tandem cells present the highest efficiencies so far, perovskite-CIGS TSCs are not too behind, with a maximum PCE of 27% recently achieved by careful optimization of the bandgap and the efficiency of the ST perovskite top cell and a flexible CIGS bottom cell.[183] Also, perovskite–perovskite tandem PVs are attracting great attention since they could deliver lower materials/fabrication costs while still enabling an efficient harvest of solar energy. Recently, Xiao et al. have achieved a breakthrough on all-perovskite TSCs using perovskite materials with ideally matched bandgaps and improved stability, demonstrating efficiencies as high as 24.2% for tandem devices with an area over 1 cm^2, and 25.6% for small-area devices (0.049 cm^2).[184] Considering that the upper PCE limit for both 2T and 4T 2-J architectures under standard light intensity is evaluated to be about 46%,[182] the possibilities for further improvement of the practical PCEs through an optimal choice of materials and bandgaps are substantial, and the perspectives on future commercialization are encouraging (see Section 4).

Given these premises, the following sections will be devoted to describing the recent progress achieved in three different types of perovskite-based TSCs, namely perovskite/Si, perovskite/CIGS, and perovskite/perovskite TSCs. The available strategies for NIR-transparent perovskite top cells will be opportunely explored and compared, focusing on the most updated transparent electrode techniques and compositional engineering approaches, and highlighting the substantial differences of device design with respect to ST-PSCs for BIPV purposes.

3.3.1. NIR-Transparent PSCs for Tandems with Silicon

Si solar cells are undoubtedly the most investigated bottom cells for tandem PV applications, owing to their ideal bandgap value (about 1.12 eV) and outstanding efficiencies (as high as 26.7%),[29] along with excellent stabilities and relatively low fabrication costs at the module level, permitting them to occupy the largest share of the global PV market (>90%). Technologies based on perovskite tandems with Si has steadily developed in the last few years as one of the fastest routes to obtain PCE improvement of the commercially available Si modules without extensive manufacturing cost increase. On the laboratory scale, spectacular results have already been reached. The highest PCE has steadily increased from 13.4% in 2014 to 29.5% in 2021,[29] benefiting from 1) advances in the design of NIR-transparent perovskite top cells, 2) careful optimization of the active layers'

bandgaps and thicknesses, 3) light management strategies to reduce parasitic optical losses, 4) sophisticated engineering of the recombination layer or tunneling junction in 2T TSCs, and 5) alternative fabrication approaches to obtain conformal PSCs on top of (textured) Si bottom cells in 2T TSCs. The main characteristics and PV parameters of recent champion perovskite/Si 2T and 4T tandem devices are summarized in Table S1, Supporting Information. Note that the practical PCEs are still lower than the possible theoretical efficiency limit of around 45.3% for perovskite/Si TSCs,[36] due to nonradiative charge recombination mechanisms and parasitic optical losses occurring in real world devices. To help identify and reduce these losses, several simulation studies have been reported, focusing on some crucial aspects such as the bandgaps of the two sub-cells, the parasitic absorptions and reflections at the semitransparent contacts and interlayers, the properties of the interconnecting layer in 2T TSCs, the silicon texturing interfaces, and the thickness of the perovskite layer.

On a technical level, the foremost issue is to develop perovskite top cells with high efficiency and suitable transparency; the low NIR absorption/reflection is the biggest challenge, especially in 4T TSCs, which comprises of three TCEs, limiting the number of low-energy photons reaching the Si bottom cell. To this aim, suitable transparent electrodes with maximized transparency in the long wavelength region are strongly needed. TCOs have been widely used to meet these requirements: in addition to sputtered ITO, alternative TCOs with high carrier mobility and low carrier density have been developed to alleviate free-carrier intraband absorption in the NIR region, including IZO, IZTO, and IZrO electrodes (see Table 1). As already mentioned in Section 3.1, DMD structures and metal NWs are also attractive candidates with respect to the trade-off between NIR transparency and sheet resistance, showing additional appealing features such as low-temperature processing and mechanical flexibility. The NIR transmission can be further improved via light trapping strategies such as the implementation of appropriate textured foils on top of the semitransparent contact to minimize parasitic reflections. Another effective approach to improve the tandem cell performance consists in employing a higher bandgap perovskite material for the top cell so as to expand the Si cell absorption spectrum. As reported in Figure 11b, the employ of detailed-balance calculation allows obtaining the optimal bandgap values for the perovskite top cell and the Si bottom cell depending on the tandem configuration: The ideal bandgap for the top cell is evaluated to be 1.73 eV (point 1) for the tandem in series, whereas this value is predicted to be 1.81 eV (point 2) for the module and the four-terminal tandem.[185] Several compositional engineering approaches for effective perovskite bandgap tuning have been proposed and used to meet these expectations, including the use of multi-cation, mixed iodide-bromide perovskite compositions. It is evident from Figure 11b that the constraints on the top-cell bandgap are more stringent in the case of monolithic tandem devices, which undergo a substantial PCE decrease as a result of small deviations of the top-cell bandgap from the ideal value, limiting the choice of available perovskite top cell materials. In this regard, a fascinating aspect recently investigated by Jager et al. is the effect of luminescent coupling, a phenomenon consisting in the re-absorption of luminescent photons emitted by the high-bandgap top cell in the low-bandgap bottom cell, which can be exploited as a means to relax those constraints and reduce spectral mismatch between the two sub-cells, allowing to shift the top-cell bandgap from 1.71 eV to values in the range of 1.60–1.65 eV.[186]

As a consequence of incorporating transparent electrodes and wider-bandgap perovskites, NIR-transparent PSCs typically show lower efficiencies than those of traditional opaque PSCs (maximum PCE of around 19% at >70% average NIR transmittance, against the record PCE of 25.5% obtained with a conventional opaque cell). Nevertheless, impressive advances have been achieved during the last few years via rational engineering of each functional layer, as thoroughly scanned in the following sections.

Design of Transparent Electrodes: Early studies mainly focused on the optimization of the semitransparent contacts. The first 4T perovskite/Si TSC was reported in 2015 by Loper et al.,[187] who proposed a MAPbI$_3$-based top cell free of metallic components, involving the use of FTO/glass as bottom electrode and MoO$_x$/ITO as TTE, and yielding a transmittance in the NIR of >55%; by combining the as-fabricated perovskite top cell with a c-Si heterojunction bottom cell, the tandem efficiency was 13.4% (top cell: 6.2%; bottom cell: 7.2%). It is worth noting that, because the TCO/glass substrate typically show higher transparency than the TTE in a ST-PSC, in 4-T devices the perovskite top cell is generally integrated with light incident from the TCO/glass side, so as to maximize the number of photons entering the solar cell and reduce the parasitic optical losses. In 2015, Mailoa and co-workers demonstrated the first monolithically integrated 2T PSC/Si tandem cell with 13.7% PCE by employing AgNWs ($R_s = 9\,\Omega\,\text{sq}^{-1}$; $T_{\text{max}} = 89.5\%$) as the top electrode and 111 nm thick LiF as an AR coating.[188] Considering the process compatibility restrictions involved in 2T devices, the monolithic integration was realized using a front-polished Si homojunction bottom cell to accommodate a MAPbI$_3$-based perovskite top cell and a suitable tunnel junction based on silicon, on top of which a 30 nm thick TiO$_2$ layer was grown by low-temperature atomic layer deposition (ALD) to serve as the n-type heterojunction for the n-i-p PSC. Returning back to 4T devices, Duong et al. produced in 2016 a mesoscopic MAPbI$_3$-based ST-PSC comprising sputtered ITO front and back electrodes with optimized thicknesses; the best device exhibited a PCE exceeding 12% and broadband NIR transmittance higher than 80%.[189] Through this strategy, an overall 4T perovskite/Si tandem efficiency of 20.1% was achieved. Another interesting work from Werner et al. reports on the effective fabrication of low-temperature NIR-transparent PSCs featuring ITO electrodes and yielding PCEs as high 14.5% for an aperture area of 1 cm^2.[190] Such PSC design was leveraged for the realization of large area (1.43 cm^2) perovskite/Si tandem cells with both 4T and 2T configurations, obtaining 23% and 20.5% PCE, respectively, at >1 cm^2 top cell aperture area. By using the simple CH$_3$NH$_3$PbI$_3$ perovskite system, the Authors critically compared the two configurations, pointing out that the former presents more challenges in terms of fabrication protocols and materials selection, whereas the 4T is more performing and easier to realize.[190]

Modulation of Perovskite Bandgap: In the search for alternative pathways to improve the tandem cell performance, researchers began to investigate the effect of deliberately altering the bandgap of the perovskite absorber by compositional engineering, aiming

at the best optical/electrical matching between the two sub-cells and at an improved stability of the perovskite system. In 2018, Zheng et al. enhanced the PCE of the monolithic perovskite/textured-homojunction-Si TSC from 17.6%, obtained with the previous design, up to 21.8% on 16 cm^2 by replacing MAPbI$_3$ with (FAPbI$_3$)$_{0.83}$(MAPbBr$_3$)$_{0.17}$ showing a higher bandgap and better quality[191]; the PCE improvement is also due to the integration of a new front top metal grid which reduces the series resistance across the device, resulting in a very high FF (78% under reverse scan). Another interesting approach was reported by Qiu et al.,[192] who fabricated 2T perovskite/Si tandem devices with different Si/ITO/SnO$_2$/perovskite (1.65–1.72 eV)/Spiro-OMeTAD/MoO$_x$/ITO compositions; the tandem device based on the 1.69 eV bandgap perovskite (FA$_{0.5}$MA$_{0.38}$Cs$_{0.12}$PbI$_{2.04}$Br$_{0.96}$) showed the highest performance, with a PCE over 22%. The proposed perovskite system was found to favorably alter the crystal growth, reducing the formation of defects whilst maintaining the NIR transmittance at values higher than 50%. Bush and co-workers further improved the PCE to the remarkable value of 23.6% in a 2T configuration by combining a Cs$_{0.17}$FA$_{0.83}$Pb(I$_{0.83}$Br$_{0.17}$)$_3$-based perovskite top cell with an infrared-tuned Si heterojunction bottom cell.[193] The stable perovskite tolerates the deposition of a SnO$_2$/ZTO window bilayer by either ALD or pulsed chemical vapor deposition (CVD), allowing for the sputtering of an ITO-based front contact; importantly, NiO$_x$ was employed as the HTL, thus preventing stability issues and parasitic optical losses related to use of doped Spiro-OMeTAD. A step to efficiencies higher than 26% (26.4%) in a 4T configuration was demonstrated by Duong et al. using a perovskite system based on Rubidium with Cs/FA/MA (Rb-FA$_{0.75}$ MA$_{0.15}$Cs$_{0.1}$PbI$_2$Br), which allowed to obtain an ideal 1.73 eV bandgap and to fabricate performing NIR-transparent PSCs with steady-state PCE of up to 16% and excellent T_{avg} of 84% in the 720–1100 nm range.[194] The study shows the beneficial impact of increasing the cation composition complexity on the light stability of the device, as well as the effective improvement of the transparency by replacing the FTO bottom electrode with an ITO transparent contact showing less than 5% absorption in the IR. More recently, an in-depth investigation of the synergic effect triggered by methylammonium chloride (MACl) additive on the performance of 4T cells was reported by He and collaborators,[195] demonstrating that the MA cation and the Cl anion allow to control the quality of the (Cs, FA)$_x$(MACl)$_{1-x}$PbBr$_{3y}$I$_{3-3y}$ perovskite film in terms of its thickness, bandgap, phase stability, and defect density. The proposed system resulted in 4 T PSC/Si tandem cell with an open-circuit voltage of 1.74 V and overall PCE of 25.9%. An investigation worth to mention due to its practical relevance is the one from De Bastiani and co-workers,[196] who developed a monolithic tandem design featured with a transparent back electrode to absorb the albedo light, enhancing the current generation in the bottom cell. By employing (Cs,FA)$_x$(MA)$_{1-x}$PbBr$_{3y}$I$_{3-3y}$ perovskites at tunable bandgaps in the range 1.59–1.7 eV, the authors found that halide segregation can be prevented by minimizing the bromide ratio, allowing to improve the stability of the resulting device and obtaining PCEs as high as 25.2% in a 2T configuration.

Advanced Strategies Toward >29% PCE: Further progress in Si/perovskite TSCs was mainly achieved by combining the aforementioned perovskite bandgap tuning strategies with advanced

electrodes design. To improve the electrode transparency deposited on top of the Cs/FA/MA perovskite layer, Ying and co-workers devised a strategy to prepare IZO electrodes having R_s of 15.9 Ω sq^{-1} and T_{avg} in the NIR higher than 80% by sputtering suitable for integration into buffer-layer-free ST-PSCs[86]; the vacuum evaporated C$_{60}$/BCP ETL is proved to be stable to the sputtered IZO top contact. They ultimately demonstrated a conversion efficiency of 16.23% for the single perovskite cell, and 24.60% PCE for a 4T tandem with c-Si. In another remarkable example of electrodes design, Jung et al. engineered indium oxide electrodes doped with titanium and tantalum, resulting in films with T_{avg} in the NIR as high as 91.6%[89]; the improved NIR transparency is explained in terms of higher carrier mobility and reduced free-carrier absorption compared to ITO. Through this strategy, they successfully realized ST perovskite cells based on (FAPbI$_3$)$_{0.95}$(MAPbBr$_3$)$_{0.05}$ with PCEs over 17%, and 4T perovskite-Si tandem with PCEs over 26%. A different, TCO-free electrode for 4T Si/perovskite devices was proposed by Wang and co-workers,[98] who developed a sandwiched gold nanomesh having MoO$_x$ (20 nm)/Au (7 nm)/MoO$_x$ (80 nm) DMD composition, sheet resistance of 19.6 Ω sq^{-1}, and average NIR transmittance of 74%, resulting in an efficient NIR-transparent n-i-p PSC yielding 18.3% PCE under reverse scan; combined with a heterojunction Si solar cells, the summed efficiency of the 4T tandem cell reached 27.0%. Note that, in their work, the proposed MoO$_x$/Au/MoO$_x$ electrode was carefully optimized toward the highest NIR transmittance, with the thicknesses of each constituting layer being substantially different compared to those employed for instance by Della Gaspera et al. for BIPV purposes.[96] This further highlights the importance of an application-orientated design of the transparent electrodes, aimed to achieve either the best visible transparency (when the target application is BIPVs) or the highest NIR transmittance (when the device is to be integrated in TSCs). In 2020, Chen et al. further enhanced the PCE of 4T TSCs through a new synergic approach consisting in the increase of the speed of the antisolvent spinning procedure (a strategy they defined boosted solvent extraction), combined with the incorporation of urea, a Lewis base, resulting in an effective modulation of the Cs$_{0.05}$FA$_{0.81}$MA$_{0.14}$PbI$_{2.55}$Br$_{0.45}$ perovskite thickness and grain size and an increase of the size of the electrons diffusion up to 2.3 μm.[197] The resulting ST perovskite cell, having an impressive 19% PCE and a transmittance higher than 70% in the NIR region, was further coupled with a Si bottom cell in a 4T tandem configuration, permitting to reach PCE values as high as 28.2% (see **Figure 12**a). In a jointed computational and experimental study, Yang et al. implemented an in-depth optimization protocol to obtain a high-efficiency 4T cell based on the Cs$_{0.05}$FA$_{0.95}$PbI$_3$ perovskite absorber, coupling high transmittance in the NIR (>60%) of the top cell with an excellent tandem PCE of 28.3%.[94] This was possible by the sophisticated engineering of an ultrathin TTE consisting in a compact Au film (7 nm) grown under the Frank–van der Merwe mechanism on top of a Cr seed layer (1 nm).

To obtain high-efficiency and marketable PSC/Si tandem PVs, it is also necessary to optimize the c-Si bottom cell. With the aim to produce industrially scalable 2T devices, Köhnen and co-workers investigated the integration of 100 μm thick Si obtained by industrial fabrication through the Czochralski (CZ) method for 2T device based on the Cs$_{0.05}$(MA$_{0.23}$FA$_{0.77}$)$_{0.95}$

$Pb(Br_{0.23}I_{0.77})_3$ perovskite formulation (see Figure 12b).[198] Their results are encouraging, since the optimal PCE they obtained—27.9%—by coupling the as-fabricated Si bottom cell with a p-i-n perovskite top cell is not too much lower than the reference value (28.2%) obtained with the commonly used front-side polished FZ-Si, which is about three times thicker. Another important aspect concerns the selection of suitable charge-transport layers for the top PSC. The management of the hole extraction has been investigated by Al-Ashouri et al.,[199] who designed a new methyl-substituted carbazole self-assembled mono-layer, that is, 2-(3,6-Dimethoxy-9H-carbazol-9-yl) ethyl]-phosphonic acid, as HTL in a 2T perovskite/Si cell based on a $Cs_{0.05}(FA_{0.77}MA_{0.23})_{0.95}Pb(I_{0.77}Br_{0.23})_3$ perovskite system with a bandgap of 1.68 eV. As a result, they obtained a certified PCE equal to 29.15%. Focusing on the impact of the top cell architecture, a very recent report by Aydin et al. showed the first integration of a noninverted perovskite n-i-p cell, based on the $Cs_{0.05}MA_{0.15}FA_{0.8}Pb(I_{0.75}Br_{0.25})_3$ absorber, in tandem with textured bottom silicon cells, resulting in PCEs as high as 27.1%.[200] This was achieved by designing novel hole- and electron-transport layers consisting in 2,20,7,70-tetra(N,N-di-p-tolyl) amino-9,9-spirobifluorene (spiro-TTB)/vanadium oxide and amorphous niobium oxide with ligand-bridged C_{60}, respectively. This report can boost future researches aiming at the integration of record-efficiency, regular n–i–p PSCs within the context of tandem PVs, whose most relevant results have mainly originated from the inverted structure configuration.

3.3.2. Perovskite-CIGS Tandem Solar Cells

A truly convenient alternative to Si-based bottom cells is constituted by the CIGS solar cells, due to the optimal bandgap value of about 1.1 eV for the state-of-the-art devices. CIGS has other advantages, namely direct bandgap properties and a high absorption coefficient (10^5 cm^{-1}), which result in the possibility to reduce its thickness and the associated manufacturing costs, making this material ideally suitable for large-scale production. Similar to perovskites, the bandgap for CIGS can be favorably tuned in the interval of 1.0–1.7 eV by varying the [Ga]/([Ga] + [In]) ratio,[201] providing CIGS/perovskite tandem PVs with high versatility and great potential to achieve high efficiencies through an optimal choice of materials and bandgaps. From theoretical calculations, it is known that the tandem cells reach the maximum efficiencies when the bandgap of the top cell is in the range 1.6–1.8 eV, whereas the optimal bandgap value for the bottom cell is around 1.0–1.2 eV.[202] For this reason, CIGS could be well integrated both as the top or the bottom cell. CIGS devices are also characterized by remarkable stability against space radiation: While perovskite/Si TSCs were found to be unsuitable
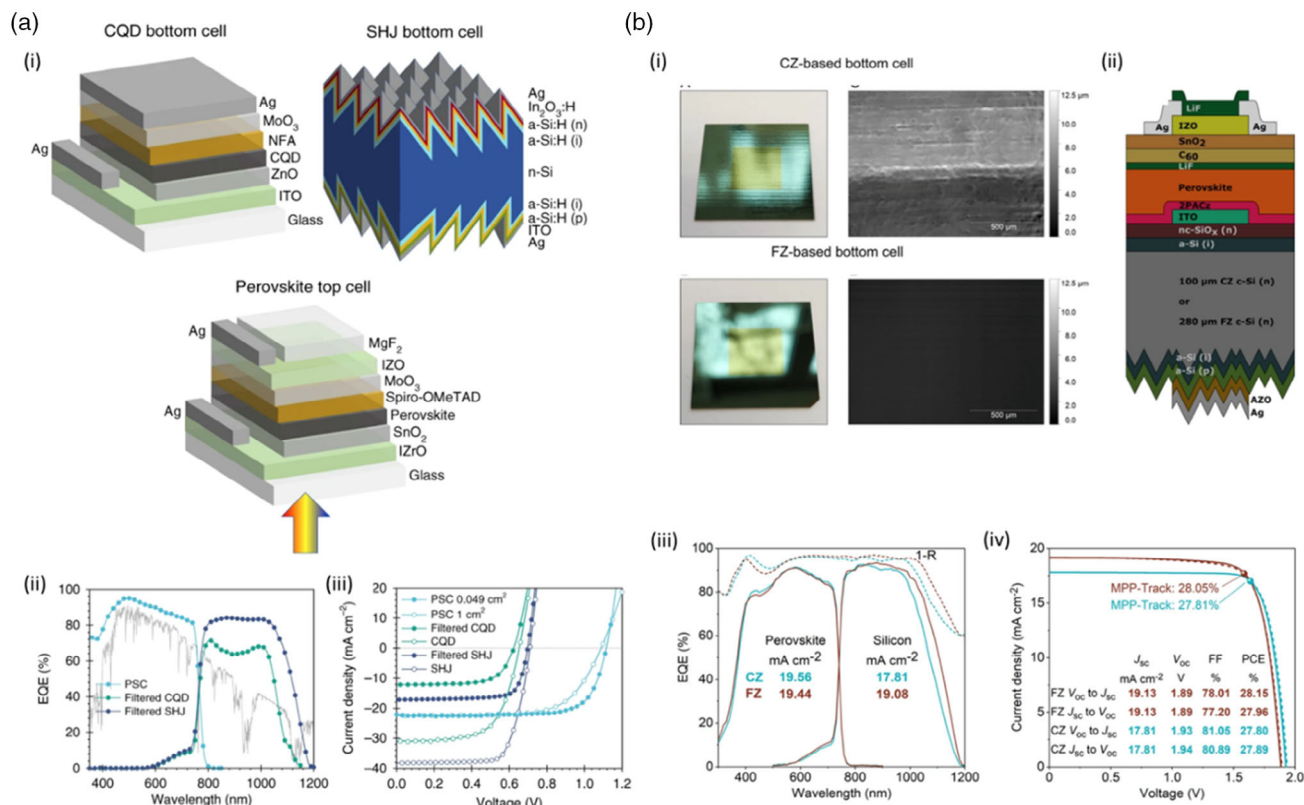

Figure 12. Structural features of efficient perovskite/Si TSCs. a) i) Schemes, ii) external quantum efficiency (EQE) characterization and *J–V* curves of 4T tandem cells made from $Cs_{0.05}FA_{0.81}MA_{0.14}PbI_{2.55}Br_{0.45}$ perovskite, mechanically stacked with colloidal quantum dot cell and Si-cell. Reproduced with permission.[197] Copyright 2020, Nature Publishing Group. b) i) Optical photographs, confocal laser scanning microscopy images, and ii) scheme of the monolithic perovskite/silicon tandem cell prepared by using planarized float-zone (FZ) or industrial Czochralski (CZ) silicon. iii) EQE and iv) *J–V* measurement of tandem solar cells based on FZ and thin CZ silicon. Reproduced with permission.[198] Copyright 2021, John Wiley & Sons, Inc.

to withstand the harsh radiation environment in space, it was demonstrated that the perovskite/CIGS cells can retain over 85% of their initial efficiency under AM0 solar illumination even after 68 MeV proton irradiation at a dose of $2 \times 10^{12} \text{ p}^+ \text{ cm}^{-2}$.[203] This makes perovskite/CIGS TSCs a promising cheap, radiation-hard, flexible, and ultra-lightweight PV technology for future space applications. These advantages are even more valuable when considering the rapid progress that perovskite/CIGS TSCs have experienced in just a few years in terms of efficiency. The evolution and PV parameters of recent champion perovskite/CIGS 2T and 4T tandem devices are summarized in Table S2, Supporting Information. Detailed theoretical analyses have permitted to shed light on the maximum efficiencies obtainable by perovskite/CIGS TSCs. According to recent simulation results,[204] tandem PCEs as high as 31.13% can be achieved by careful optimization of the bandgaps and thicknesses of both perovskite and CIGS, improvements of the perovskite film quality, use of antireflection coatings, and rational design of the ICL (in 2T devices), the transparent electrodes, and the charge-transport layers to minimize parasitic absorptions and reflections.

2-Terminal CIGS/Perovskite TSCs: Despite the promising theoretical performances, the perovskite/CIGS implementation into real devices has not been simple, though. One of the very first examples of perovskite/CIGS 2T TSCs was reported in 2015 by Todorov et al.,[205] who designed a reactor for precise control of the optical properties of the perovskite layer via vapor-based halide exchange reactions, enabling continuous and reversible bandgap tuning from 1.58 eV (pure iodide) to 2.29 eV (pure bromide). Efficiencies exceeding 10–12% were demonstrated for the stand-alone perovskite devices in the optimum bandgap range of 1.65–1.75 eV. For 2T tandem integration, the authors examined the performance of two different front transparent electrodes, namely a 10–15 nm thick Al-based electrode (50% optical transmission) and a Ca-based electrode having similar thickness but higher optical transmission (80%) and including a BCP layer of ≈5 nm with the dual function of an n-selective layer and a Ca diffusion barrier; the analysis resulted in tandem PCEs equal to 8.0% and 10.9%, respectively. The efficiencies were still much lower than the performance of the individual CIGS or perovskite sub-cells, but many other reports followed and paved the way toward substantial PCE improvements through various strategies. For instance, a remarkable advancement in the 2T configuration was presented in 2018 by Han and co-workers,[206] who developed a functional ICL using a sufficiently thick ITO film, chemically polished with a commercial SiO_2 slurry, to reduce the roughness of the underlying boron-doped ZnO (BZO) layer. They also optimized the $Cs_{0.09}FA_{0.77}MA_{0.14}Pb(I_{0.86}Br_{0.14})_3$ perovskite composition (1.59 eV bandgap) and employed a 100 nm thick ITO front electrode, resulting in an overall tandem efficiency of 22.4%. A similarly high value of PCE (21.6%) was obtained by Jošt et al.,[207] who developed thin conformal HTLs to improve the quality of the above deposited $Cs_{0.05}(MA_{0.17}FA_{0.83})Pb_{1.1}(I_{0.83}Br_{0.17})_3$ perovskite layer for effective integration onto rough bottom cell surfaces without any additional polishing step. Specifically, a thin NiO_x layer was conformally deposited by ALD on the front contact of the CIGS bottom cells, and an additional PTAA layer was incorporated at the NiO_x/perovskite interface to further enhance

the performance; the complete 2T tandem device also comprised a highly transparent IZO front contact, a silver frame around the active area, and a LiF AR coating. In a recent comprehensive report, Jacobsson and colleagues explored all the issues of 2T perovskite/CIGS TSCs by reporting on the characterization of a significant number (169) of 2T cells, highlighting the main challenges related to the surface roughness of the CIGS bottom cell and the uniformity of the ICLs between the CIGS and perovskite sub-cells.[208] They used $Cs_{0.05}FA_{0.79}MA_{0.16}PbBr_{0.49}I_{2.51}$, doped with Rb and with a surplus of PbI_2, as the perovskite absorber, a sputtered i-ZnO/AZO bilayer as the mid TCO, and SnO_2/ITO as the front contact. Their efforts brought to acceptable tandem PCEs in the range 15–16%. They also analyzed devices using the same perovskite composition in a 4T tandem configuration. To this aim, they fabricated perovskite cells using FTO as the bottom electrode, onto which NiO (15–20 nm) was deposited to serve as the HTL, and i-ZnO (80 nm)/AZO (300 nm) as the top contact, which was sputtered on top of a 10 nm thick SnO_2 layer; the as-fabricated ST-PSCs showed average PCEs of around 12% and good transmittance in the NIR (>60%); in this case, they obtained PCE values in the range 16–17%.

4-Terminal CIGS/Perovskite TSCs: As expected, the researches provide a quite different scenario when 4T cells are considered, with the engineering of the TCEs becoming a fundamental aspect of the studies. In this regard, it is worth to mention the work by Shen and coworkers,[209] who employed opportunely designed transparent electrodes, together with a multi-cation $Cs_{0.1}Rb_{0.05}FA_{0.75}MA_{0.15}PbI_{1.8}Br_{1.2}$ perovskite absorber, to fabricate high-performance perovskite/CIGS 4T cells. The perovskite top cell was realized on a 100 nm thick ITO bottom electrode, onto which a compact TiO_2 (70 nm) layer and a mesoporous TiO_2 (60 nm) film were deposited, whereas the top electrode consisted in a 10 nm thick MoO_x anode buffer layer and a 40 nm thick IZO conductive layer onto which a 180 nm thick MgF_2 AR coating was deposited, resulting in an excellent overall NIR transmittance (>70%) and high PCE (18.1% at a perovskite bandgap of 1.62 eV, and 16.5% at 1.75 eV). By mechanically stacking the high bandgap (≈1.75 eV) ST-PSC with a 16.5% CIGS (≈1.13 eV) bottom cell, a 4T tandem efficiency of 23.4% was achieved, along with excellent device stability against oxygen-induced degradation.

A clever strategy to improve the performance of 4T perovskite/CIGS TSCs was shown by Gharibzadeh and co-workers,[210] who employed a 2D/3D perovskite heterostructure comprising a bulk 3D double-cation $FA_{0.83}Cs_{0.17}Pb(I_{1-y}Br_y)_3$ system and a 2D passivation agent based on n-butylammonium bromide (BABr), resulting in greatly enhanced V_{oc} and PCE values. The authors tuned the bromide concentration to control the bandgap value of the 3D perovskite absorber layer in the range between 1.65 and 1.85 eV; the highest stabilized PCE (equal to 17.5%) for the stand-alone perovskite top cell was obtained at a bandgap of 1.65 eV, whereas significantly lower PCEs were observed for $E_g > 1.74$ eV. The semitransparency was guaranteed by the employ of both top and bottom ITO electrodes processed by sputtering (active area 10.5 mm²), resulting in transmittance values >50% in the NIR. The NIR transmittance of the perovskite cells was characterized as a function of the perovskite bandgap, as shown in **Figure 13**a. The authors realized 4T TSCs by
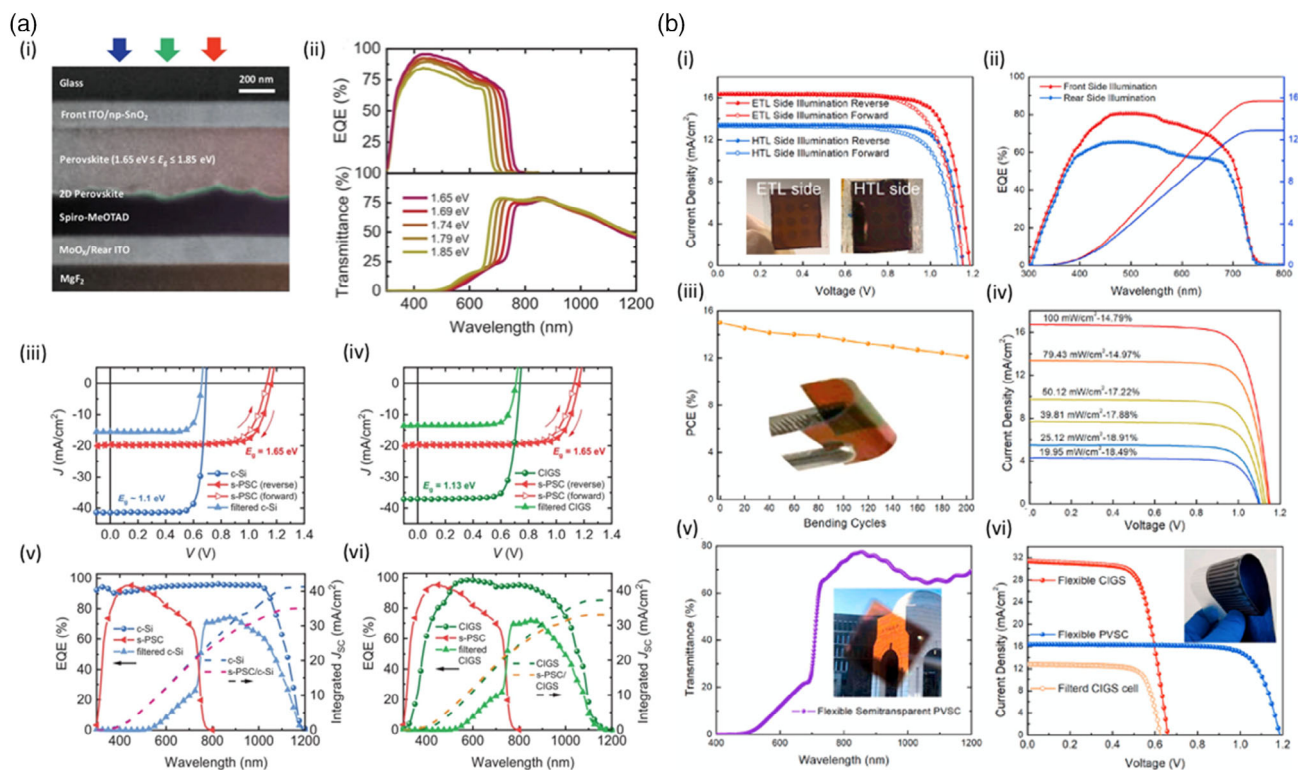
Figure 13. Representative examples of perovskite-CIGS tandem PVs. a) i) SEM cross-section characterization of the $FA_{0.83}Cs_{0.17}Pb(I_{0.6}Br_{0.4})_3$-based ST-PSC and ii) effect of perovskite bandgap (in the range 1.65–1.85 eV) on the EQE and transmittance. The bandgap tuning is realized by modifying the amount of bromide ($0.24 \leq \gamma \leq 0.56$) in the precursor solution used for preparing the 3D perovskite system $FA_{0.83}Cs_{0.17}Pb(I_{1-y}Br_y)_3$. iii) J–V curves, iv) integrated J_{sc} and EQE characterizations of the 1.65 eV ST-PSC coupled with Si bottom cell (v) or with CIGS bottom cell (vi). Reproduced with permission.[210] Copyright 2020, John Wiley & Sons, Inc. b) i) J–V curves and (ii) EQE spectra of the semitransparent $FA_{0.8}Cs_{0.2}Pb(I_{0.7}Br_{0.3})_3$ perovskite cell illuminated from (the front which has) the ETL side and from the (rear which has the) HTL side; effect of bending (iii) and of illumination intensity (iv) on the PCE; v) Transmittance values of the flexible semitransparent PSC, with inset showing a photograph of the device. vi) J–V curves of the perovskite/CIGS 4-T tandem device. The photograph in the inset shows a flexible CIGS cell. Reproduced with permission.[211] Copyright 2020, Elsevier.

combining the above perovskite cells with CIGS bottom cells ($E_g = 1.13$ eV; PCE = 21.2%), demonstrating overall tandem PCEs as high as 25.0%, which is quite similar to the performance the same authors obtained using silicon bottom cells (25.7%). In another interesting report, Li et al. demonstrated the first example of efficient all-flexible perovskite/CIGS tandem device yielding a PCE of 21.06% (see Figure 13b).[211] To this aim, the authors fabricated a flexible perovskite cell onto an ITO/PET substrate using a high-bandgap $FA_{0.8}Cs_{0.2}Pb(I_{0.7}Br_{0.3})_3$ perovskite system ($E_g = 1.75$ eV) and a triple-layer electron-selective contact made of trans-1,2-diaminocyclohexane-N,N,N′,N′-tetraacetic (CyDTA), SnO₂, and CyDTA-complexed SnO₂. On top of the perovskite layer, they deposited spiro-OMeTAD by spin-coating to serve as the HTL, followed by thermal evaporation of 1 nm Au and 10 nm MoO_x films and sputtering of 100 nm thick ITO as the top electrode. As a result, flexible perovskite cells with a PCE of 15.02% and an excellent light transparency of around 70% beyond 700 nm were demonstrated. By coupling such devices with flexible CIGS cells in a 4T configuration, tandem PCEs as high as 21.06% were achieved. Such design flexibility of perovskite/CIGS TSCs is a remarkable advantage over

traditional silicon-based tandems, since this makes them viable for unconventional PV applications including BIPVs.

Lastly, it is worth to mention the recent work by Nakamura et al.,[212] who employed a 775-nm spectral splitting mirror to direct the low-energy photons only to the CIGS cell ($E_g = 1.02$ eV) and the high-energy photons to a perovskite cell based on a $Cs_{0.1}Rb_{0.05}FA_{0.75}MA_{0.15}PbI_{1.8}Br_{1.2}$ system ($E_g = 1.59$ eV). Through this strategy, they obtained an overall PCE as high as 28.0%. However, the main disadvantages of such approach are the high costs associated with the optical splitting system, as well as the complexity of manufacture and scale-up. By contrast, mechanically stacked and monolithically integrated perovskite/Si TSCs have demonstrated superior potential for commercial applications, presenting high efficiency along with cost-effectiveness and reliability. At present, the record research-cell PCE for perovskite/CIGS 2T TSCs is 24.2%, as certified by the NREL,[29] whereas the ultimate record for perovskite/CIGS 4T tandem devices is claimed to be 27%, obtained by coupling a 18.6% efficient perovskite top cell with a bandgap-optimized CIGS flexible bottom cell, as a result of the joint efforts between the company MiaSolé Hi-Tech Corp and European Solliance Solar Research.[183]

3.3.3. All-Perovskite Tandem Devices

As mentioned in the previous sections, the perovskite bandgap can be conveniently tuned by engineering the chemical composition, obtaining values higher than 1.5 eV (suitable for tandem integration as top cell) and inferior than 1.4 eV (suitable for the bottom cell).[213] For instance, the possibility to produce alloys between Pb and Sn in metal halide perovskites allows obtaining narrow bandgaps which can be set down to 1.17 eV if the Sn amount is in the range 50–60%.[214] In contrast, the bandgap of lead halide perovskites can be readily tuned from 1.5 to 2.5 eV by adjusting the I/Br ratio. Such extraordinary bandgap tunability enables perovskite–perovskite (all-perovskite) TSCs to be constructed using a wide-bandgap ST-PSC as the top cell and a narrow-bandgap PSC as the bottom cell.

The first example of all-perovskite 2T tandem device was reported in 2016 by Jiang and co-workers,[215] who engineered a very simple device structure in which they used $CH_3NH_3PbI_3$ perovskite, FTO as the back electrode, spiro-OMeTAD/PEDOT:PSS/PEI/PCBM:PEI as the ICL, and a thin film (40 nm) of PEDOT:PSS as the front contact, resulting in a glass/FTO/c-TiO$_2$/m-TiO$_2$/CH$_3$NH$_3$PbI$_3$/spiroOMeTAD/PEDOT:PSS/PEI/PCBM:PEI/CH$_3$NH$_3$PbI$_3$/spiro-OMeTAD/PEDOT:PSS device stack. However, the noncomplementary absorption region of the two sub-cells (both based on $CH_3NH_3PbI_3$) resulted in a limited overall PCE as low as 7%. Further development of all-perovskite TSCs has mainly benefited from the advances in the design of efficient narrow-bandgap (1.1–1.2 eV) perovskite cells, as well as of appropriate semitransparent contacts and ICLs. Figure S3, Supporting Information, summarizes the efficiency evolution of recent champion all-perovskite 2T and 4T tandem devices.

Tandems with Narrow-Bandgap Perovskite Bottom Cells: Aiming at an ideal bandgap matching between the two sub-cells, researchers began to focus their attention on the fabrication of efficient low-bandgap perovskite films for the bottom cell to be coupled with high-bandgap, mixed iodide-bromide perovskite absorbers in the top cell. As a first groundbreaking report, Eperon and co-workers investigated the effect of adding Cs to perovskite to prepare highly stable and efficient all-perovskite TSCs.[216] In particular, the authors employed a 1.2 eV bandgap $FA_{0.75}Cs_{0.25}Sn_{0.5}Pb_{0.5}I_3$ perovskite absorber which was coupled with a 1.6 eV bandgap $FA_{0.83}Cs_{0.17}Pb(I_{0.83}Br_{0.17})_3$ to obtain a 4T tandem device yielding a PCE of 20.3% with an aperture area of 0.2 cm^2 (16.0% for 1 cm^2 devices). In this configuration, an ITO layer deposited by sputtering was employed to realize the top contact of the p-i-n perovskite top cell. A 2T tandem device was also developed by the authors using a 1.8 eV bandgap $FA_{0.83}Cs_{0.17}Pb(I_{0.5}Br_{0.5})_3$ perovskite in the monolithic structure in combination with the 1.2 eV bandgap $FA_{0.75}Cs_{0.25}Sn_{0.5}Pb_{0.5}I_3$ perovskite; a recombination layer obtained by tin oxide coated with sputtered ITO was employed, resulting in PCE values reaching 17.0% (see **Figure 14a**).

Another experimental investigation worth to mention in the field of 2T devices is the 2018 work from Zhao and co-workers,[217] who incorporated chloride ions in a narrow-bandgap perovskite system ($\approx$1.25 eV) to improve the grain morphology and the resulting carrier mobilities. The incorporation of 2.5% Cl was found to increase grain size, crystallinity, and carrier mobility in (FASnI$_3$)$_{0.6}$(MAPbI$_3$)$_{0.4}$:Cl perovskite films with a thickness of $\approx$750 nm, enabling an improved performance of devices featuring thick absorber layers. Through this strategy, 2T all-perovskite TSCs showing PCEs up to 21% and promising operational stability were successfully fabricated. The remarkable result from the authors was the engineering of a semitransparent interconnection layer Ag (1 nm)/MoO$_x$ (3 nm)/ITO ($\approx$120 nm), possessing a transmittance >60% in the NIR; the transmittance of the 1.75 eV high-bandgap FA$_{0.8}$Cs$_{0.2}$Pb(I$_{0.7}$Br$_{0.3}$)$_3$ perovskite film ($\approx$250 nm) deposited onto glass/ITO/PTAA was also very high (>70%). Comparable performances had already been demonstrated by the same research group also in the 4T configuration.[218] To this end, the authors thoroughly improved the thickness (up to $\approx$1000 nm), crystallinity and the resulting carrier lifetimes of the (FASnI$_3$)$_{0.6}$(MAPbI$_3$)$_{0.4}$ perovskite absorber, obtaining >80% external quantum efficiency (EQE) in the IR region as well as carrier lifetimes higher than 0.25 μs; the result was an impressive PCE of the stand-alone low-bandgap perovskite cell equal to 17.6%. The authors stacked this perovskite-based cell with a ST high-bandgap ($\approx$1.58 eV) perovskite top cell based on FA$_{0.3}$MA$_{0.7}$PbI$_3$, obtaining 4T tandem efficiencies approaching 21%. The $\approx$18% efficient n-i-p top cell was produced on FTO/glass, while the transparent top electrode consisted in a MoO$_x$ (10 nm)/Au (8.5 nm)/MoO$_x$ (10 nm) stack deposited by thermal evaporation; the authors characterized the transmission spectra of the resulting entire wide-bandgap cell, finding acceptable transmittance values (>50%) in the NIR. A further improvement of the 4T tandem PCE up to 23% was obtained by coupling the 1.25 eV narrow-bandgap (FASnI$_3$)$_{0.6}$(MAPbI$_3$)$_{0.4}$ bottom cell with a wider bandgap ST-PSC based on FA$_{0.8}$Cs$_{0.2}$Pb-(I$_{0.7}$Br$_{0.3}$)$_3$ (1.75 eV). In this new configuration, the authors employed a more transparent MoO$_x$/ITO electrode in place of MoO$_x$/Au/MoO$_x$, which resulted in a top cell transmittance up to 70% beyond 700 nm.

Latest Advances toward >25% PCE: The most recent researches on the field of all-perovskite TSCs have mainly focused on the optimization of the narrow-bandgap PSC in terms of PV performance and device lifetime. An interesting study on the engineering of mixed Pb–Sn narrow-bandgap PSCs was reported in 2019 by Lin and co-workers,[219] who leveraged the comproportionation reaction of tin (Sn + Sn^{4+} → 2 Sn^{2+}) to improve perovskite stability; in particular, by introducing metallic tin in the perovskite film precursor ink, the resulting MA$_{0.3}$FA$_{0.7}$Pb$_{0.5}$Sn$_{0.5}$I$_3$ (1.22 eV) perovskite film presented a higher resistance to oxidation under ambient conditions. As a result, they could increase the carrier diffusion length up to an outstanding value of 3 μm, ultimately resulting in PCE values as high as 21.1% for the stand-alone narrow-bandgap solar cell. By coupling this device with a wide-bandgap (1.71 eV) Cs$_{0.2}$Fa$_{0.8}$PbI$_{1.8}$Br$_{1.2}$-based top cell via an ALD-SnO$_2$-based tunnel recombination junction, they obtained overall 2T tandem PCEs equal to 24.8% for small-area devices (0.049 cm^2) and 22.1% for large-area devices (1.05 cm^2). Their efforts were mainly focused on characterizing the perovskite precursor ink to demonstrate the reduction of the Sn^{4+} precursor solution by a blue-shift in the transmittance spectra; indeed, the Sn^{2+}-rich solution was yellowish, whereas the oxidized Sn^{4+} form was red colored. A breakthrough in the morphology control of mixed Pb–Sn perovskite films was obtained one year
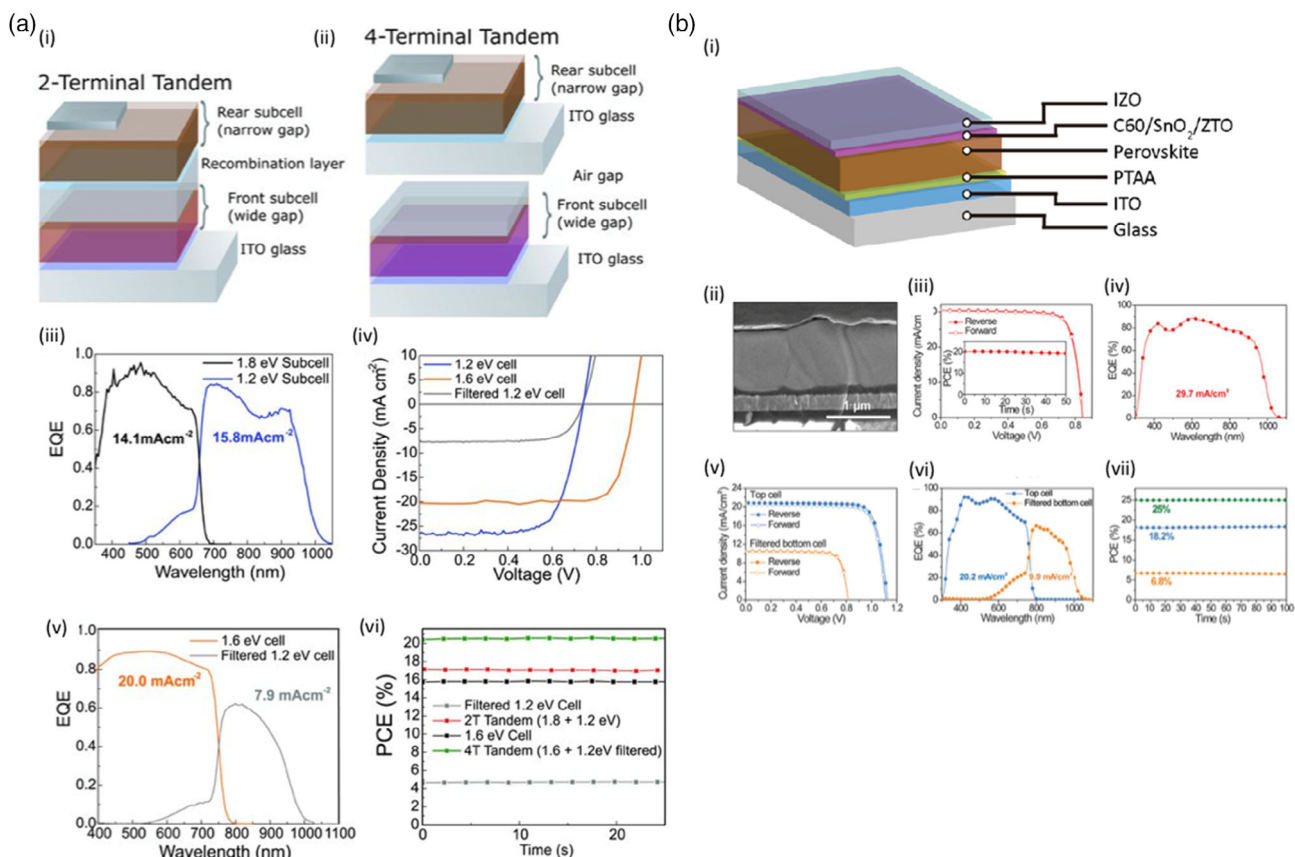
Figure 14. Representative examples of all-perovskite tandem PVs. a) Scheme of 2T (i) and 4T (ii) all-perovskite TSCs based on monolithic assembly of the $FA_{0.83}Cs_{0.17}Pb(I_{0.5}Br_{0.5})_3$ (1.8 eV bandgap) and $FA_{0.75}Cs_{0.25}Sn_{0.5}Pb_{0.5}I_3$ (1.2 eV bandgap); for the 4T tandem, the $FA_{0.83}Cs_{0.17}Pb(I_{0.83}Br_{0.17})_3$ (1.6 eV bandgap) is employed. iii) EQE spectra of the 1.2 and 1.8 eV perovskite cells; iv) J–V curves and v) EQE spectra of the 1.2 eV (also filtered) and 1.6 eV perovskite cells. Reproduced with permission.[216] Copyright 2020, American Association for the Advancement of Science (AAAS). b) i) Scheme of the high–bandgap ST-PSC using the $Cs_{0.05}FA_{0.8}MA_{0.15}PbI_{2.55}Br_{0.45}$ perovskite system. ii) Cross-sectional SEM image of the narrow-bandgap cell based on the GuaSCN-modified $(FASnI_3)_{0.6}(MAPbI_3)_{0.4}$ perovskite film. iii) J–V curve and iv) EQE characterization of the tandem device. The integrated photocurrent density is indicated in the inset. v) J–V curves and vi) EQE characterization of the top wide–bandgap ST-PSC and the filtered low–bandgap bottom PSC. The inset shows the integrated photocurrent densities for the two cells. Reproduced with permission.[220] Copyright 2019, The Authors, some rights reserved; exclusive licensee American Association for the Advancement of Science.

later by the same research group, who introduced formamidine sulfinic acid (FSA) as a suitable additive to reduce the nonradiative recombination and increase the stability of Sn^{2+} in narrow-bandgap perovskite films under ambient conditions.[184] The authors studied the effect of FSA concentration, finding that the best performances were obtained at 0.3 mol%, resulting in a 2T tandem PCE equal to 24.7% (the one certified was 24.2%) on an area over 1 cm². In-lab power conversion efficiencies of 25.6% and 21.4% for 0.049 and 12 cm², respectively, were also demonstrated.

A remarkable breakthrough in the field of 4T devices was achieved by Tong et al.,[220] who leveraged guanidinium thiocyanate (GuaSCN) for improving the structural and optoelectronic properties of Sn-Pb mixed, low-bandgap perovskite films. The GuaSCN additive allowed for carrier lifetimes >1 μs and diffusion lengths >2 μm when added at concentration of about 7% in the 1.25 eV low-bandgap, 1 μm thick $(FASnI_3)_{0.6}(MAPbI_3)_{0.4}$ perovskite layer. The resulting PCE of the complete narrow-bandgap cell having glass/ITO/PEDOT:PSS/GuaSCN-modified$(FASnI_3)_{0.6}(MAPbI_3)_{0.4}$/$C_{60}$/BCP/Ag composition was

>20%. When combined with a semitransparent 1.63 eV wide-bandgap top cell based on the $Cs_{0.05}FA_{0.8}MA_{0.15}PbI_{2.55}Br_{0.45}$ perovskite absorber, it was possible to obtain a PCE as high as 25% in the 4T configuration (see Figure 14b). The top cell was realized on a glass/ITO substrate onto which PTAA was deposited by spin-coating to act as the HTL. On top of the perovskite film, the semitransparent electron-collecting electrode was fabricated as follows: C_{60} (40 nm) was deposited by thermal evaporation, while ALD was employed to deposit SnO_x (6 nm) and ZTO (2 nm); then, the films were covered by a sputtered 250 nm thick IZO layer. The NIR transmittance of the as-fabricated ST-PSC was higher than 60%.

In conclusion, both 2T and 4T all-perovskite tandem devices have already reached practical PCEs exceeding 25%, demonstrating performances competitive with those of other perovskite-based TSCs and offering additional exciting opportunities for cost reduction and modern PV applications (e.g., flexible PVs). According to recent analyses, further advances toward commercially viable all-perovskite TSCs can be achieved through a careful optimization of the device composition (absorber layers, ICLs,

transparent electrodes) and by improving the stability of the narrow-bandgap perovskite cells.

4. Challenges and Perspectives

Within a few years of intensive research efforts, ST-PSCs have experienced tremendous progress and have opened up promising pathways toward a terawatt-scale PV deployment. The possibility to combine light transparency with sustainable power generation constitute a unique opportunity to expand the market potential of solar PVs. The highly modulable shapes, colors, and aesthetic features of ST-PSCs enable creative applications and an effective approach to "near-zero energy" building design via innovative BIPV solutions. Both neutral-colored and colorful ST-PSCs showing a wide range of PCE-AVT values have been reported, demonstrating remarkable potential for future integration as electricity-generating solar windows, facades, or other architectural elements. Perovskite ST devices with switchable optical properties have also been developed in the perspective of smart window applications. Parallelly, the rapid progress of NIR-transparent PSCs has boosted the efficiency of perovskite-based TSCs up to the current world record of 29.5%.[29] At present, the evolution of ST-PSCs for BIPV and tandem applications is considered as one of the most effective and feasible ways to promote the transition from the laboratory to real-world deployment of PSCs in the near future. To this aim, the following challenges and possible solutions about device lifetime, efficiency/transparency trade-off, manufacturing scale-up, and perovskite toxicity should be seriously considered for future advances.

4.1. Current Issues in Device Design and Manufacturing

4.1.1. Stability of Materials

The main obstacle hindering the commercialization of perovskite-based PVs is the short device lifetime. In the case of commercial Si solar panels, a device lifespan of more than 25 years is typically guaranteed, whereas laboratory-scale PSCs generally last a few months. The inherent instability of hybrid halide perovskites (e.g., thermal decomposition, photo-induced phase segregation, ion migration), as well as their degradation induced by the permeation of oxygen and moisture from the atmosphere, are the major reasons, which are common to both opaque and ST devices. In addition, it was found that the defects and trap states located at the surface and grain boundaries (GBs) of perovskite play a critical role in PSC performance deterioration, influencing the aforementioned decomposition phenomena. Stability issues may not only come from perovskites, but also from adjacent materials and interfaces; in fact, PSCs are composed of several layers with different compositions, and the possible corrosion or formation of complexes induced by chemical interactions at the interfaces must also be considered. For instance, the commonly used HTL additives like lithium bis(trifluoromethanesulfonyl)imide (LiTFSI) and 4-*tert*-butylpyridine (TBP) can facilitate device degradation by interacting with moisture (LiTFSI is highly hygroscopic) or forming complexes with PbI_2 (TBP can dissolve PbI_2, forming $PbI_2 \cdot TBP$ complexes). As far as the electrode interface is concerned,

Kato et al. detected iodine from the perovskite at the Ag top contact after aging in the dark under inert atmosphere and proposed a mechanism for AgI formation[221]; the corrosion was even more severe when the devices were aged under humidity, thermal stressing, and light soaking. In addition to Ag, other metals such as Au or Cu can diffuse and generate impurities inside the device, resulting in solar cell degradation.[222] Metal diffusion or self-aggregation may also cause the loss of electrical percolation in UTM film-based TCEs, which would not be no longer able to extract charge carriers efficiently.[73] In this regard, the conductivity degradation of TCEs over time is an additional critical issue in ST solar cells with respect to traditional opaque counterparts. Thus, a careful choice of materials and interfaces is necessary to prolong the device lifetime. Moreover, in new applications such as BIPVs and TSCs, long-term stability of the device appearance (optical properties, aesthetics) should also be guaranteed, and this constitutes a fundamental challenge requiring further attention.

During the last decade, a substantial research emphasis has been placed on developing effective strategies to prevent both intrinsic and extrinsic degradation mechanisms, and considerable advances have been achieved through rational interfacial engineering, perovskite composition tuning, defect passivation, and hermetic encapsulation solutions.[30,223] Almost all the studies reported to date are based on opaque PSC, with only few reports being focused on ST-PSCs stability. Nevertheless, many concepts and developments are applicable in both opaque and ST devices. While degradation from extrinsic environmental factors can be effectively solved by advanced encapsulation techniques, perovskite cation engineering is an important strategy to address thermal instability. The incorporation of inorganic cations (e.g., Cs, Rb) in multi-cation perovskites was found to prolong device lifetime, whereas organic cations (e.g., MA) typically destabilize materials and devices; however, this interpretation is based on accelerated ageing tests performed at higher-than-operating temperatures (e.g., 140 °C). Interestingly, a very recent work by Zhao et al. highlights that the impact of cations is reversed below 100 °C (temperature-induced stability reversal), underlining the importance of the specific temperature regime in which the solar cell will operate and shedding light on the complex phenomena behind perovskite decomposition from a kinetic perspective.[224] In another thoughtful report, Xu and co-workers developed a strategy to prevent photo-induced phase segregation in wide-bandgap perovskites: The authors employed triple-halide alloys (Cl, Br, I) to tailor the bandgap and stabilize the semiconductor under illumination, ultimately demonstrating NIR-transparent PSCs with less than 4% degradation after 1000 h at maximum power point operation suitable for tandem integration.[225] Remarkable device lifetimes as long as 10 000 h have recently been demonstrated by employing multi-dimensional perovskites.[226] Parallelly, numerous approaches have been proposed to obtain perovskite crystals with larger grain size (and consequently reduced GBs) and to passivate the surface/bulk defects and trap states, including the antisolvent dripping method, the use of additives, and various surface post-treatments.[68,223] Tremendous efforts have also been dedicated to develop novel dopant-free HTLs to replace the traditional unstable spiro-OMeTAD, with encouraging results. [227] In contrast, the incorporation of suitable interfacial layers, diffusion

barriers, and buffer layers has often proved to be effective in stabilizing materials and their interfaces, but further efforts are needed to fabricate devices and TCEs with stable morphological and opto-electrical properties. Despite the tremendous progress achieved during the last years, it is recognized that practical ST-PSCs would not last as long as a building or a c-Si bottom cell. Nevertheless, ST-PSCs can be potentially installed into BIPV or TSC systems and replaced periodically in a cost-effective manner, thanks to the short energy/cost payback times and easy recycling.[28] In this perspective, precise stability targets and replacement logistics should be defined, and new strategies for periodic module replacement and materials recycling should be developed to accelerate market entry.

4.1.2. Efficiency/Transparency Trade-off

In addition to the lifetime, another key parameter to be considered for assessing the technical feasibility for commercialization of a given PV technology is the efficiency. In ST-PSCs, obtaining high PCEs is complicated by the requirement of light transparency, which varies by application. Generally speaking, to make ST-PSCs a competitive technology, their efficiency should be maximized for each transparency level, and their transparency should be easy to control according to need. For BIPV purposes, further attention must be paid on the device appearance and aesthetic factors, since widespread adoption would require the compound optimization of PCE, AVT, haze, and color metrics. As previously discussed, ST-PSCs showing PCEs beyond 5–10% and AVT higher than 25%, along with neutral color and minimized haze, would be suitable for building integration as solar windows. In this regard, a topic that should be explored more is the morphological and structural optimization of the perovskite layer to obtain color neutrality while maintaining high efficiency. In the context of TSCs, the general aim of the research becomes that of maximizing the overall tandem PCE. To this end, the perovskite top cell must be optimized toward the best trade-off between efficiency and NIR transparency. This article has reviewed three different tandem technologies, namely perovskite/Si, perovskite/CIGS, and all-perovskite TSCs, whose rapid evolution was mainly attributed to the remarkable advances in NIR-transparent PSC design. Further improvements in tandem PCEs can be obtained through an optimal choice of materials and bandgaps toward the best optical/electrical matching between the top and the bottom cell, as well as by developing highly transparent electrodes and advanced light management strategies to suppress parasitic absorptions and reflections. A more application-orientated design aimed at achieving the optimum trade-off between PCE and NIR transparency in the perovskite top cell would certainly give perovskite-based tandem PVs an extra push toward commercialization.

4.1.3. Scale-up and Cost of Manufacturing

To fabricate marketable ST-PSCs, researchers also need to mitigate the costs associated with the materials used and the manufacturing process. As widely discussed earlier, solution processability is one of the key advantages of perovskite cells over traditional PV devices, as this property allows for the use of low-cost solution-based fabrication techniques. However, some of the PSC components, such as spiro-OMeTAD, are very expensive, at least at the laboratory scale. Most of the organic HTMs used in PSCs are synthesized by coupling reaction using palladium, an expensive metal, as a catalyst, thereby increasing the overall manufacturing costs. A possible solution consists in employing low-cost and more stable inorganic HTMs, such as NiOx, CuO, and CuSCN, which have recently led to respectable PCEs.[228] The employ of precious metals (Au, Ag) as top electrode materials could represent a further obstacle to a large-scale commercialization. In this regard, the ST technology permits to substantially reduce the content of such expensive metals by using for example ultrathin Au or Ag films as transparent electrodes; however, silver-, gold-, and indium-free TCEs (e.g., carbon-, polymer-, or copper-based electrodes) should be rather selected for a cost-effective design. Similarly, the costs associated with ETMs and perovskites should be reduced, for example, by selecting heart-abundant materials or replacing the conventional sintering procedure of metal oxides with other low-temperature processes.

In addition to cost, the other important challenge in ST-PSC manufacturing is the scaling up. For instance, scaling ST-PSCs to the sizes necessary for window integration requires the use of fabrication techniques compatible with the industrial large-scale production and capable of reproducing the high performance of the constituent materials and interfaces over a large area. On a laboratory scale, the spin-coating method has achieved great success in fabricating small-area devices, leading to the highest efficiencies reported to date. However, the deposition of uniform and high-quality perovskite films over large areas using spin-coating is very challenging; the same issue is valid for the other layers. Alternative scalable techniques such as slot-die coating, doctor blading, and inkjet printing should be explored more for a timely development. In addition to the uniformity and quality of the perovskite and charge-transport layers, the conductivity of the TCOs is vital to maintain high performances, and this could be an issue over large-area substrates that needs to be addressed before practical use. Adding metal grids can be an effective strategy on this front, though at the expense of transparency.

4.1.4. Toxicity Issues

The PV community is also aware about the toxicity issues associated with the lead content in perovskite-based PV technologies. Lead has largely proven to be the superior metal cation constituent in perovskite PV compounds, both in terms of performance and stability; however, the environmental impact of its usage is becoming an important issue for commercial PSC development. Alternative lead-free perovskite absorbers have been extensively explored, but the corresponding devices generally suffer from lower efficiencies and short lifetime. Moreover, the total or partial substitution of the B cation in the perovskite crystal structure has a substantial impact on the bandgap, making it challenging to reduce the Pb content in ST-PSCs without compromising on the performance of the target PV system; this is especially the case for TSCs, which require an optimal bandgap matching between the top and bottom cell to achieve high PCEs. Anyway, it has been calculated that the possible contamination

from lead-based PSCs would be relatively insignificant compared to the amount of lead released by other human activities, for example though a coal burning power station.[229] In addition, it has been demonstrated that high-efficiency PSCs can also be fabricated using lead from recycled lead-acid batteries or isolating PbI_2 from previous devices, an encouraging result from a recycling and lifecycle perspective.[230] Nevertheless, studies on lead-free PSCs cannot be neglected, and further efforts are needed in this direction.

4.2. Future Outlook

In summary, the current limitations impeding the commercialization of PSCs are now well known and tackled by numerous research groups around the world. PSCs have already reached excellent efficiencies and acceptable levels of stability. The future perspectives are encouraging, especially in terms of efficiency-to-cost ratios: Based on recent analyses, the PSC technology seems to have all the trumps to emerge as a cost leader in the future energy market.[231] Different from conventional applications in rooftops and power plants, the ST design offers alternative and potentially faster pathways toward commercialization, even without achieving PCE comparable to the dominating Si modules. With preliminary demonstrations already exceeding the expectations in terms of PCE, AVT, haze, and color metrics values, ST-PSCs will probably find complementary applications and markets in the near future, especially in the context of BIPVs. To this regard, one has to consider the rising global market of BIPVs, which is expected to have a compound annual growth rate of 23.9% for the period of 2020–2025.[232] At the European Community level, this growth is also sustained by the urgent need of increasing the energy performance of buildings. This requirement was in particular defined by the European Directive 31/2010/EU (effective since 2010) which was, in turn, based on the Kyoto protocol (effective since 2015) toward strict emission reduction targets. In this scenario, the future role played by PSCs might be crucial, given the lower manufacturing costs compared to silicon-based technologies, as clearly quantified in some recent studies. By considering PCE values higher than 22% in the case of single-junction devices and higher than 30% in the case of tandem solar cells, Zafoschnig et al.[233] estimated that perovskite-based technology can lead to a reduction of about 11–19% relative decrease (0.4–0.7 \$cents kWh^{-1}) of LCOE compared with silicon-based PVs for utility-scale panels, and to 14–17% relative decrease (0.9–1.1 \$cents kWh^{-1}) for the residential panels. In absolute terms, the economic analysis showcases the great potentialities of PSCs in the residential case. Another in-depth analysis based on a BIPV system has been provided by Cannavale and co-workers,[234] reporting as example the headquarters of the Regional Departments of Apulia located in Bari, Italy. They considered the replacement of glazing with ST-PSCs (PCE = 6%), and also shade systems with opaque all-perovskite tandem solar cells (PCE = 16%). The application of ST-PSCs returned 27.9 MWh $year^{-1}$, which can be further expanded to 42.0 MWh $year^{-1}$ by also including the PV shades. The authors also estimated the resulting electricity saving up to 18%. Although this investigation is based on an existing

building, the low PCE numbers clearly underestimate the great potential of ST-PSCs for BIPVs.

In the context of tandem PVs, the recent progress achieved in the fabrication of highly efficient (>19% PCE), NIR-transparent ($T_{avg} > 70\%$ in the 800–1200 nm range) PSCs offers a tremendous opportunity to cut off the LCOE and boost the competitiveness of well-established solar PVs by combining them with ST perovskite top cells in tandem double-junction PV devices. The review revealed that the efficiency of perovskite/Si 2-J TSCs is already approaching that of mature GaAs-based tandem PVs, while CIGS/perovskite and perovskite/perovskite tandem devices are also reaching competitive performances, offering additional exciting possibilities to further reduce the manufacturing costs and make the tandem technology compatible with flexible and transparent solar cell applications. As far as the life cycle assessment of perovskite-based TSCs is concerned, a recent holistic estimation from Tian et al. analyzed the beneficial effect in terms of energy payback time and CO_2 emission per kWh, with particular regard to the all-perovskite tandem PVs compared to the established Si-based PV.[235] While the latter shows values equal to 1.52 years and $24.6 \times g$ CO_2-eq kWh^{-1}, all-perovskite tandem PVs permits to significantly reduce these numbers down to 0.35 years and $10.7 \times g$ CO_2-eq kWh^{-1}, ultimately offering an advantageous alternative not just for the economy scale but also environmentally wise due to the predicted reduction of the produced CO_2. In a subsequent report,[28] the same authors also highlighted the key role played by rigorous recycling strategies for single-junction perovskite cells. They investigated the life cycle assessment, comparing six different types of state-of-the-art PSC. Recycling significantly reduces the energy payback time and the greenhouse gas emission to values higher than 70% with respect to the landfill scenario. Remarkably, recycling perovskite modules might be a convenient strategy to further reduce the CO_2 emission with respect to the silicon-based panels.

With further research efforts dedicated to addressing stability, scalability, and toxicity issues, it is expected that ST-PSCs will experience a transition from laboratory scale to commercial deployment very soon; looking at the current trends, the 2T PSC/Si tandem solar cells will likely be the first perovskite-based technology to enter the PV market. We believe that a more judicious ST-PSC design primarily focused on the target application would accelerate this revolution, and we hope that our review succeeded in providing the readers with clear guidelines and strategic tools to proceed in this direction.

Supporting Information

Supporting Information is available from the Wiley Online Library or from the author.

Acknowledgements

Conflict of Interest

The authors declare no conflict of interest.

Keywords

[1] Intergovernmental Panel on Climate Change (IPCC), *AR6 Climate Change 2021: The Physical Science Basis*, Cambridge University Press, Cambridge **2021**.

[2] National Aeronautics and Space Administration (NASA), *Climate Change and Global Warming*, **2021**, https://climate.nasa.gov/ (accessed: August 2021).

[3] United Nations Department of Economic and Social Affairs (UN DESA), *The 17 Goals of Sustainable Development*, **2021**, https://sdgs.un.org/goals (accessed: August 2021).

[4] International Energy Agency (IEA), *Net Zero by 2050 – A Roadmap for the Global Energy Sector*, **2021**, https://www.iea.org/reports/net-zero-by-2050 (accessed: August 2021).

[5] International Renewable Energy Agency (IRENA), *World Energy Transitions Outlook: 1.5°C Pathway*, **2021**, https://www.irena.org/publications/2021/Jun/World-Energy-Transitions-Outlook (accessed: August 2021).

[6] C. Breyer, D. Bogdanov, A. Gulagi, A. Aghahosseini, L. S. N. S. Barbosa, O. Koskinen, M. Barasa, U. Caldera, S. Afanasyeva, M. Child, J. Farfan, P. Vainikka, *Prog. Photovolt. Res. Appl.* **2017**, *25*, 727 (accessed: August 2021).

[7] P. K. Nayak, S. Mahesh, H. J. Snaith, D. Cahen, *Nat. Rev. Mater.* **2019**, *4*, 269.

[8] D. M. Chapin, C. S. Fuller, G. L. Pearson, *J. Appl. Phys.* **1954**, *25*, 676.

[9] REN21, *Renewables 2021: Global Status Report*, **2021**, https://www.ren21.net/gsr-2021.

[10] International Energy Agency (IEA), *Global Energy Review 2021*, https://www.iea.org/reports/global-energy-review-2021.

[11] N. M. Haegel, R. Margolis, T. Buonassisi, D. Feldman, A. Froitzheim, R. Garabedian, M. Green, S. Glunz, H.-M. Henning, B. Holder, I. Kaizuka, B. Kroposki, K. Matsubara, S. Niki, K. Sakurai, R. A. Schindler, W. Tumas, E. R. Weber, G. Wilson, M. Woodhouse, S. Kurtz, *Science* **2017**, *356*, 141.

[12] G. M. Wilson, M. Al-Jassim, W. K. Metzger, S. W. Glunz, P. Verlinden, G. Xiong, L. M. Mansfield, B. J. Stanbery, K. Zhu, Y. Yan, J. J. Berry, A. J. Ptak, F. Dimroth, B. M. Kayes, A. C. Tamboli, R. Peibst, K. Catchpole, M. O. Reese, C. S. Klinga, P. Denholm, M. Morjaria, M. G. Deceglie, J. M. Freeman, M. A. Mikofski, D. C. Jordan, G. TamizhMani, D. B. Sulas-Kern, *J. Phys. Appl. Phys.* **2020**, *53*, 493001.

[13] S. Ghosh, R. Yadav, *Sustain. Energy Technol. Assess.* **2021**, *47*, 101410.

[14] M. Kokkonen, P. Talebi, J. Zhou, S. Asgari, S. A. Soomro, F. Elsehrawy, J. Halme, S. Ahmad, A. Hagfeldt, S. G. Hashmi, *J. Mater. Chem. A* **2021**, *9*, 10527.

[15] D. Zhang, M. Stojanovic, Y. Ren, Y. Cao, F. T. Eickemeyer, E. Socie, N. Vlachopoulos, J.-E. Moser, S. M. Zakeeruddin, A. Hagfeldt, M. Grätzel, *Nat. Commun.* **2021**, *12*, 1777.

[16] Y. Suleymanov, *Science* **2021**, *372*, 1301.

[17] C. Li, J. Zhou, J. Song, J. Xu, H. Zhang, X. Zhang, J. Guo, L. Zhu, D. Wei, G. Han, J. Min, Y. Zhang, Z. Xie, Y. Yi, H. Yan, F. Gao, F. Liu, Y. Sun, *Nat. Energy* **2021**, *6*, 605.

[18] A. Bonasera, G. Giuliano, G. Arrabito, B. Pignataro, *Molecules* **2020**, *25*, 2200.

[19] A.-G. Gereanu, C. Sartorio, A. Bonasera, G. Giuliano, S. Cataldo, M. Scopelliti, G. Arrabito, B. Pignataro, *Coatings* **2021**, *11*, 586.

[20] J. Y. Kim, J.-W. Lee, H. S. Jung, H. Shin, N.-G. Park, *Chem. Rev.* **2020**, *120*, 7867.

[21] T. Wu, Z. Qin, Y. Wang, Y. Wu, W. Chen, S. Zhang, M. Cai, S. Dai, J. Zhang, J. Liu, Z. Zhou, X. Liu, H. Segawa, H. Tan, Q. Tang, J. Fang, Y. Li, L. Ding, Z. Ning, Y. Qi, Y. Zhang, L. Han, *Nano-Micro Lett.* **2021**, *13*, 152.

[22] M. Jeong, I. W. Choi, E. M. Go, Y. Cho, M. Kim, B. Lee, S. Jeong, Y. Jo, H. W. Choi, J. Lee, J.-H. Bae, S. K. Kwak, D. S. Kim, C. Yang, *Science* **2020**, *369*, 1615.

[23] G. Kim, H. Min, K. S. Lee, D. Y. Lee, S. M. Yoon, S. I. Seok, *Science* **2020**, *370*, 108.

[24] J. Jeong, M. Kim, J. Seo, H. Lu, P. Ahlawat, A. Mishra, Y. Yang, M. A. Hope, F. T. Eickemeyer, M. Kim, Y. J. Yoon, I. W. Choi, B. P. Darwich, S. J. Choi, Y. Jo, J. H. Lee, B. Walker, S. M. Zakeeruddin, L. Emsley, U. Rothlisberger, A. Hagfeldt, D. S. Kim, M. Grätzel, J. Y. Kim, *Nature* **2021**, *592*, 381.

[25] J. J. Yoo, G. Seo, M. R. Chua, T. G. Park, Y. Lu, F. Rotermund, Y.-K. Kim, C. S. Moon, N. J. Jeon, J.-P. Correa-Baena, V. Bulović, S. S. Shin, M. G. Bawendi, J. Seo, *Nature* **2021**, *590*, 587.

[26] M. Giannouli, *Int. J. Photoenergy* **2021**, *2021*, e6692858.

[27] J. Gong, S. B. Darling, F. You, *Energy Environ. Sci.* **2015**, *8*, 1953.

[28] X. Tian, S. D. Stranks, F. You, *Nat. Sustain.* **2021**, *4*, 821.

[29] National Renewable Energy Laboratory (NREL), *Best Research-Cell Efficiency Chart*, **2021**, https://www.nrel.gov/pv/cell-efficiency.html.

[30] W. Xiang, S. (Frank) Liu, W. Tress, *Energy Environ. Sci.* **2021**, *14*, 2090.

[31] C. J. Traverse, R. Pandey, M. C. Barr, R. R. Lunt, *Nat. Energy* **2017**, *2*, 849.

[32] B. Shi, L. Duan, Y. Zhao, J. Luo, X. Zhang, *Adv. Mater.* **2020**, *32*, 1806474.

[33] M. Mujahid, C. Chen, J. Zhang, C. Li, Y. Duan, *InfoMat* **2021**, *3*, 101.

[34] M. Batmunkh, Y. L. Zhong, H. Zhao, *Adv. Mater.* **2020**, *32*, 2000631.

[35] A. Roy, A. Ghosh, S. Bhandari, S. Sundaram, T. K. Mallick, *Buildings* **2020**, *10*, 129.

[36] Z. Wang, Z. Song, Y. Yan, S. (Frank) Liu, D. Yang, *Adv. Sci.* **2019**, *6*, 1801704.

[37] R. K. Kothandaraman, Y. Jiang, T. Feurer, A. N. Tiwari, F. Fu, *Small Methods* **2020**, *4*, 2000395.

[38] Z. Zhang, Z. Li, L. Meng, S.-Y. Lien, P. Gao, *Adv. Funct. Mater.* **2020**, *30*, 2001904.

[39] J. W. Jung, C.-C. Chueh, A. K.-Y. Jen, *Adv. Energy Mater.* **2015**, *5*, 1500486.

[40] V. M. Goldschmidt, *Naturwissenschaften* **1926**, *14*, 477.

[41] C. Li, X. Lu, W. Ding, L. Feng, Y. Gao, Z. Guo, *Acta Crystallogr. B* **2008**, *64*, 702.

[42] W. Xu, X. Yao, H. Wu, T. Zhu, X. Gong, *Emergent Mater.* **2020**, *3*, 727.

[43] C. K. Møller, *Nature* **1958**, *182*, 1436.

[44] A. Kojima, K. Teshima, Y. Shirai, T. Miyasaka, *J. Am. Chem. Soc.* **2009**, *131*, 6050.

[45] J. H. Noh, S. H. Im, J. H. Heo, T. N. Mandal, S. I. Seok, *Nano Lett.* **2013**, *13*, 1764.

[46] N. Pellet, P. Gao, G. Gregori, T.-Y. Yang, M. K. Nazeeruddin, J. Maier, M. Grätzel, *Angew. Chem., Int. Ed.* **2014**, *53*, 3151.

[47] J. Chen, J. Xu, L. Xiao, B. Zhang, S. Dai, J. Yao, *ACS Appl. Mater. Interfaces* **2017**, *9*, 2449.

[48] Y. Zhang, G. Grancini, Y. Feng, A. M. Asiri, M. K. Nazeeruddin, *ACS Energy Lett.* **2017**, *2*, 802.

[49] A. Maqsood, Y. Li, J. Meng, D. Song, B. Qiao, S. Zhao, Z. Xu, *Nanoscale Res. Lett.* **2020**, *15*, 89.

[50] E. Gutierrez-Partida, H. Hempel, S. Caicedo-Dávila, M. Raoufi, F. Peña-Camargo, M. Grischek, R. Gunder, J. Diekmann, P. Caprioglio, K. O. Brinkmann, H. Köbler, S. Albrecht, T. Riedl, A. Abate, D. Abou-Ras, T. Unold, D. Neher, M. Stolterfoht, *ACS Energy Lett.* **2021**, *6*, 1045.

[51] M. Saliba, T. Matsui, J.-Y. Seo, K. Domanski, J.-P. Correa-Baena, M. K. Nazeeruddin, S. M. Zakeeruddin, W. Tress, A. Abate, A. Hagfeldt, M. Grätzel, *Energy Environ. Sci.* **2016**, *9*, 1989.

[52] T. Singh, T. Miyasaka, *Adv. Energy Mater.* **2018**, *8*, 1700677.

[53] S. Ašmontas, A. Čerškus, J. Gradauskas, A. Grigucevičienė, K. Leinartas, A. Lučun, K. Petrauskas, A. Selskis, A. Sužiedėlis, E. Širmulis, R. Juškėnas, *Coatings* **2021**, *11*, 279.

[54] F. Ünlü, E. Jung, J. Haddad, A. Kulkarni, S. Öz, H. Choi, T. Fischer, S. Chakraborty, T. Kirchartz, S. Mathur, *APL Mater.* **2020**, *8*, 070901.

[55] A. D. Taylor, Q. Sun, K. P. Goetz, Q. An, T. Schramm, Y. Hofstetter, M. Litterst, F. Paulus, Y. Vaynzof, *Nat. Commun.* **2021**, *12*, 1878.

[56] F. Zuo, S. T. Williams, P.-W. Liang, C.-C. Chueh, C.-Y. Liao, A. K.-Y. Jen, *Adv. Mater.* **2014**, *26*, 6454.

[57] N. Glück, T. Bein, *Energy Environ. Sci.* **2020**, *13*, 4691.

[58] H.-S. Kim, C.-R. Lee, J.-H. Im, K.-B. Lee, T. Moehl, A. Marchioro, S.-J. Moon, R. Humphry-Baker, J.-H. Yum, J. E. Moser, M. Grätzel, N.-G. Park, *Sci. Rep.* **2012**, *2*, 591.

[59] C.-C. Chueh, C.-Z. Li, A. K.-Y. Jen, *Energy Environ. Sci.* **2015**, *8*, 1160.

[60] Z. Yang, B. H. Babu, S. Wu, T. Liu, S. Fang, Z. Xiong, L. Han, W. Chen, *Sol. RRL* **2020**, *4*, 1900257.

[61] Y. Li, M. Cheng, E. Jungstedt, B. Xu, L. Sun, L. Berglund, *ACS Sustain. Chem. Eng.* **2019**, *7*, 6061.

[62] Y. Y. Xiao, Y. Meng, H. Gao, Y. Chen, Q. Meng, Y. Bai, H. Wang, Y. Zhang, H. Yan, C. B. Han, *Sustain. Energy Fuels* **2020**, *4*, 824.

[63] X. Meng, Z. Cai, Y. Zhang, X. Hu, Z. Xing, Z. Huang, Z. Huang, Y. Cui, T. Hu, M. Su, X. Liao, L. Zhang, F. Wang, Y. Song, Y. Chen, *Nat. Commun.* **2020**, *11*, 3016.

[64] L. A. Castriotta, R. Fuentes Pineda, V. Babu, P. Spinelli, B. Taheri, F. Matteocci, F. Brunetti, K. Wojciechowski, A. Di Carlo, *ACS Appl. Mater. Interfaces* **2021**, *13*, 29576.

[65] J. Chung, S. S. Shin, K. Hwang, G. Kim, K. W. Kim, D. S. Lee, W. Kim, B. S. Ma, Y.-K. Kim, T.-S. Kim, J. Seo, *Energy Environ. Sci.* **2020**, *13*, 4854.

[66] N. Ren, B. Chen, R. Li, P. Wang, S. Mazumdar, B. Shi, C. Zhu, Y. Zhao, X. Zhang, *Sol. RRL* **2021**, *5*, 2000795.

[67] X. Liu, L. Hu, R. Wang, J. Li, H. Gu, S. Liu, Y. Zhou, G. Tu, *Polymers* **2019**, *11*, 427.

[68] N. K. Tailor, M. Abdi-Jalebi, V. Gupta, H. Hu, M. I. Dar, G. Li, S. Satapathi, *J. Mater. Chem. A* **2020**, *8*, 21356.

[69] S. D. Stranks, G. E. Eperon, G. Grancini, C. Menelaou, M. J. P. Alcocer, T. Leijtens, L. M. Herz, A. Petrozza, H. J. Snaith, *Science* **2013**, *342*, 341.

[70] J. Burschka, N. Pellet, S.-J. Moon, R. Humphry-Baker, P. Gao, M. K. Nazeeruddin, M. Grätzel, *Nature* **2013**, *499*, 316.

[71] M. Liu, M. B. Johnston, H. J. Snaith, *Nature* **2013**, *501*, 395.

[72] Q. Chen, H. Zhou, Z. Hong, S. Luo, H.-S. Duan, H.-H. Wang, Y. Liu, G. Li, Y. Yang, *J. Am. Chem. Soc.* **2014**, *136*, 622.

[73] G. Giuliano, A. Bonasera, M. Scopelliti, D. Chillura Martino, T. Fiore, B. Pignataro, *ACS Appl. Electron. Mater.* **2021**, *3*, 1813.

[74] V. M. Le Corre, M. Stolterfoht, L. Perdigón Toro, M. Feuerstein, C. Wolff, L. Gil-Escrig, H. J. Bolink, D. Neher, L. J. A. Koster, *ACS Appl. Energy Mater.* **2019**, *2*, 6280.

[75] X.-L. Trinh, H.-C. Kim, *Energy Rep.* **2020**, *6*, 1297.

[76] G. E. Eperon, V. M. Burlakov, A. Goriely, H. J. Snaith, *ACS Nano* **2014**, *8*, 591.

[77] Z. Song, C. Chen, C. Li, S. Rijal, L. Chen, Y. Li, Y. Yan, *Sustain. Energy Fuels* **2021**, *5*, 2865.

[78] S. Kim, T. T. Trinh, J. Park, D. P. Pham, S. Lee, H. B. Do, N. N. Dang, V.-A. Dao, J. Kim, J. Yi, *Sci. Rep.* **2021**, *11*, 15524.

[79] J.-D. Chen, T.-Y. Jin, Y.-Q. Li, J.-X. Tang, *Nanoscale* **2019**, *11*, 18517.

[80] C.-Y. Chen, G.-H. Tan, H.-L. Hsu, C.-P. Chen, H.-W. Lin, *Adv. Energy Sustain. Res.* **2020**, *1*, 2000035.

[81] Y. Xu, J. Wang, L. Sun, H. Huang, J. Han, H. Huang, L. Zhai, C. Zou, *J. Mater. Chem. C* **2021**, *9*, 9102.

[82] S. Zhu, X. Yao, Q. Ren, C. Zheng, S. Li, Y. Tong, B. Shi, S. Guo, L. Fan, H. Ren, C. Wei, B. Li, Y. Ding, Q. Huang, Y. Li, Y. Zhao, X. Zhang, *Nano Energy* **2018**, *45*, 280.

[83] F. J. Ramos, S. Jutteau, J. Posada, A. Bercegol, A. Rebai, T. Guillemot, R. Bodeux, N. Schneider, N. Loones, D. Ory, C. Broussillou, G. Goaer, L. Lombez, J. Rousset, *Sci. Rep.* **2018**, *8*, 16139.

[84] A. J. Bett, K. M. Winkler, M. Bivour, L. Cojocaru, Ö. Ş. Kabakli, P. S. C. Schulze, G. Siefer, L. Tutsch, M. Hermle, S. W. Glunz, J. C. Goldschmidt, *ACS Appl. Mater. Interfaces* **2019**, *11*, 45796.

[85] N. Li, F. Meng, F. Huang, G. Yu, Z. Wang, J. Yan, Y. Zhang, Y. Ai, C. Shou, Y. Zeng, J. Sheng, B. Yan, J. Ye, *ACS Appl. Energy Mater.* **2020**, *3*, 9610.

[86] Z. Ying, Y. Zhu, X. Feng, J. Xiu, R. Zhang, X. Ma, Y. Deng, H. Pan, Z. He, *Adv. Mater. Interfaces* **2021**, *8*, 2001604.

[87] S.-H. Lim, H.-J. Seok, M.-J. Kwak, D.-H. Choi, S.-K. Kim, D.-H. Kim, H.-K. Kim, *Nano Energy* **2021**, *82*, 105703.

[88] E. Aydin, M. D. Bastiani, X. Yang, M. Sajjad, F. Aljamaan, Y. Smirnov, M. N. Hedhili, W. Liu, T. G. Allen, L. Xu, E. V. Kerschaver, M. Morales-Masis, U. Schwingenschlögl, S. D. Wolf, *Adv. Funct. Mater.* **2019**, *29*, 1901741.

[89] H. Jung, G. Kim, G. S. Jang, J. Lim, M. Kim, C. S. Moon, X. Hao, N. J. Jeon, J. S. Yun, H. H. Park, J. Seo, *ACS Appl. Mater. Interfaces* **2021**, *13*, 30497.

[90] J. Yun, *Adv. Funct. Mater.* **2017**, *27*, 1606641.

[91] C. Roldán-Carmona, O. Malinkiewicz, R. Betancur, G. Longo, C. Momblona, F. Jaramillo, L. Camacho, H. J. Bolink, *Energy Environ. Sci.* **2014**, *7*, 2968.

[92] Z. Li, H. Li, L. Chen, J. Huang, W. Wang, H. Wang, J. Li, B. Fan, Q. Xu, W. Song, *Sol. Energy* **2020**, *206*, 294.

[93] B. Chen, Y. Bai, Z. Yu, T. Li, X. Zheng, Q. Dong, L. Shen, M. Boccard, A. Gruverman, Z. Holman, J. Huang, *Adv. Energy Mater.* **2016**, *6*, 1601128.

[94] D. Yang, X. Zhang, Y. Hou, K. Wang, T. Ye, J. Yoon, C. Wu, M. Sanghadasa, S. (Frank) Liu, S. Priya, *Nano Energy* **2021**, *84*, 105934.

[95] J. C. Bernède, L. Cattin, *Asian J. Eng. Technol.* **2019**, *7*, https://doi.org/10.24203/ajet.v7i3.5710.

[96] E. Della Gaspera, Y. Peng, Q. Hou, L. Spiccia, U. Bach, J. J. Jasieniak, Y.-B. Cheng, *Nano Energy* **2015**, *13*, 249.

[97] Z. Ren, J. Zhou, Y. Zhang, A. Ng, Q. Shen, S. H. Cheung, H. Shen, K. Li, Z. Zheng, S. K. So, A. B. Djurišić, C. Surya, *Sol. Energy Mater. Sol. Cells* **2018**, *179*, 36.

[98] Z. Wang, X. Zhu, S. Zuo, M. Chen, C. Zhang, C. Wang, X. Ren, Z. Yang, Z. Liu, X. Xu, Q. Chang, S. Yang, F. Meng, Z. Liu, N. Yuan, J. Ding, S. (Frank) Liu, D. Yang, *Adv. Funct. Mater.* **2020**, *30*, 1908298.

[99] Y. (Michael) Yang, Q. Chen, Y.-T. Hsieh, T.-B. Song, N. D. Marco, H. Zhou, Y. Yang, *ACS Nano* **2015**, *9*, 7714.

[100] J. Zhao, K. O. Brinkmann, T. Hu, N. Pourdavoud, T. Becker, T. Gahlmann, R. Heiderhoff, A. Polywka, P. Görrn, Y. Chen, B. Cheng, T. Riedl, *Adv. Energy Mater.* **2017**, *7*, 1602599 (accessed: August 2021).

[101] C. D. Bailie, M. G. Christoforo, J. P. Mailoa, A. R. Bowring, E. L. Unger, W. H. Nguyen, J. Burschka, N. Pellet, J. Z. Lee, M. Grätzel, R. Noufi, T. Buonassisi, A. Salleo, M. D. McGehee, *Energy Environ. Sci.* **2015**, *8*, 956.

[102] K. Han, M. Xie, L. Zhang, L. Yan, J. Wei, G. Ji, Q. Luo, J. Lin, Y. Hao, C.-Q. Ma, *Sol. Energy Mater. Sol. Cells* **2018**, *185*, 399.

[103] C. O. R. Quiroz, Y. Shen, M. Salvador, K. Forberich, N. Schrenker, G. D. Spyropoulos, T. Heumüller, B. Wilkinson, T. Kirchartz, E. Spiecker, P. J. Verlinden, X. Zhang, M. A. Green, A. Ho-Baillie, C. J. Brabec, *J. Mater. Chem. A* **2018**, *6*, 3583.

[104] B. Vaagensmith, K. M. Reza, M. N. Hasan, H. Elbohy, N. Adhikari, A. Dubey, N. Kantack, E. Gaml, Q. Qiao, *ACS Appl. Mater. Interfaces* **2017**, *9*, 35861.

[105] J. H. Lee, J. H. Heo, S. H. Im, O. O. Park, *ACS Appl. Mater. Interfaces* **2020**, *12*, 10527.

[106] P. You, Z. Liu, Q. Tai, S. Liu, F. Yan, *Adv. Mater.* **2015**, *27*, 3632.

[107] J. Yoon, H. Sung, G. Lee, W. Cho, N. Ahn, H. S. Jung, M. Choi, *Energy Environ. Sci.* **2017**, *10*, 337.

[108] Z. Yao, D. Qu, Y. Guo, H. Huang, *J. Mater. Sci.* **2019**, *54*, 11564.

[109] V.-D. Tran, S. V. N. Pammi, B.-J. Park, Y. Han, C. Jeon, S.-G. Yoon, *Nano Energy* **2019**, *65*, 104018.

[110] Z. Li, S. A. Kulkarni, P. P. Boix, E. Shi, A. Cao, K. Fu, S. K. Batabyal, J. Zhang, Q. Xiong, L. H. Wong, N. Mathews, S. G. Mhaisalkar, *ACS Nano* **2014**, *8*, 6797.

[111] C. Lee, S.-W. Lee, S. Bae, A. Shawky, V. Devaraj, A. Anisimov, E. I. Kauppinen, J.-W. Oh, Y. Kang, D. Kim, I. Jeon, S. Maruyama, H.-S. Lee, *Sol. RRL* **2020**, *4*, 2000353.

[112] F. Guo, H. Azimi, Y. Hou, T. Przybilla, M. Hu, C. Bronnbauer, S. Langner, E. Spiecker, K. Forberich, C. J. Brabec, *Nanoscale* **2015**, *7*, 1642.

[113] D. Bryant, P. Greenwood, J. Troughton, M. Wijdekop, M. Carnie, M. Davies, K. Wojciechowski, H. J. Snaith, T. Watson, D. Worsley, *Adv. Mater.* **2014**, *26*, 7499.

[114] D. S. Hecht, L. Hu, G. Irvin, *Adv. Mater.* **2011**, *23*, 1482.

[115] Y. Wang, S. W. Tong, X. F. Xu, B. Özyilmaz, K. P. Loh, *Adv. Mater.* **2011**, *23*, 1514.

[116] Z. Liu, P. You, S. Liu, F. Yan, *ACS Nano* **2015**, *9*, 12026.

[117] M. Achenza, G. Desogus, Guidelines on the Building Integration of Photovoltaic in the Mediterranean Area University of Cagliari - Dipartimento di Ingegneria Civile, Ambientale e Architettura (UNICA-DICAAR), Cagliari, Italy **2015**.

[118] *BIPV: Building Integrated Photovoltaics*, **2021**, https://www.vpsolar.com/bipv-building-integrated-photovoltaics (accessed: August 2021).

[119] F. Martellotta, A. Cannavale, U. Ayr, *Energy Procedia* **2017**, *126*, 219.

[120] V. Stockhausen, L. Andrade, D. Ivanou, B. Stannowski, A. Mendes, *Sol. Energy Mater. Sol. Cells* **2019**, *191*, 451.

[121] A. Cannavale, U. Ayr, F. Martellotta, *Energy Procedia* **2017**, *126*, 636.

[122] C. Yang, D. Liu, M. Bates, M. C. Barr, R. R. Lunt, *Joule* **2019**, *3*, 1803.

[123] K. Lee, H.-D. Um, D. Choi, J. Park, N. Kim, H. Kim, K. Seo, *Cell Rep. Phys. Sci.* **2020**, *1*, 100143.

[124] P. Boyce, C. Hunter, O. Howlett, *The Benefits of Daylight through Windows*, Rensselaer Polytechnic Institute, Troy, NY **2003**.

[125] *International Glazing Database, n.d*, https://windows.lbl.gov/software/igdb (accessed: August 2021).

[126] L. K. Ono, S. Wang, Y. Kato, S. R. Raga, Y. Qi, *Energy Environ. Sci.* **2014**, *7*, 3989.

[127] G. Giuliano, S. Cataldo, M. Scopelliti, F. Principato, D. C. Martino, T. Fiore, B. Pignataro, *Adv. Mater. Technol.* **2019**, *4*, 1800688.

[128] J. C. Yu, J. Sun, N. Chandrasekaran, C. J. Dunn, A. S. R. Chesman, J. J. Jasieniak, *Nano Energy* **2020**, *71*, 104635.

[129] S. Bag, M. F. Durstock, *Nano Energy* **2016**, *30*, 542.

[130] C. O. R. Quiroz, I. Levchuk, C. Bronnbauer, M. Salvador, K. Forberich, T. Heumüller, Y. Hou, P. Schweizer, E. Spiecker, C. J. Brabec, *J. Mater. Chem. A* **2015**, *3*, 24071.

[131] M. T. Hörantner, W. Zhang, M. Saliba, K. Wojciechowski, H. J. Snaith, *Energy Environ. Sci.* **2015**, *8*, 2041.

[132] G. E. Eperon, D. Bryant, J. Troughton, S. D. Stranks, M. B. Johnston, T. Watson, D. A. Worsley, H. J. Snaith, *J. Phys. Chem. Lett.* **2015**, *6*, 129.

[133] L. Zhang, M. T. Hörantner, W. Zhang, Q. Yan, H. J. Snaith, *Sol. Energy Mater. Sol. Cells* **2017**, *160*, 193.

[134] J. H. Heo, M. H. Jang, M. H. Lee, H. J. Han, M. G. Kang, M. L. Lee, S. H. Im, *J. Mater. Chem. A* **2016**, *4*, 16324.

[135] H.-C. Kwon, A. Kim, H. Lee, D. Lee, S. Jeong, J. Moon, *Adv. Energy Mate.r* **2016**, *6*, 1601055.

[136] D. Liu, C. Yang, R. R. Lunt, *Joule* **2018**, *2*, 1827.

[137] H. Kim, H.-S. Kim, J. Ha, N.-G. Park, S. Yoo, *Adv. Energy Mater.* **2016**, *6*, 1502466.

[138] H. Wang, J. Li, H. A. Dewi, N. Mathews, S. Mhaisalkar, A. Bruno, *J. Phys. Chem. Lett.* **2021**, *12*, 1321.

[139] G. E. Eperon, S. D. Stranks, C. Menelaou, M. B. Johnston, L. M. Herz, H. J. Snaith, *Energy Environ. Sci.* **2014**, *7*, 982.

[140] H. Fang, P. Jena, *J. Mater. Chem. A* **2016**, *4*, 4728.

[141] D. Cui, Z. Yang, D. Yang, X. Ren, Y. Liu, Q. Wei, H. Fan, J. Zeng, S. Liu, *J. Phys. Chem. C* **2016**, *120*, 42.

[142] C. Chen, Y. Wu, L. Liu, Y. Gao, X. Chen, W. Bi, X. Chen, D. Liu, Q. Dai, H. Song, *Adv. Sci.* **2019**, *6*, 1802046.

[143] P. Luo, Y. Zhou, W. Xia, S. Zhou, J. Liu, Y. Lu, C. Xu, L. Sun, *Ceram. Int.* **2018**, *44*, 12783.

[144] S. Xiong, J. Song, J. Yang, J. Xu, M. Zhang, R. Ma, D. Li, X. Liu, F. Liu, C. Duan, M. Fahlman, Q. Bao, *Sol. RRL* **2020**, *4*, 1900529.

[145] Y. Jiang, B. Luo, B. Jiang, F. Jiang, C. Fuentes-Hernandez, T. Liu, L. Mao, S. Xiong, Z. Li, T. Wang, B. Kippelen, Y. Zhou, *Nano Lett.* **2016**, *16*, 7829.

[146] H. Wang, H. A. Dewi, T. M. Koh, A. Bruno, S. Mhaisalkar, N. Mathews, *ACS Appl. Mater. Interfaces* **2020**, *12*, 484.

[147] J. Li, H. Wang, X. Y. Chin, H. A. Dewi, K. Vergeer, T. W. Goh, J. W. M. Lim, J. H. Lew, K. P. Loh, C. Soci, T. C. Sum, H. J. Bolink, N. Mathews, S. Mhaisalkar, A. Bruno, *Joule* **2020**, *4*, 1035.

[148] K. Deng, Z. Liu, M. Wang, L. Li, *Adv. Funct. Mater.* **2019**, *29*, 1900830.

[149] Y. Wang, Y. Lan, Q. Song, F. Vogelbacher, T. Xu, Y. Zhan, M. Li, W. E. I. Sha, Y. Song, *Adv. Mater.* **2021**, *33*, 2008091.

[150] W. Wang, Y. He, L. Qi, *Sci. China Mater.* **2020**, *63*, 35.

[151] J. Y. Lee, K.-T. Lee, S. Seo, L. J. Guo, *Sci. Rep.* **2014**, *4*, 4192.

[152] K.-T. Lee, M. Fukuda, S. Joglekar, L. J. Guo, *J. Mater. Chem. C* **2015**, *3*, 5377.

[153] J.-H. Lu, Y.-L. Yu, S.-R. Chuang, C.-H. Yeh, C.-P. Chen, *J. Phys. Chem. C* **2016**, *120*, 4233.

[154] K.-T. Lee, J.-Y. Jang, N. Y. Ha, S. Lee, H. J. Park, *Nano Res.* **2018**, *11*, 2553.

[155] Y. Guo, K. Shoyama, W. Sato, E. Nakamura, *Adv. Energy Mater.* **2016**, *6*, 1502317.

[156] S. Schlisske, F. Mathies, D. Busko, N. Strobel, T. Rödlmeier, B. S. Richards, U. Lemmer, U. W. Paetzold, G. Hernandez-Sosa, E. Klampaftis, *ACS Appl. Energy Mater.* **2019**, *2*, 764.

[157] C. O. Ramírez Quiroz, C. Bronnbauer, I. Levchuk, Y. Hou, C. J. Brabec, K. Forberich, *ACS Nano* **2016**, *10*, 5104.

[158] J.-H. Lee, Y. Song, K. Jung, M.-J. Lee, *Mater. Lett.* **2021**, *282*, 128828.

[159] K.-T. Lee, J.-Y. Jang, J. Zhang, S.-M. Yang, S. Park, H. J. Park, *Sci. Rep.* **2017**, *7*, 10640.

[160] S. Nundy, A. Mesloub, B. M. Alsolami, A. Ghosh, *J. Clean. Prod.* **2021**, *301*, 126854.

[161] S. D. Rezaei, S. Shannigrahi, S. Ramakrishna, *Sol. Energy Mater. Sol. Cells* **2017**, *159*, 26.

[162] A. Cannavale, U. Ayr, F. Fiorito, F. Martellotta, *Energies* **2020**, *13*, 1449.

[163] A. Cannavale, G. E. Eperon, P. Cossari, A. Abate, H. J. Snaith, G. Gigli, *Energy Environ. Sci.* **2015**, *8*, 1578.

[164] G. A. Niklasson, C. G. Granqvist, *J. Mater. Chem.* **2006**, *17*, 127.

[165] X. Xia, Z. Ku, D. Zhou, Y. Zhong, Y. Zhang, Y. Wang, M. J. Huang, J. Tu, H. J. Fan, *Mater. Horiz.* **2016**, *3*, 588.

[166] F. Zhou, Z. Ren, Y. Zhao, X. Shen, A. Wang, Y. Y. Li, C. Surya, Y. Chai, *ACS Nano* **2016**, *10*, 5900.

[167] M. Pugliese, F. Bisconti, A. Rizzo, S. Colella, C. T. Prontera, G. Gigli, V. Maiorano, P. Cossari, *ACS Appl. Energy Mater.* **2020**, *3*, 10453.

[168] H. Ling, J. Wu, F. Su, Y. Tian, Y. J. Liu, *Nat. Commun.* **2021**, *12*, 1010.

[169] Y. Liu, J. Wang, F. Wang, Z. Cheng, Y. Fang, Q. Chang, J. Zhu, L. Wang, J. Wang, W. Huang, T. Qin, *Nat. Commun.* **2021**, *12*, 3360.

[170] M. I. Saidaminov, A. L. Abdelhady, B. Murali, E. Alarousu, V. M. Burlakov, W. Peng, I. Dursun, L. Wang, Y. He, G. Maculan, A. Goriely, T. Wu, O. F. Mohammed, O. M. Bakr, *Nat. Commun.* **2015**, *6*, 7586.

[171] M. De Bastiani, M. I. Saidaminov, I. Dursun, L. Sinatra, W. Peng, U. Buttner, O. F. Mohammed, O. M. Bakr, *Chem. Mater.* **2017**, *29*, 3367.

[172] J. Lin, M. Lai, L. Dou, C. S. Kley, H. Chen, F. Peng, J. Sun, D. Lu, S. A. Hawks, C. Xie, F. Cui, A. P. Alivisatos, D. T. Limmer, P. Yang, *Nat. Mater.* **2018**, *17*, 261.

[173] Y. Zhang, C. Y. Tso, J. S. Iñigo, S. Liu, H. Miyazaki, C. Y. H. Chao, K. M. Yu, *Appl. Energy* **2019**, *254*, 113690.

[174] J. Li, X. Liu, P. Cui, J. Li, T. Ye, X. Wang, C. Zhang, Y. S. Zhao, *Sci. China Chem.* **2019**, *62*, 1257.

[175] S. Liu, Y. W. Du, C. Y. Tso, H. H. Lee, R. Cheng, S.-P. Feng, K. M. Yu, *Adv. Funct. Mater.* **2021**, *31*, 2010426.

[176] Y. Zhang, Z. Wang, S. Hu, P. Yan, H. Li, C. Sheng, *ACS Appl. Mater. Interfaces* **2021**, *13*, 12042.

[177] W. Shockley, H. J. Queisser, *J. Appl. Phys.* **1961**, *32*, 510.

[178] C. Li, Y. Wang, W. C. H. Choy, *Small Methods* **2020**, *4*, 2000093.

[179] A. D. Vos, *J Phys Appl Phys* **1980**, *13*, 839.

[180] J. F. Geisz, R. M. France, K. L. Schulte, M. A. Steiner, A. G. Norman, H. L. Guthrey, M. R. Young, T. Song, T. Moriarty, *Nat Energy* **2020**, *5*, 326.

[181] M. Jaysankar, M. Filipič, B. Zielinski, R. Schmager, W. Song, W. Qiu, U. W. Paetzold, T. Aernouts, M. Debucquoy, R. Gehlhaar, J. Poortmans, *Energy Environ. Sci.* **2018**, *11*, 1489.

[182] S. P. Bremner, M. Y. Levy, C. B. Honsberg, *Prog Photovolt Res Appl* **2008**, *16*, 225.

[183] A. Bhambhani, *28.7% Efficiency Reported For 4T Tandem Solar Cell*, **2021**, http://taiyangnews.info/technology/28-7-efficiency-reported-for-4t-tandem-solar-cell/ (accessed: August 2021).

[184] K. Xiao, R. Lin, Q. Han, Y. Hou, Z. Qin, H. T. Nguyen, J. Wen, M. Wei, V. Yeddu, M. I. Saidaminov, Y. Gao, X. Luo, Y. Wang, H. Gao, C. Zhang, J. Xu, J. Zhu, E. H. Sargent, H. Tan, *Nat. Energy* **2020**, *5*, 870.

[185] M. H. Futscher, B. Ehrler, *ACS Energy Lett.* **2016**, *1*, 863.

[186] K. Jäger, P. Tillmann, E. A. Katz, C. Becker, *Sol. RRL* **2021**, *5*, 2000628.

[187] P. Löper, B. Niesen, S.-J. Moon, S. Martín de Nicolas, J. Holovsky, Z. Remes, M. Ledinsky, F.-J. Haug, J.-H. Yum, S. De Wolf, C. Ballif, *IEEE J. Photovolt.* **2014**, *4*, 1545.

[188] J. P. Mailoa, C. D. Bailie, E. C. Johlin, E. T. Hoke, A. J. Akey, W. H. Nguyen, M. D. McGehee, T. Buonassisi, *Appl. Phys. Lett.* **2015**, *106*, 121105.

[189] T. Duong, N. Lal, D. Grant, D. Jacobs, P. Zheng, S. Rahman, H. Shen, M. Stocks, A. Blakers, K. Weber, T. P. White, K. R. Catchpole, *IEEE J. Photovolt.* **2016**, *6*, 679.

[190] J. Werner, L. Barraud, A. Walter, M. Bräuninger, F. Sahli, D. Sacchetto, N. Tétreault, B. Paviet-Salomon, S.-J. Moon, C. Allebé, M. Despeisse, S. Nicolay, S. De Wolf, B. Niesen, C. Ballif, *ACS Energy Lett.* **2016**, *1*, 474.

[191] J. Zheng, C. F. J. Lau, H. Mehrvarz, F.-J. Ma, Y. Jiang, X. Deng, A. Soeriyadi, J. Kim, M. Zhang, L. Hu, X. Cui, D. S. Lee, J. Bing, Y. Cho, C. Chen, M. A. Green, S. Huang, A. W. Y. Ho-Baillie, *Energy Environ. Sci* **2018**, *11*, 2432.

[192] Z. Qiu, Z. Xu, N. Li, N. Zhou, Y. Chen, X. Wan, J. Liu, N. Li, X. Hao, P. Bi, Q. Chen, B. Cao, H. Zhou, *Nano Energy* **2018**, *53*, 798.

[193] K. A. Bush, A. F. Palmstrom, Z. J. Yu, M. Boccard, R. Cheacharoen, J. P. Mailoa, D. P. McMeekin, R. L. Z. Hoye, C. D. Bailie, T. Leijtens, I. M. Peters, M. C. Minichetti, N. Rolston, R. Prasanna, S. Sofia, D. Harwood, W. Ma, F. Moghadam, H. J. Snaith, T. Buonassisi, Z. C. Holman, S. F. Bent, M. D. McGehee, *Nat. Energy* **2017**, *2*, 17009.

[194] T. Duong, Y. Wu, H. Shen, J. Peng, X. Fu, D. Jacobs, E.-C. Wang, T. C. Kho, K. C. Fong, M. Stocks, E. Franklin, A. Blakers, N. Zin, K. McIntosh, W. Li, Y.-B. Cheng, T. P. White, K. Weber, K. Catchpole, *Adv. Energy Mater.* **2017**, *7*, 1700228.

[195] Y. He, Z. Tang, L. Mao, S. Yang, T. Yang, M. Xie, Q. Chang, L. Ding, B. He, C. Peng, C. Yu, X. Hao, J. Zhang, K. Zheng, C. Han, Y. Zhang, H. Yan, X. Xu, *PSS RRL* **2021**, 2100119.

[196] M. De Bastiani, A. J. Mirabelli, Y. Hou, F. Gota, E. Aydin, T. G. Allen, J. Troughton, A. S. Subbiah, F. H. Isikgor, J. Liu, L. Xu, B. Chen, E. Van Kerschaver, D. Baran, B. Fraboni, M. F. Salvador, U. W. Paetzold, E. H. Sargent, S. De Wolf, *Nat. Energy* **2021**, *6*, 167.

[197] B. Chen, S.-W. Baek, Y. Hou, E. Aydin, M. De Bastiani, B. Scheffel, A. Proppe, Z. Huang, M. Wei, Y.-K. Wang, E.-H. Jung, T. G. Allen, E. Van Kerschaver, F. P. García de Arquer, M. I. Saidaminov, S. Hoogland, S. De Wolf, E. H. Sargent, *Nat. Commun.* **2020**, *11*, 1257.

[198] E. Köhnen, P. Wagner, F. Lang, A. Cruz, B. Li, M. Roß, M. Jošt, A. B. Morales-Vilches, M. Topič, M. Stolterfoht, D. Neher, L. Korte, B. Rech, R. Schlatmann, B. Stannowski, S. Albrecht, *Sol. RRL* **2021**, *5*, 2100244.

[199] A. Al-Ashouri, E. Köhnen, B. Li, A. Magomedov, H. Hempel, P. Caprioglio, J. A. Márquez, A. B. Morales Vilches, E. Kasparavicius, J. A. Smith, N. Phung, D. Menzel, M. Grischek, L. Kegelmann, D. Skroblin, C. Gollwitzer, T. Malinauskas, M. Jošt, G. Matič, B. Rech, R. Schlatmann, M. Topič, L. Korte, A. Abate, B. Stannowski, D. Neher, M. Stolterfoht, T. Unold, V. Getautis, S. Albrecht, *Science* **2020**, *370*, 1300.

[200] E. Aydin, J. Liu, E. Ugur, R. Azmi, G. T. Harrison, Y. Hou, B. Chen, S. Zhumagali, M. De Bastiani, M. Wang, W. Raja, T. G. Allen, A. Ur Rehman, A. S. Subbiah, M. Babics, A. Babayigit, F. H. Isikgor, K. Wang, E. Van Kerschaver, L. Tsetseris, E. H. Sargent, F. Laquai, S. De Wolf, *Energy Environ. Sci* **2021**, *14*, 4377.

[201] A. Morales-Acevedo, in *Proc. Inorganic Nanostructured Photovoltaics—E-MRS 2009 Symp. B*, Energy Procedia, E-MRS Spring Meeting 2009, Symposium B, Strasbourg, France Vol. *2*, **2010**, p. 169.

[202] Z. (Jason) Yu, M. Leilaeioun, Z. Holman, *Nat. Energy* **2016**, *1*, 16137.

[203] F. Lang, M. Jošt, K. Frohna, E. Köhnen, A. Al-Ashouri, A. R. Bowman, T. Bertram, A. B. Morales-Vilches, D. Koushik, E. M. Tennyson, K. Galkowski, G. Landi, M. Creatore, B. Stannowski, C. A. Kaufmann, J. Bundesmann, J. Rappich, B. Rech, A. Denker, S. Albrecht, H.-C. Neitzert, N. H. Nickel, S. D. Stranks, *Joule* **2020**, *4*, 1054.

[204] P. Zhao, L. Feng, Z. Lin, J. Wang, J. Su, Z. Hu, J. Zhang, X. Ouyang, J. Chang, Y. Hao, *Sol. RRL* **2019**, *3*, 1900303.

[205] T. Todorov, T. Gershon, O. Gunawan, Y. S. Lee, C. Sturdevant, L.-Y. Chang, S. Guha, *Adv. Energy Mater.* **2015**, *5*, 1500799.

[206] Q. Han, Y.-T. Hsieh, L. Meng, J.-L. Wu, P. Sun, E.-P. Yao, S.-Y. Chang, S.-H. Bae, T. Kato, V. Bermudez, Y. Yang, *Science* **2018**, *361*, 904.

[207] M. Jošt, T. Bertram, D. Koushik, J. A. Marquez, M. A. Verheijen, M. D. Heinemann, E. Köhnen, A. Al-Ashouri, S. Braunger, F. Lang, B. Rech, T. Unold, M. Creatore, I. Lauermann, C. A. Kaufmann, R. Schlatmann, S. Albrecht, *ACS Energy Lett.* **2019**, *4*, 583.

[208] T. J. Jacobsson, A. Hultqvist, S. Svanström, L. Riekehr, U. B. Cappel, E. Unger, H. Rensmo, E. M. J. Johansson, M. Edoff, G. Boschloo, *Sol. Energy* **2020**, *207*, 270.

[209] H. Shen, T. Duong, J. Peng, D. Jacobs, N. Wu, J. Gong, Y. Wu, S. K. Karuturi, X. Fu, K. Weber, X. Xiao, T. P. White, K. Catchpole, *Energy Environ. Sci.* **2018**, *11*, 394.

[210] S. Gharibzadeh, I. M. Hossain, P. Fassl, B. A. Nejand, T. Abzieher, M. Schultes, E. Ahlswede, P. Jackson, M. Powalla, S. Schäfer, M. Rienäcker, T. Wietler, R. Peibst, U. Lemmer, B. S. Richards, U. W. Paetzold, *Adv. Funct. Mater.* **2020**, *30*, 1909919.

[211] S. Li, C. Wang, D. Zhao, Y. An, Y. Zhao, X. Zhao, X. Li, *Nano Energy* **2020**, *78*, 105378.

[212] M. Nakamura, K. Tada, T. Kinoshita, T. Bessho, C. Nishiyama, I. Takenaka, Y. Kimoto, Y. Higashino, H. Sugimoto, H. Segawa, *iScience* **2020**, *23*, 101817.

[213] M. Jošt, L. Kegelmann, L. Korte, S. Albrecht, *Adv. Energy Mater.* **2020**, *10*, 1904102.

[214] S. Gu, R. Lin, Q. Han, Y. Gao, H. Tan, J. Zhu, *Adv. Mater.* **2020**, *32*, 1907392.

[215] F. Jiang, T. Liu, B. Luo, J. Tong, F. Qin, S. Xiong, Z. Li, Y. Zhou, *J. Mater. Chem. A* **2016**, *4*, 1208.

[216] G. E. Eperon, T. Leijtens, K. A. Bush, R. Prasanna, T. Green, J. T.-W. Wang, D. P. McMeekin, G. Volonakis, R. L. Milot, R. May, A. Palmstrom, D. J. Slotcavage, R. A. Belisle, J. B. Patel, E. S. Parrott, R. J. Sutton, W. Ma, F. Moghadam, B. Conings, A. Babayigit, H.-G. Boyen, S. Bent, F. Giustino, L. M. Herz, M. B. Johnston, M. D. McGehee, H. J. Snaith, *Science* **2016**, *354*, 861.

[217] D. Zhao, Y. Yu, C. Wang, W. Liao, N. Shrestha, C. R. Grice, A. J. Cimaroli, L. Guan, R. J. Ellingson, K. Zhu, X. Zhao, R.-G. Xiong, Y. Yan, *Nat. Energy* **2017**, *2*, 17018.

[218] D. Zhao, C. Wang, Z. Song, Y. Yu, C. Chen, X. Zhao, K. Zhu, Y. Yan, *ACS Energy Lett.* **2018**, *3*, 305.

[219] R. Lin, K. Xiao, Z. Qin, Q. Han, C. Zhang, M. Wei, M. I. Saidaminov, Y. Gao, J. Xu, M. Xiao, A. Li, J. Zhu, E. H. Sargent, H. Tan, *Nat. Energy* **2019**, *4*, 864.

[220] J. Tong, Z. Song, D. H. Kim, X. Chen, C. Chen, A. F. Palmstrom, P. F. Ndione, M. O. Reese, S. P. Dunfield, O. G. Reid, J. Liu, F. Zhang, S. P. Harvey, Z. Li, S. T. Christensen, G. Teeter, D. Zhao, M. M. Al-Jassim, M. F. A. M. van Hest, M. C. Beard, S. E. Shaheen, J. J. Berry, Y. Yan, K. Zhu, *Science* **2019**, *364*, 475.

[221] Y. Kato, L. K. Ono, M. V. Lee, S. Wang, S. R. Raga, Y. Qi, *Adv. Mater. Interfaces* **2015**, *2*, 1500195.

[222] W. Ming, D. Yang, T. Li, L. Zhang, M.-H. Du, *Adv. Sci.* **2018**, *5*, 1700662.

[223] Y. Cheng, L. Ding, *Energy Environ. Sci.* **2021**, *14*, 3233.

[224] Y. Zhao, J. Zhang, Z. Xu, S. Sun, S. Langner, N. T. P. Hartono, T. Heumueller, Y. Hou, J. Elia, N. Li, G. J. Matt, X. Du, W. Meng, A. Osvet, K. Zhang, T. Stubhan, Y. Feng, J. Hauch, E. H. Sargent, T. Buonassisi, C. J. Brabec, *Nat. Commun.* **2021**, *12*, 2191.

[225] J. Xu, C. C. Boyd, Z. J. Yu, A. F. Palmstrom, D. J. Witter, B. W. Larson, R. M. France, J. Werner, S. P. Harvey, E. J. Wolf, W. Weigand, S. Manzoor, M. F. A. M. van Hest, J. J. Berry, J. M. Luther, Z. C. Holman, M. D. McGehee, *Science* **2020**, *367*, 1097.

[226] G. Grancini, C. Roldán-Carmona, I. Zimmermann, E. Mosconi, X. Lee, D. Martineau, S. Narbey, F. Oswald, F. De Angelis, M. Graetzel, M. K. Nazeeruddin, *Nat. Commun.* **2017**, *8*, 15684.

[227] X. Yin, Z. Song, Z. Li, W. Tang, *Energy Environ. Sci.* **2020**, *13*, 4057.

[228] A. M. Elseman, S. Sajid, A. E. Shalan, S. A. Mohamed, M. M. Rashad, *Appl. Phys. A* **2019**, *125*, 476.

[229] D. Fabini, *J. Phys. Chem. Lett.* **2015**, *6*, 3546.

[230] P.-Y. Chen, J. Qi, M. T. Klug, X. Dang, P. T. Hammond, A. M. Belcher, *Energy Environ. Sci.* **2014**, *7*, 3659.

[231] Z. Song, C. L. McElvany, A. B. Phillips, I. Celik, P. W. Krantz, S. C. Watthage, G. K. Liyanage, D. Apul, M. J. Heben, *Energy Environ. Sci.* Energy and Environmental Science, RSC, **2017**, *10*, 1297.

[232] BCC Publishing Staff, *Building-Integrated Photovoltaics (BIPV): Technologies and Global Markets*, **2021**.

[233] L. A. Zafoschnig, S. Nold, J. C. Goldschmidt, *IEEE J. Photovolt.* **2020**, *10*, 1632.

[234] A. Cannavale, L. Ierardi, M. Hörantner, G. E. Eperon, H. J. Snaith, U. Ayr, F. Martellotta, *Appl. Energy* **2017**, *205*, 834.

[235] X. Tian, S. D. Stranks, F. You, *Sci. Adv.* **2020**, *6*, 55.

Giuliana Giuliano received her B.Sc. in chemistry at the University of Palermo. She pursued her M.Sc. in photochemistry and molecular materials at the University of Bologna. She obtained her Ph.D. degree (2020) in materials science and nanotechnologies from the University of Catania. She is currently a postdoctoral scientist at the University of Palermo. Her research interests span across the fields of nanostructured materials, organic electronics, energy conversion, and thin-film solar cells.

Aurelio Bonasera received his B.Sc. and M.Sc. in chemistry from the University of Messina. He pursued his Ph.D. in chemistry at the University of Trieste under the supervision of Prof. M. Prato. He was appointed Erasmus-fellow at the University of Mons. He underwent his post-doctoral training as MSCA-fellow at Humboldt-Universität zu Berlin under the supervision of Prof. Stefan Hecht; then, he was visiting scientist at University College London and BASF SE. He is currently an independent researcher at the University of Palermo. His research interests include dyes, photochromic compounds, and supramolecular architectures for light harvesting and organic solar cells fabrication.

Giuseppe Arrabito received his B.Sc. in chemistry and M.Sc. in biomolecular chemistry at the Scuola Superiore di Catania. He received his Ph.D. (2012) in nanoscience from Scuola Superiore di Catania. He was postdoctoral fellow in the group of Prof. C.M. Niemeyer at the Technical University of Dortmund and in the group of Dr C. Falconi at the University of Rome—Tor Vergata. He is currently a post-doctoral scientist at the University of Palermo. His research interests are in the field of synthetic biology, biointerfaces, DNA nanotechnology, and ZnO-based nanodevices.

Bruno Pignataro obtained his Ph.D. degree in materials science from the University of Catania. He is a full professor of physical chemistry at the University of Palermo. He is referee and editorial board member for different international journals and expert evaluator for national and international research proposals. He is the project leader of the District of High Technology for innovation in the field of Cultural Heritage in Sicily, and the delegate for project planning at the Department of Physics and Chemistry in Palermo. His research interests are in the topics of nanotechnology, molecular surfaces, plastic electronics, and biotechnology.